A supercritical R-744 heat transfer simulation implementing various Nusselt number correlations

Philip van Zyl Venter

B.Eng. (Mechanical),

Hons.B.Sc. (Actuarial Science), Hons.B.Sc. (Mathematics)

Dissertation submitted in partial fulfilment of the degree

Master of Engineering

in the

School of Mechanical Engineering,

Faculty of Engineering

at the

North-West University

Supervisor: Dr. Martin van Eldik

Potchefstroom

South Africa

2010

Abstract

During the past decade research has shown that global warming may have disastrous effects on our planet. In order to limit the damage that the human race seems to be causing, it was acknowledged that substances with a high global warming potential (GWP) should be phased out. In due time, R-134a with a GWP = 1300, may probably be phased out to make way for nature friendly refrigerants with a lower GWP. One of these contenders is carbon dioxide, R-744, with a GWP = 1.

Literature revealed that various Nusselt number (*Nu*) correlations have been developed to predict the convection heat transfer coefficients of supercritical R-744 in cooling. No proof could be found that any of the reported correlations accurately predict Nusselt numbers (Nu^s) and the subsequent convection heat transfer coefficients of supercritical R-744 in cooling.

Although there exist a number of *Nu* correlations that may be used for R-744, eight different correlations were chosen to be compared in a theoretical simulation program forming the first part of this study. A water-to-transcritical R-744 tube-in-tube heat exchanger was simulated. Although the results emphasise the importance of finding a more suitable *Nu* correlation for cooling supercritical R-744, no explicit conclusions could be made regarding the accuracy of any of the correlations used in this study.

For the second part of this study experimental data found in literature were used to evaluate the accuracy of the different correlations. Convection heat transfer coefficients, temperatures, pressures and tube diameter were employed for the calculation of experimental Nusselt numbers (Nu_{exp}). The theoretical *Nu* and Nu_{exp} were then plotted against the length of the heat exchanger for different pressures. It was observed that both Nu_{exp} and *Nu* increase progressively to a maximal value and then decline as the tube length increases. From these results it were possible to group correlations according to the general patterns of their *Nu* variation over the tube length.

Graphs of Nu_{exp} against Nu^s, calculated according to the Gnielinski correlation, generally followed a linear regression, with $R^2 > 0.9$, when the temperature is equal or above the pseudocritical temperature. From this data a new correlation, *Correlation I*, based on average gradients and intersects, was formulated. Then a modification on the Haaland friction factor was used with the Gnielinski correlation to yield a second correlation, namely *Correlation II*. A third and more advanced correlation, *Correlation III*, was then formulated by employing graphs where gradients and y-intercepts were plotted against pressure. From this data a new parameter, namely the turning point pressure ratio of cooling supercritical R-744, was defined.

It was concluded that the employed *Nu* correlations under predict *Nu* values (a minimum of 0.3% and a maximum of 81.6%). However, two of the correlations constantly over predicted Nu^s at greater tube lengths, *i.e.* below pseudocritical temperatures. It was also concluded that *Correlation III* proved to be more accurate than both *Correlations I* and *II*, as well as the existing correlations found in the literature and employed in this study. *Correlation III* Nu^s for cooling supercritical R-744 may only be valid for a diameter in the order of the experimental diameter of 7.73 mm, temperatures that are equal or above the pseudocritical temperature and at pressures ranging from 7.5 to 8.8 MPa.

Key words

Convection heat transfer coefficient.
New correlation,.
Nusselt number.
Pseudocritical.
Supercritical.

Opsomming

Navorsing gedurende die laaste dekade het getoon dat globale verwarming die aarde nadelig kan beïnvloed. Om die skade wat moontlik deur die mensdom veroorsaak kan word te verminder, is dit noodsaaklik dat verbindings wat oor ‘n hoë globale verhittings potensiaal (GVP) beskik uitgefasseer moet word. Ter gelegener tyd sal R-134a, met ‘n GVP = 1300, bes moontlik uitgeskakel word ten gunste van natuurvriendelike vloeiers met ‘n lae GVP. Een van laasgenoemde aanspraak makers is koolsuurgas, R-744, met ‘n GVP = 1.

Dit volg uit die literatuur dat verskeie Nusseltgetal-korrelasies (*Nu*-korrelasies)ontwikkel is wat die konveksie hitte oordrag koeffisiënte, van superkritiese R-744 onder verkoeling, kan voorspel. Geen bewyse kon egter gevind word dat enige van hierdie voorgestelde korrelasies die Nusseltgetalle (Nu^s) en die daaropvolgende konveksie hitte oordrag koeffisiënte, van superkritiese R-744 onder verkoeling, akkuraat kan voorspel nie.

Alhoewel daar verskeie *Nu*-korrelasies bestaan, is slegs agt verskillende korrelasies gekies en deur middel van ’n teoretise simulasie program, in die eerste gedeelte van hierdie studie, met mekaar vergelyk. Hierdie program simmuleer ’n water-tot-transkritiese R-744 buis-in-buis hitte uitruier. Alhoewel die verkreë resultate die belangrikheid van die soeke na ‘n meer bruikbare *Nu*-korrelasie, vir superkritiese R-744 beklemtoon, kon daar egter geen gevolgtrekkings gemaak word ten opsigte van die akkuraatheid van die korrelasies wat vir die simmulasie program gebruik is nie.

In die tweede gedeelte van hierdie studie was eksperimentele data uit die literatuur aangewend om die akkuraatheid van die onderskeie korrelasies te evalueer. Konveksie hitte oordrag koeffisiënte, temperature, drukke en buis deursnee is aangewend vir die berekening van die eksperimentele Nusseltgetalle (Nu_{exp}). Teoretiese Nu^s en Nu_{exp} is grafies, by verskillende drukke, uitgeteken teenoor die lengte van die hitte uitruiler. Daar is waargeneem dat Nu_{exp} en *Nu* progressief verhoog tot by ’n maksimale waarde, en dat dit dan verminder namate de pyplengte toeneem. Die $Nu_{exp}{}^s$ en die teoretiese Nu^s is met mekaar vergelyk. Hierdie resultate het die moontlikheid gebied om die korrelasies volgens die algemene patrone van hul *Nu* variasies oor die pyplengte te groepeer

Grafieke van Nu_{exp} teenoor Nu^s, wat deurmiddel van die Gnielinski-korrelasie bereken is, het oor die algemeen lineêre regressies met, $R^2 > 0.9$, gelewer vir temperature groter of gelyk aan die pseudokritiese temperatuur. Uit hierdie data is ‘n nuwe korrelasie, *Korrelasie I*, gebaseer op gemiddelde hellings en snypunte saamgestel. Die Gnielinski-korrelasie, saam met ’n veranderde

Haaland-wrywingsfaktor, het aanleiding gegee tot die formulering van ‘n tweede korrelasie, naamlik *Korrelasie II*. ’n Derde, en meer gevorderde korrelasie, *Korrelasie III*, is saamgestel deur die gebruikmaking van grafieke waarin hellings en y-assnypunte teenoor druk uitgeteken is. Uit hierdie data is ’n nuwe parameter, naamlik die draaipunt-drukverhouding van superkritiese R-744 onder verkoeling, gedefinieer.

Daar is tot die gevolgtrekking gekom dat die aangewende *Nu*-korrelasies oor die algemeen te lae *Nu*-waardes voorspel (met ‘n minimum van 0.3% teenoor ‘n maksimum van 81.6%). Twee van die korrelasies het egter te hoë *Nu*-waardes by langer pyplengtes voorspel. Laasgenoemde geskied wanneer die temperatuur benede die pseudokritiese temperatuur daal. Daar is ook tot die gevolgtrekking gekom dat *Korrelasie III* akkurater is as beide *Korrelasies I* en *II*, asook die gepubliseerde korrelasies wat in hierdie studie gebruik is. *Korrelasie III-Nu* vir die verkoeling van R-744 is waarskynlik slegs geldig vir ‘n buisdiameter in die orde van die eksperimentele waarde van 7.73 mm, temperature gelyk aan of hoër as die pseudokritiese temperature en by die bepaalde drukke van 7.5 tot 8.8 MPa wat gebruik is.

Sleutelwoorde

Konveksie hitte oordrag koeffisiënt.
Nuwe korrelasie.
Nusseltgetal.
Pseudokrities.
Superkrities.

Acknowledgements

The author of this thesis is very grateful and would like to thank:

- my supervisor, Dr. Martin van Eldik, for his insight, enthusiasm, time and support which inspired me until the very end of this study;
- my father, Prof. Daan Venter for his enthusiasm, time, support, encouragement and invaluable technical assistance throughout my study;
- the rest of my family, my mother Sylvia Venter for all her love and prayers, my brother and sisters, Danro, Nadia, and especially Brianda, for their love and support; and
- my financial sponsors, Dr. Martin van Eldik and the NRF, who made it possible for me to study fulltime.

My Father who art in heaven, hallowed be thy Name. In humbleness I thank thee my Lord for never-ending grace and mercy.

Table of Contents

Nomenclature

c_p	Specific heat capacity at constant pressure	J/kg-K
$c_{p,b}$	c_p at the bulk temperature	J/kg-K
$c_{p,w}$	c_p at the wall temperature	J/kg-K
ε	Relative tube roughness	m
f	Friction factor	Dimensionless
f_{mH}	Modified Haaland friction factor	Dimensionless
f_w	Friction factor at the wall	Dimensionless
g	Gravitational acceleration constant	m/s^2
h	Enthalpy	J/kg
h_b	Enthalpy at the bulk	J/kg
h_c	Convection heat transfer coefficient	W/m^2-K
h_e	Enthalpy at the outlet	J/kg
h_i	Enthalpy at the inlet	J/kg
h_w	Enthalpy at the wall	J/kg
k	Conduction heat transfer coefficient	W/m-K
$\dot{m}$	Mass flow rate	kg/s
$\dot{m}_e$	Mass flow rate at outlet	kg/s
$\dot{m}_i$	Mass flow rate at inlet	kg/s
p	Pressure	Pa or bar
p_e	Pressure at outlet	Pa or bar
p_i	Pressure at inlet	Pa or bar
q	Heat flux	W/m^2
q_w	Heat flux at the wall	W/m^2
u	Internal energy	J/kg
t	Time	s
z	Elevation height	m
z_e	Elevation height at outlet	m
z_i	Elevation height at inlet	m
A	Area	m^2
A_f	Fin area	m^2
A_{ff}	Face flow area	m^2

D_H	Hydraulic diameter	m
D_{ii}	Inner diameter of the inner tube	m
$D_{i,o}$	Outer diameter of the inner tube	m
$D_{o,i}$	Inner diameter of the outer tube	m
D_t,	Pipe thickness	m
G	Mass flux	kg/s-m^2
K	Absolute temperature	ºK
L	Length	m
Nu	Nusselt number	Dimensionless
Nu^s	Nusselt numbers	Dimensionless
Nu_{DB}	Nusselt number *via* the Dittus-Boelter correlation	Dimensionless
Nu_{exp}	Experimental Nusselt number	Dimensionless
$Nu_{exp}^{\ s}$	Experimental Nusselt numbers	Dimensionless
Nu_F	Nusselt number *via* the Fang correlation	Dimensionless
Nu_G	Nusselt number *via* the Gnielinski correlation	Dimensionless
Nu_{GH}	*Nu via* the Gnielinski correlation with the Haaland friction factor	Dimensionless
$Nu_{G,M}$	Nusselt number *via* the Modified Gnielinski correlation	Dimensionless
Nu_H	Nusselt number *via* the Huai correlation	Dimensionless
Nu_{KKP}	*Nu via* the Krasnoshchekov-Kuraeva-Protopopov correlation	Dimensionless
Nu_P	Nusselt number *via* the Pitla correlation	Dimensionless
Nu_{PK}	Nusselt number *via* the Petukhov-Kirillov correlation	Dimensionless
Nu_{PP}	Nusselt number *via* the Petrov-Popov correlation	Dimensionless
Nu_{SP}	Nusselt number *via* the Son-Park correlation	Dimensionless
Nu_Y	Nusselt number *via* the Yoon correlation	Dimensionless
Nu_b	Nusselt number at the bulk	Dimensionless
Nu_w	Nusselt number at the wall	Dimensionless
Pr	Prandtl number	Dimensionless
Pr_b	Prandtl number at the bulk	Dimensionless
Pr_w	Prandtl number at the wall	Dimensionless
P_w	Wetted perimeter	m
$\dot{Q}$	Heat transfer rate	W
Re	Reynolds number	Dimensionless
Re_b	Reynolds number at the bulk	Dimensionless
Re_w	Reynolds number at the wall	Dimensionless

$R''_{f,p}$	Surface foulness factor for the primary stream	Dimensionless
$R''_{f,s}$	Surface foulness factor for the secondary stream	Dimensionless
R_w	Thermal wall resistance	K/W
T	Temperature	ºC
T_b	Temperature at the bulk	ºC
$T_{b,in}$	Inlet bulk temperature	ºC
$T_{b,out}$	Outlet bulk temperature	ºC
T_e	Temperature at the outlet	ºC
T_i	Temperature at the inlet	ºC
T_{lm}	Temperature *via* log mean temperature difference method	ºC
T_{pc}	Pseudocritical temperature	ºC
$T_{p,e}$	Outlet temperature of the primary stream	ºC
$T_{p,i}$	Inlet temperature of the primary stream	ºC
$T_{s,e}$	Outlet temperature of the secondary stream	ºC
$T_{s,i}$	Inlet temperature of the secondary stream	ºC
T_w	Temperature at the wall	ºC
UA	Overall heat transfer coefficient	W/K
V	Velocity	m/s
$\dot{W}$	Rate of work transfer	W

Greek symbols

μ	Viscosity	Ns/m^2
ρ	Density	kg/m^3
ρ_b	Density at the bulk	kg/m^3
ρ_{pc}	Density at the pseudocritical temperature	kg/m^3
ρ_w	Density at the wall	kg/m^3
η_o	Overall surface efficiency	Dimensionless
η_f	Fin efficiency	Dimensionless
Δp_L	Pressure loss over the length	Pa or bar
ΔT_{lm}	Difference in T_{lm}	ºC

List of Figures

Chapter 1

Chapter 2

Chapter 3

Chapter 4

Chapter 5

List of Tables

Chapter 2

Chapter 3

Chapter 5

CHAPTER

Introduction 1

1.1. History and problem statement

During the 19th century scientists started to grasp the fundamentals of thermodynamics. These understandings led to the rise of refrigeration systems, as it is known today.

A vapour-compression refrigeration system was first patented by Jacob Perkins during 1834 (Pearson, 2005). This was a closed refrigeration cycle using ethyl ether as the refrigerant. The patent included a compressor, condenser, expansion valve and an evaporator. All four of these basic units are still used in modern vapour-compression cycles. Ongoing research, following this patent, was directed in finding the best possible refrigerant.

According to Pearson (2005) ethyl ether was a few years later dismissed as a refrigerant and already during Perkins' time, ammonia, sulphur dioxide and carbon dioxide were available to be used as refrigerants. However, due to complex compressors needed, air and water were rather used as refrigerants. In 1872 David Boyle was the first to design and build an ammonia compressor for a refrigeration system (Pearson, 2005). Ammonia may be seen as the almost perfect refrigerant, but it has one major disadvantage; it is highly toxic. Due to this disadvantage, the less toxic refrigerants have always been opted for in refrigeration systems.

The first carbon dioxide refrigeration system was designed in 1862 by Thaddeus Lowe (Pearson, 2005). The refrigeration system used a compressor, but unfortunately this system was problematic due to the unavailability of high pressure system components needed when using carbon dioxide as refrigerant. During the later half of the 19th century, methyl chloride (CH_3Cl), the predecessor of halocarbon refrigerants, came to the scene as the new refrigerant. Methyl chloride is odourless, but also toxic and flammable, therefore it is considered to be a very dangerous refrigerant (Pearson, 2005).

The search for better performing refrigerants continued during the 20th century. Thomas Midgeley (Pearson, 2005) was assigned the task to find a refrigerant with the following qualities:

- Stable.
- Non-toxic.
- Non-flammable.
- Miscible with lubricating oil.
- Operating above atmospheric pressure.
- Good insulator towards electricity.
- Low compression index, in order for the compressor to function at low temperatures.
- Operation pressures correlating to those of ammonia, methyl chloride and propane.

Midgeley alleged that halocarbons could possibly be stable refrigerants and dichlorodifluoromethane (CCl_2F_2), more commonly known as R-12, resulted from his research. Midgeley's choice was an excellent one and it was the beginning of the halocarbon refrigerant era. After the discovery of the refrigerant R-12, a number of new CFC (chlorofluorocarbons) and HCFC (hydro chlorofluorocarbons) refrigerants, namely R-22 ($CHClF_2$), R-115 ($CClF_2{\cdot}CF_3$) and R-502 (an azeotropic mixture of R-22 and R-115), were introduced (Pearson, 2005).

In 1985, the discovery of a dwindling ozone layer over Antarctica marked the beginning of the end for the CFC and HCFC refrigerants. It was suspected that these refrigerants are a possible cause for the ozone depletion. After the Montreal Protocol in 1987, the use of these refrigerants was systematically being phased out. This gave rise to the new refrigerant R-134a ($CH_2F{\cdot}CF_3$). Although R-134a does not perform as well as R-22, it is, however, a non-ozone depleting refrigerant (Pearson, 2005).

During the past decade research has shown that global warming may have disastrous effects on our planet. In order to limit the damage that the human race seems to be causing, it was acknowledged that substances with a high global warming potential (GWP) should be phased out. In due time, R-134a with a GWP = 1300, may probably be phased out to make way for refrigerants with a lower GWP. One of these contenders is carbon dioxide, R-744, with a GWP = 1.

1.2. Focus of this study

This study will focus on the simulation of R-744 as refrigerant for heating purposes, namely water heating. It was reported by both Nekså and co-workers (1999) and White and co-workers (2002), that transcritical R-744 cycles may be employed to deliver water at 90 °C for industrial

purposes. Currently, direct electrical heating is used in applications where water is required above 60°C, as this is typically the limit of current heat pumps. If a heat pump cycle capable of heating water above 70 °C could be designed and manufactured for industrial purposes, it should have a substantial impact on reducing energy consumption.

The prediction of the functionality of a heat pump cycle depends on accurate simulation processes. Without an accurate simulation process, it may be difficult to design a system that operates at maximum efficiency. Part of the simulation process of a heat pump cycle is the simulation of two heat exchangers, namely the condenser and the evaporator. For accurate simulation of a heat exchanger, the convection heat transfer coefficients must be accurately simulated. The convection heat transfer coefficient is determined *via* knowledge of the Nusselt number, whereas the Nusselt number is calculated *via* a suitable empirical correlation. Cheng and co-workers (2008) reported that there exist a number of supercritical R-744 Nusselt number correlations for the prediction of the heat transfer coefficient, but not enough data are available to verify which Nusselt number correlation is the most suitable to use.

An R-744 transcritical heat pump cycle does not consist of a condenser, but rather a gas cooler. In this study a water-to-R-744 tube-in-tube heat exchanger (gas cooler) will be simulated by implementing the various Nusselt number correlations reported by Cheng and co-workers (2008).

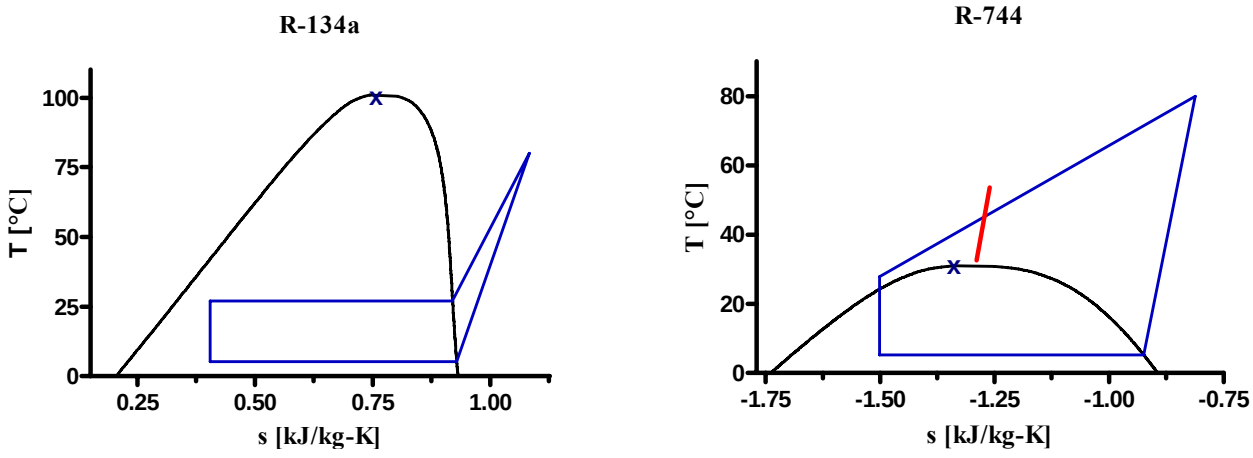

Figure 1.1. Representation of a vapour compression heat pump cycle for R-134a and R-744 respectively. The respective critical points (*i.e.* when T = critical T and p = critical pressure) of the fluids is indicated by X. The red line represents the pseudocritical temperature of R-744 over a range of pressures.

Figure 1.1 illustrate some of the terms used in this study. Data points were arbitrarily chosen to represent a typical R-134a and an R-744 vapour compression heat pump cycle. For R-134a, the

saturated vapour exiting the evaporator is compressed into a superheated vapour, whereas the R-744 is compressed into the supercritical phase. The supercritical phase exists when the temperature and pressure of a fluid are above the respective critical temperature and pressure of the fluid (point "X" in Figure 1.1 represents the critical point, *i.e*. the point where a fluid is at critical temperature and pressure).

The red line, at the top of the R-744 cycle, represents the pseudocritical temperature of R-744 over a range of pressures. The pseudocritical temperature may be defined as the temperature where the specific heat capacity at constant pressure is a maximum, for a constant pressure line.

A cycle as depicted in Figure 1.1 for R-744, is known as a transcritical cycle.

1.3. Aims of this study

The aims of this study are the following:

- Theoretical investigation of a selected number of Nusselt number correlations used for cooling of R-744 in turbulent flow at supercritical conditions.
- Compare theoretically obtained Nusselt numbers, of turbulent supercritical R-744 in cooling, to published experimental Nusselt numbers.
- Development of a new Nusselt number correlation, for cooling of turbulent supercritical R-744, by utilising experimental data published by Yoon and co-workers (2003). The newly proposed correlation should be an improvement on existing correlations.

1.4. Method of investigation

A theoretical simulation program for R-744 will be presented in Chapter 4. The program will simulate a water-to-transcritical R-744 tube-in-tube heat exchanger[1]. The program code EES (Engineering Equation Solver) will be employed for the simulation process. Various Nusselt number correlations will be implemented, and the different simulation outcomes will be compared. However, the theoretical simulated Nusselt numbers will not be compared to experimental Nusselt numbers; so that no conclusion will be drawn regarding the accuracy of any of the correlations used in Chapter 4.

In Chapter 5 experimental Nusselt numbers obtained from Yoon and co-workers (2003) will be compared to theoretical Nusselt numbers. No simulation program will be developed. Yoon and co-workers (2003) provided adequate information for the calculation of all the required

[1] In this study a water-to-transcritical R-744 heat exchanger refers to a counter-flow heat exchanger for a transcritical cycle, with water and supercritical R-744 as fluids.

theoretical Nusselt numbers. It is important to note that these Nusselt numbers will be calculated[2], and not computed[3]. The theoretical Nusselt numbers will be compared to the experimental Nusselt numbers. The Gnielinski Nusselt number correlation will be used as basis for presenting a new Nusselt number correlation for the cooling of turbulent supercritical R-744.

[2] Results directly obtained, *i.e.* exact values, through applicable equations.
[3] Results obtained through an iterative process. Results are not necessarily exact and the accuracy of these values may be dependant on the number of iterations and/or the size of the chosen roster.

CHAPTER

Literature survey 2

A brief overview on the history of refrigerants was given in Chapter 1. It was mentioned that since the implementation of refrigerants commenced, there has been a continuous search for more suitable working fluids. This chapter will concentrate on the available literature concerning supercritical carbon dioxide as a working fluid for heating purposes, thermodynamic properties of R-744 and correlations that may be applied to R-744.

2.1. R-744 employed for heating purposes

A prototype heat pump water heater was constructed by Nekså and co-workers (1998), using R-744 as refrigerant. Water was heated from 10 to 60 °C. The system was reported to have a COP of 4.3 at an evaporation temperature of 0 °C. The mass flow rate of the water was reduced to deliver water at 80 °C with a COP of 3.6. Nekså and co-workers (1998) claimed that the heating of water to a temperature of 60 °C, using an R-744 heat pump water heater, can reduce the energy consumption by 75% when compared to electrical and gas fired water heater systems. The high process efficiency for an R-744 heat pump water heater, using R-744, was ascribed to good heat transfer characteristics and efficient compression. According to Nekså and co-workers (1999), an efficient compression may be achieved when an R-744 system operates near the critical pressure of R-744. It was also claimed that an R-744 heat pump water heater, without any operational problems and only a small loss in efficiency, may be constructed to deliver water with a temperature of up to 90 °C.

White and co-workers (2002) also constructed a prototype transcritical R-744 heat pump system. The performance of this system was measured under operating conditions, when the compressor was operating at full speed. It was found that when heating water to 90 °C, the prototype system was able to reach an optimum heating COP of almost 3. The authors of the article claimed that an optimum heating COP of 2.46 may be obtained if water was to be heated to 120 °C *via* the prototype system (White *et al.*, 2002).

Due to the high volumetric capacity of R-744, compact compressors can be designed even when the system operates at extremely high working pressures. The volumetric capacity of R-744 relative to the alternative refrigerants in use, are in ratio, 5 to 10 times larger (Dorin, 1999). The high volumetric efficiency of R-744 gives rise to small flow areas. In combination with good heat transfer characteristics, this may result in an opportunity to manufacture cost efficient and compact heat pump systems (Nekså *et al.*, 1999).

Bredesen and co-workers (1997a; 1997b) argued that supercritical R-744 consists of good heat transfer characteristics and together with the high volumetric capacity, efficiently compact heat exchangers may be designed and produced for an R-744 refrigerant cycle.

2.2. Thermodynamic properties of the supercritical state

The most prominent property of a fluid above the critical point is the absence of a two phase flow. Above the critical point there are very distinct variations in the thermodynamic and transport properties of R-744 as the temperature and pressure varies. Andresen, (2007) stated that a fluid at supercritical pressure experiences significant thermodynamic property fluctuations when the transition temperature is approached. Furthermore, a fluid is considered to behave as a liquid for temperatures beneath the transition temperature and behaves like a gas for temperatures greater than the transition temperature. Every pressure has a unique transition temperature (Andresen, 2007).

When supercritical R-744, near the critical point, undergoes an increase in temperature, then a sudden reduction in density, thermal conductivity and viscosity may take place (Aldana *et al.*, 2002). The authors of this article argued that the thermo-physical properties of the supercritical R-744 transform from 'liquid-like' to 'gas-like' values and referred to this region as the so-called pseudocritical region. It was further stated that the specific heat at constant pressure, c_p, will approach, by definition, infinity at the critical point. Aldana and co-workers (2002) defined the pseudocritical temperature as follows: it is the temperature at a constant pressure line where the c_p value experiences a maximum value.

In Figures 2.1 to 2.4[4] the fluctuations in specific heat at constant pressure c_p[5], density ρ, thermal conductivity k and the viscosity μ can be seen as R-744 passes through the transition temperature. Figure 2.1 clearly shows a spike in c_p, *i.e.* when R-744 transforms from a liquid-like to a gas-like state over the transition point. The temperature corresponding to the maximum

[4] All the graphs values were obtained from EES at the chosen pressures.
[5] The specific heat at constant pressure, c_p, represents the energy required to increase the temperature of a fluid by a specific quantity.

c_p, for every pressure, is referred to as the pseudocritical temperature, T_{pc}. As the pressure line approaches the critical pressure of 73.8 bar, the more volatile the values become (Andresen, 2007).

It can also be seen in Figure 2.1 that as the pressure increases above the critical pressure, c_p decreases in magnitude, whereas T_{pc} rises. For supercritical flow, the transition between the liquid-like and gas-like stage occurs over a small temperature interval, resulting in a high c_p (Andresen, 2007). The variation in thermodynamic properties at the transition temperature

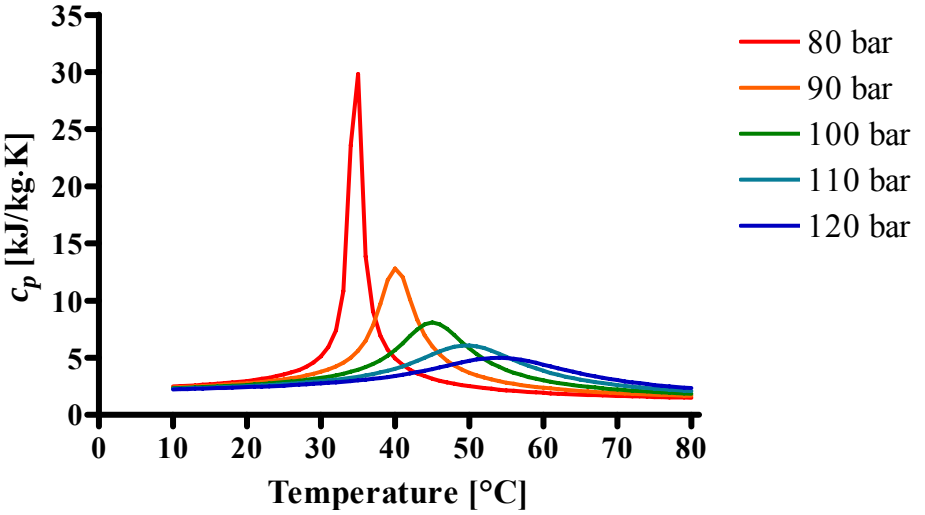

Figure 2.1. Specific heat over constant pressure, c_p, is plotted against the temperature for various constant pressure lines. The temperature corresponding to the maximum c_p, of a constant pressure line, is referred to as the pseudocritical temperature for that specific pressure.

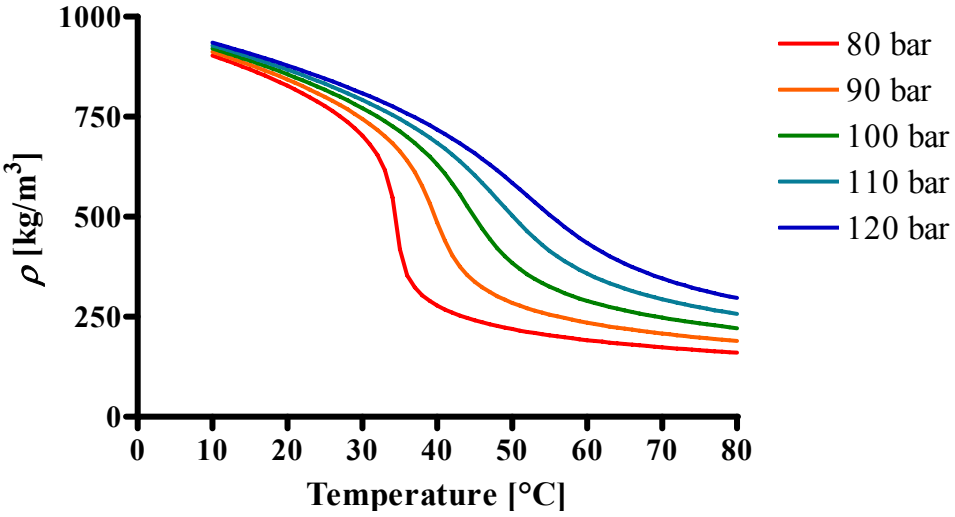

Figure 2.2. Density, ρ, is plotted against the temperature for various constant pressure lines.

result in a spike in the convection heat transfer coefficient close to the transition point. In Figure 2.2 it can be seen that the density drops quite substantially when R-744 is heated over the transition temperature. Lower densities result in higher velocities (momentum conservation), which in turn results in higher pressure drops (Andresen, 2007).

Numerous experimental and theoretical studies during the past five decades (Bruch *et al.*, 2009) have been carried out on supercritical fluids, in an attempt to acquire the design requirements for industrial heat pump systems. The fluids mainly used for these studies were water, helium, hydrogen or carbon dioxide (Bruch *et al.*, 2009). Several researchers (Pethukov, 1970;

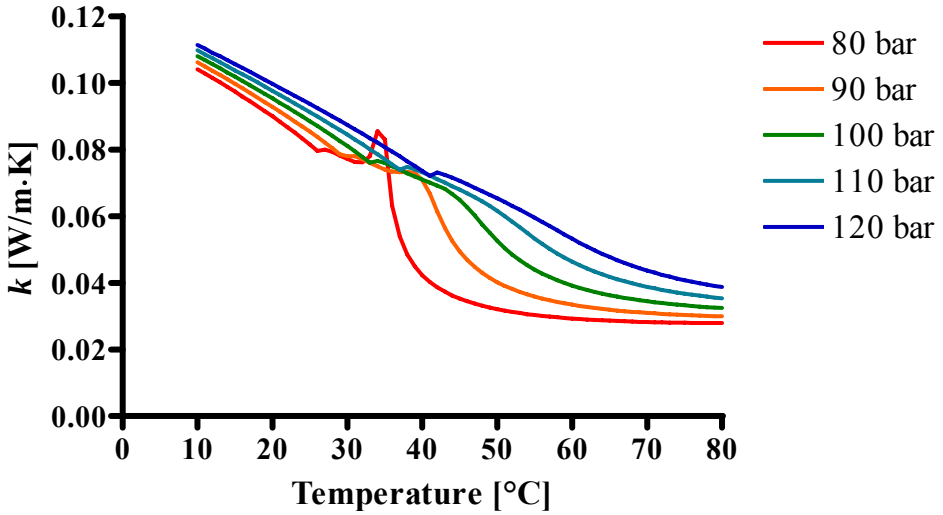

Figure 2.3. Conduction heat transfer coefficient, *k*, is plotted against the temperature for various constant pressure lines.

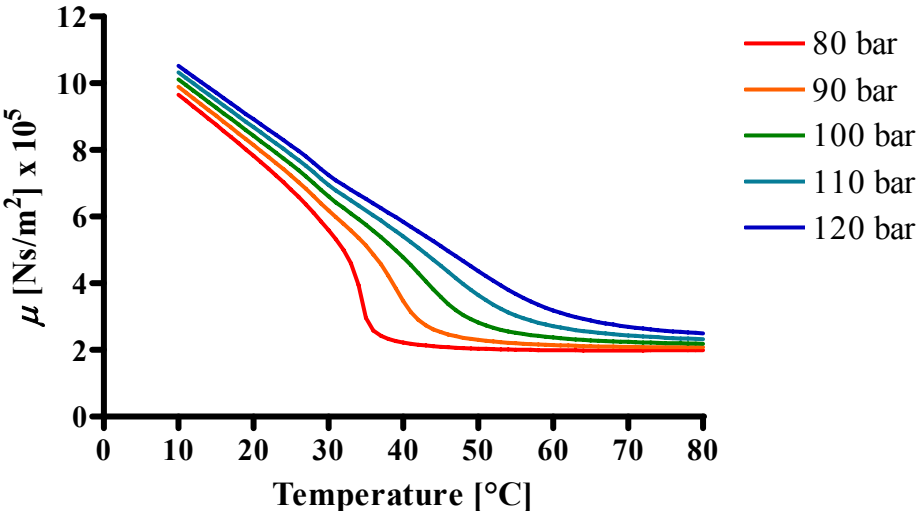

Figure 2.4. Viscosity, μ, is plotted against the temperature for various constant pressure lines.

(Jackson & Hall, 1979) investigated heat transfer coefficients under heating for supercritical fluid flows. These researchers came to the conclusion that heat flux and flow direction have a great impact on the supercritical heat transfer coefficient. Mixed convection is a general phenomenon for supercritical fluid flows, and this can be attributed to the huge fluctuations of thermo-physical properties of the fluid over a small temperature difference (Bruch *et al.*, 2009). It was observed, that a reduction in the heat transfer coefficient take place as the buoyancy forces increases, when a turbulent fluid is flowing vertical upwards (Jackson & Hall, 1979; Aicher & Martin, 1997). The explanation forwarded for this finding was that it may be attributed to an alteration in the velocity profile by means of Archimedes forces, which in turn reduces the turbulence flow of the fluid. Alternatively, for downward vertical fluid flow, the heat transfer coefficient increases due to free convection that is taking place (Bruch *et al.*, 2009). It was suggested by Aicher and Martin (1997) that when mixed convection is taking place, it will be irrelevant whether cooling or heating is taking place. Unfortunately, no thorough study exists to confirm this speculation.

2.3. Supercritical R-744 *Nu* correlations

The accuracy of recognized heat transfer correlations have been investigated for a range of geometries, by the mainstream of supercritical and pseudocritical researchers (Aldana *et al.*, 2002). Petukhov and co-workers (1961) produced a supercritical heat transfer R-744 correlation that unfortunately did not account for variations in temperature in the thermo-physical properties. Gnielinski (1976), however, modified this correlation for constant thermo-physical properties. According to Olsen and Allen (1998) this newly modified correlation from Gnielinski may be seen as the most accurate constant property correlation for in-tube heat transfer.

When a fluid possesses a bulk temperature above the critical temperature with the wall temperature below the critical temperature, an improvement in the convection heat transfer coefficient was found (Shitsman, 1963; Krasnoshchekov *et al.*, 1969; Tanaka *et al.*, 1971). Krasnoshchekov and co-workers (1969) argued that near the wall of the tube a liquid-like layer forms, resulting in higher convection heat transfer coefficients. The authors of this article further reported that the thermal conductivity found at the liquid-like layer is greater than that of the bulk fluid, resulting in higher convection heat transfer coefficients. It was further reported that a gas-like layer may exist near the wall of the tube when the fluid is in heating, resulting in lower convection heat transfer coefficients. The lower convection heat transfer coefficients may be the result of a lower thermal conductivity found at the gas-like layer, as compared to the bulk of the fluid.

Various researchers have stated that property corrections need to be introduced in Nusselt number correlations to compensate for the considerable large variations of thermodynamic properties found near the critical region (Mitra, 2005; Andresen, 2007). In most of the previous studies emphases was laid on supercritical heating experiments, with the bulk temperature of the fluid below the inner wall temperature (Mitra, 2005; Andresen, 2007). Higher wall temperatures result in lower thermal conductivities and viscosities. For supercritical cooling, the wall temperatures are lower than the fluid bulk temperatures, resulting in higher thermal conductivities and viscosities. It was also reported that the bulk-to-wall temperature difference is expected to exert a great influence on frictional pressure drops and the convection heat transfer coefficients. Andresen (2007) eventually came to the conclusion that supercritical heating correlations will not be adequate for supercritical cooling correlation predictions.

Kurganov (1998a; 1998b) conducted a study on the heating of supercritical R-744. Three intervals were defined to classify the state of R-744 in heating, namely, liquid-like, pseudo-phase transition and gas-like states. Nusselt number and pressure drop correlations were published for all three states.

The cooling process of supercritical R-744 has not received as much attention as the counterpart, namely, the heating process. The relative slow rate at which research is conducted on the cooling process may be ascribed to the unavailability of adequate equipment (Bruch *et al.*, 2009). A study on horizontal flowing supercritical cooling of R-744 was conducted by Bruch and co-workers (2009). All the experiments showed that the maximum heat transfer coefficient will be reached in a small interval around the pseudocritical temperature.

Despite intensive research programs, where emphasis was laid on the thermal-hydraulic behaviour off fluids, a total understanding of the fundamental phenomena in mass and energy transfers in supercritical fluids are still lacking (Bruch *et al.*, 2009).

Existing empirical correlations were compared by Ghajar and Asadi (1986) for determining R-744 convection heat transfer coefficients near the critical point. Ghajar and Asadi reported the following inconsistencies that were found in the literature:

- Thermodynamic property values differed between the researchers.
- Property variations.
- Heat flux and buoyancy effects.

Ghajar and Asadi (1986) published a new Nusselt number correlation, using the Dittus-Boelter correlation as foundation, as well as the criteria reported by Jackson and Fewster (1975).

An in depth literature survey was carried out by Pitla and co-workers (1998) on supercritical R-744 convection heat transfer and pressure drop coefficients. Emphasis was laid on thermo-physical properties including friction factors, heating and cooling convection heat transfer coefficients, *i.e.* Nusselt number correlations, factors influencing *Nu* and heat transfer calculation at supercritical pressures through numerical methods.

To predict the heat transfer coefficient of a fluid Pitla and co-workers (2002) presented a new correlation that may be employed to calculate Nusselt numbers (Nu^s) for supercritical R-744 in cooling. This correlation is based on Pitla's experimental data together with published data reported in the literature. Bulk and wall temperatures of any supercritical fluid may vary, and thus result in a varying heat transfer of the fluid (Pitla *et al.*, 2002). A steep upward spike in the heat transfer was noted when the R-744 thermodynamic properties were approaching the pseudocritical region. Bulk and wall Nu^s, as predicted by the Gnielinski correlation, were used by these authors in an attempt to develop an equation that may be employed to calculate the mean *Nu*. It was claimed that the new correlation is accurate within a range of 20% for up to 85% of the calculated values. This new correlation of Pitla and co-workers (2002) displayed an increased accuracy for *Nu* prediction when it was compared with three known *Nu* correlations, *i.e.* namely the Krasnoshchekov Kuraeva Protopopov correlation (Krasnoshchekov *et al.*, 1969), the Baskov Kuraeva Protopopov correlation (Baskov *et al.*, 1977) and the Gnielinski correlation (Gnielinski, 1976).

The Gnielinski correlation was manipulated by Dang and Hihara (2004). This new correlation is based on other existing correlations and experimental data obtained of cooling supercritical R-744 flowing in a tube. Four different horizontal tubes, varying in sizes from 1 to 6 mm were used. The parameters heat flux, mass flux, pressure and tube diameter were investigated, in an attempt to uncover to what extend each of these parameters affect the *Nu*, as well as the pressure drop. Dang and Hihara (2004) came to the following conclusions:

- The heat transfer coefficient and pressure drop correlate with the mass flux, thus, the increase or decrease in mass flux corresponds to the increase or decrease in the heat transfer coefficient and pressure drop.
- Pressure is influenced along the flow direction as the thermodynamic properties differ, whereas, the decline in pressure appears to be independent of the inlet pressure at sub pseudocritical temperatures. For temperatures above the pseudocritical temperature, it was found that a decrease in the pressure drop occurred as the pressure increased.

- It was claimed that the newly improved *Nu* correlation, based on the Gnielinski correlation, is accurate to within 20% of the experimental data used in the study.

Son and Park (2006) measured convection heat transfer coefficients and pressure drops of supercritical R-744 in cooling. The authors of this article came to the following conclusions:

- When entering the gas cooler, R-744 experiences a slow increase in the convection heat transfer coefficient and a decrease at the gas cooler exit. The authors reported that the specific heat of R-744 is a maximum near the pseudocritical temperature and argued that the convection heat transfer coefficient will peak when the temperature is equal to T_{pc}.
- As the gas cooler inlet pressure increases, supercritical R-744 in cooling has a lower pressure drop. The authors of the article ascribed this phenomenon to the density variation of R-744 in the supercritical region. It was also reported that according to measured data, the Blasius correlation accurately predicts the pressure drop of supercritical R-744 in cooling.
- The authors compared the measured convection heat transfer data with existing correlations as proposed by Baskov and co-workers (1977), Bringer and Smith (1957), Ghajar and Asadi (1986), Gnielinski (1976), Krasnoshchekov and co-workers (1969), Krasnoshchekov and Protopopov (1966), Petrov and Popov (1985), Petukhov and co-workers (1961) and Pitla and co-workers (1998). Son and Park (2006) reported that the Bringer and Smith correlation was the most accurate of the correlations in predicting the convection heat transfer coefficients.

A new correlation was proposed by the authors of the article, claiming that the new correlation was more accurate than any of the correlations used in the study. The newly proposed correlation included density and a specific heat ratio determined from average bulk and wall temperatures.

Liao and Zhao (2002) investigated self obtained convection heat transfer coefficients, for cooling of supercritical R-744. Six different 'mini/macro' tube diameters were used (0.50 mm, 0.70 mm, 1.10 mm, 1.40 mm, 1,55 mm and 2.16 mm). The pressure of the supercritical R-744 ranged from 74 to 120 bar with the temperature varying from 20 to 110°C. The authors of this article reported that even though the R-744 was in 'forced motion' throughout the tubes, the buoyancy effect should be taken into account. This conclusion was based on the founding that the Nusselt numbers decreased when the tube diameter was reduced. It was also reported that the buoyancy effect reduced as the tube diameter reduced in size, since the buoyancy parameter is per definition proportional to the tube diameter. Liao and Zhao (2002) claimed that the experimental

results showed that existing correlations as developed in previous studies, where experimental results were obtained, deviate substantially between large and 'mini/macro' tubes. A new Nusselt number correlation for supercritical R-744 in cooling, with dimensionless forced convection parameters, was presented by the authors. It was claimed that the published results are of great importance for a gas cooler design of a transcritical R-744 refrigeration system (Liao and Zhao, 2002).

Yoon and co-workers (2003) reported experimental data that contain heat transfer and pressure drop characteristics of cooling supercritical R-744 flow in a horizontal tube. Different mass fluxes and inlet pressures were used for R-744, whilst a variable speed gear pump was used for controlling the mass flux. The inlet pressures varied from 7.5 MPa to 8.8 MPa. The obtained experimental data was employed to investigate the accuracy of known correlations used for predicting the heat transfer coefficients and pressure drop of supercritical R-744 in cooling. Yoon and co-workers (2003) found that the following occurred during the process of supercritical cooling of R-744:

- The heat transfer coefficient rises to a maximal value and then decreases.
- The maximal heat transfer coefficient value is found nearby the pseudocritical temperature.
- Increasing the pressure resulted in a decreased maximal value of the heat transfer coefficient.
- A mass flux increase resulted in a heat transfer coefficient increase for all the pressures.
- Existing *Nu* correlations in most cases tend to under predict supercritical R-744, which directly result in an under prediction of the heat transfer coefficient.
- The Blasius correlation accurately predicts the pressure drop for cooling supercritical R-744.

A new *Nu* correlation based on the Dittus-Boelter correlation was also introduced by Yoon and co-workers (2003). Most of the newly predicted Nu^s came within a 20% deviation of the experimental data and exhibited an average deviation of 12.7% between the data.

A comprehensive study was carried out by Cheng and co-workers (2008) on heat transfer coefficient and pressure drop correlations of cooling supercritical R-744 in macro- and micro-channels. An investigation was launched into experimental studies on heat transfer coefficients

and the pressure drop of supercritical R-744 in cooling. Cheng and co-workers (2008) came to the following conclusions regarding supercritical R-744 in cooling:

- There exist a number of *Nu* correlations for the prediction of the heat transfer coefficient, but not enough data is available to verify which *Nu* correlation is the most suitable to use.
- Further investigation into the heat transfer coefficient is needed over a wide range of test parameters.
- The Blasius correlation is sufficiently accurate in predicting the pressure drop of cooling supercritical R-744. Yoon and co-workers (2003) came to this very same conclusion for predicting the supercritical pressure drop.

2.4. Summary

For supercritical R-744 there exists a pseudocritical temperature for each constant pressure line. Large thermodynamic variations exist in a small region around the pseudoctitical temperature. A gas-like behaviour of R-744 is found when the temperature is greater than the pseudocritical temperature. On the other hand, a liquid-like behaviour is found for R-744 when the temperature is lower than the pseudocritical temperature.

Many of the work on supercritical heat transfer and pressure drop correlations dealt with the heating of supercritical carbon dioxide. Table 2.1 shows a summary of the heat transfer studies reviewed in this study.

There seems to be consensus that the Blasius correlation predicts the pressure drop in cooling of supercritical R-744 with sufficient accuracy. However, further investigation is needed with regard to the heat transfer coefficient.

Table 2.1. Summary of correlations

Authors	Under investigation	Results
Petukhov *et al.* (1961)	Supercritical R-744	Published a new *Nu* correlation, not accounting for variations in temperature in the thermo-physical properties.
Gnielinski (1976)	Supercritical R-744	Modified the correlation published by Petukhov and co-workers (1961).
Kurganov (1998a; 1998b)	Heating of supercritical R-744.	Published *Nu* and pressure drop correlations by defining three interval to classify the state of R-744 in heating, namely, liquid-like, pseudo-phase transition and gas-like states.
Bruch *et al.* (2009)	Vertical flowing, cooling of supercritical R-744	Came to the conclusion that the maximum heat transfer coefficient will be reached in a small interval around the pseudocritical temperature.
Ghajar and Asadi (1986)	R-744 convection heat transfer coefficients near the critical point	Published a new *Nu* correlation, using the Dittus-Boelter correlation as foundation, as well as the criteria reported by Jackson and Fewster (1975).
Pitla *et al.* (2002)	Cooling of supercritical R-744	Bulk and wall Nu^s, as predicted by the Gnielinski correlation, were used to develop an equation that may be employed to calculate the mean *Nu*. It was claimed that the new correlation is accurate within a range of 20% for up to 85% of the calculated values.
Dang and Hihara (2004)	Cooling supercritical R-744 flowing in a tube	Published an improved *Nu* correlation, based on the Gnielinski correlation, and claimed to be accurate within 20% of the experimental data used in their study.
Son and Park (2006)	Supercritical R-744 in cooling	The new correlation, based on the Dittus-Boelter correlation, included density and a specific heat ratio determined from average bulk and wall temperatures.
Liao and Zhao (2002)	Cooling of supercritical R-744	A new Nusselt number correlation for supercritical R-744 in cooling, with dimensionless forced convection parameters, was presented.
Yoon *et al.* (2003)	Cooling of supercritical R-744	A new *Nu* correlation based on the Dittus-Boelter correlation was introduced. Most of the newly predicted Nu^s came within a 20% deviation of the experimental data and exhibited an average deviation of 12.7% between the data. The Blasius correlation accurately predicts the pressure drop for cooling supercritical R-744.
Cheng and co-workers (2008)	Heat transfer coefficient and pressure drop correlations of cooling supercritical R-744 in macro- and micro-channels	There exist a number of *Nu* correlations for the prediction of the heat transfer coefficient, but not enough data are available to verify which *Nu* correlation is the most suitable to use. The Blasius correlation is sufficiently accurate in predicting the pressure drop of cooling supercritical R-744.

CHAPTER

Theoretical background 3

The current chapter presents the theoretical background that is necessary for the successful development and operation of the simulation programs used in this study. A water-to-transcritical R-744 heat exchanger will be simulated in this study and a detailed analysis will be performed on the simulated heat exchanger. Cheng and co-workers (2008) reported that there are currently a number of applicable *Nu* correlations that may be used for the cooling of supercritical R-744, but due to a lack of published data, no conclusions may be drawn as to which of these *Nu* correlations are the most suited for the use of cooling supercritical R-744 (see Chapter 2).

Simulation implies that the characteristics of the system are known and models must be set up to predict its functionality and performance level. For the simulation of a thermal fluid system, the relevant engineering sciences and mathematics are a pre-requisite. The relevant engineering sciences and mathematics include (Rousseau, 2007):

- The laws of conservation of mass, momentum and energy. It is important to know whether the flow in question is compressible or incompressible.
- One should distinguish between laminar and turbulent flow.
- Friction factor correlations for calculating pressure losses.
- The formulation of non-dimensional *Nu*, *Pr* and *Re*.
- The effectiveness of NTU (Number of Transfer Units) and LMTD (Log Mean Temperature Difference) methods for the simulation performance of a heat exchanger.

The generic structure of any simulation model must incorporate the following:

- Conservation laws, *i.e.* mass, momentum and energy.
- Component characteristics, *i.e.* component dimensions, pressure drops and heat transfer rates.

- Fluid properties, *i.e.* gas laws and thermodynamic property tables.
- Boundary values, *i.e.* temperatures and pressures.

3.1. Conservation Laws[6]

Science is a series of logical arguments that evolve from fundamental definitions and assumptions. A science is therefore only as good as the foundation it is build upon. For thermal fluid systems the conservation laws of mass, momentum and energy form part of the foundation of fundamental assumptions. These laws are important for expanding the science of thermal fluid systems and are vital for the simulation of any thermal fluid system model.

3.1.1. Conservation of mass

For the conservation of mass, the following generic equation is valid:

$$V\frac{\partial \rho}{\partial t} + \dot{m}_e - \dot{m}_i = 0 \tag{3.1}$$

where V is the velocity, ρ the density, t the time and $\dot{m}$ [7] the mass flow rate.

If a steady state flow is assumed, no change will take place over time and $\partial\rho/\partial t = 0$. It follows now that under steady state conditions the mass conservation of the flow is given by:

$$\dot{m}_e - \dot{m}_i = 0 \tag{3.2}$$

From Eq (3.2) it follows that the out- and inlet mass flow rates are equal for a steady state and, therefore, only a single symbol, $\dot{m}$, may be used to represent the mass flow rate:

$$\dot{m} = \dot{m}_i = \dot{m}_e \tag{3.3}$$

3.1.2. Conservation of momentum

For the conservation of momentum, the following generic equation is valid for an incompressible flow:

$$\rho L\frac{\partial V}{\partial t} + (p_e - p_i) + \rho g(z_e - z_i) + \Delta p_L = 0 \tag{3.4}$$

where L is the incremental length, p the pressure, g the constant gravitational acceleration, z the elevation height and Δp_L the pressure loss over the length.

---

[6] The discussions in Sections 3.1.1 to 3.5.1 are based on the works of Rousseau (2007), Incropera *et al*. (2006) and Sonntag *et al*. (2003).

[7] In this study the subscripts e and i always denote outlet and inlet, respectively.

If a steady state prevails, then, $\partial V/\partial t = 0$ and the following equation will be valid for the conservation of momentum:

$$(p_e - p_i) + \rho g(z_e - z_i) + \Delta p_L = 0 \tag{3.5}$$

3.1.3. Conservation of energy

For the conservation of energy, the following generic equation is valid:

$$\dot{Q} + \dot{W} = V\frac{\partial(\rho h - p)}{\partial t} + \dot{m}_e h_e - \dot{m}_i h_i + \dot{m}_e g z_e - \dot{m}_i g z_i \tag{3.6}$$

where $\dot{Q}$ is the total rate of heat transfer to the fluid, $\dot{W}$ the total rate of work done on the fluid and h the enthalpy. For steady state conditions $\partial(\rho h - p)/\partial t = 0$. Substitution of Eq (3.3) into this newly obtained equation for steady state, gives:

$$\dot{Q} + \dot{W} = \dot{m}\left(h_e - h_i\right) + \dot{m}g\left(z_e - z_i\right) \tag{3.7}$$

In all heat exchangers thermal energy is transferred from a warm fluid to a cold fluid. During this process no work is done, resulting in $\dot{W} = 0$. In this study it will also be assumed that there is no elevation height difference when simulating a heat exchanger, therefore, $z_e - z_i = 0$. Eq (3.7) now reduces to:

$$\dot{Q} = \dot{m}(h_e - h_i) \tag{3.8}$$

The heat transfer in a fluid between two points may be calculated according to Eq. (3.8).

3.2. Mass flow rate

An overview of the conservation laws was given in Section 3.1. It follows from Eq (3.8) that the mass flow rate is required in order to calculate the heat transfer rate. The mass flow rate is defined by:

$$\dot{m} = \rho V A_{ff} \tag{3.9}$$

where A_{ff} is the face flow area, *i.e.* the area perpendicular to the flow.

The heat exchanger to be used in the transcritical simulation process described in Chapter 5 will be of a tube-in-tube configuration. In this heat exchanger there are thus two face flow areas, namely, one inside the inner tube and the other located between the two tubes, also known as the annulus. The face flow area for the inner tube is defined by:

$$A_{ff} = \frac{1}{4}\pi D_{i,i}^{\ 2} \tag{3.10}$$

where D_{ii} represents the inner diameter of the inner tube.

The face flow area, located in the annulus, is defined by:

$$A_{ff} = \frac{1}{4}\pi (D_{o,i}^{\ 2} - D_{i,o}^{\ 2}) \tag{3.11}$$

where $D_{o,i}$ represents the inner diameter of the outer tube and $D_{i,o}$ the outer diameter of the inner tube.

3.3. Heat transfer rate

In the simulation model for the heat exchanger a number of equations must be employed to calculate the heat transfer at the various positions along the length of the exchanger. Eq (3.8) represent one of these equations, whilst all the other methods will be given in this section.

3.3.1. Heat transfer between bulk temperatures

Eq (3.8) may be used to calculate the heat transfer between two points in a fluid, thus, it may be used to calculate the heat transfer between the bulk temperatures of the same fluid. This same heat transfer rate exists between the bulk and the wall temperatures, the conduction through the tube and the pattern of heat transfer between the fluids.

3.3.2. Heat transfer rate through convection

Heat is transferred from the fluid to the wall *via* convection. The heat transfer rate, in a tube, through convection is given by:

$$\dot{Q} = \pi D L h_c \Delta T \tag{3.12}$$

where h_c is the convection heat transfer coefficient and ΔT the temperature difference between the wall and bulk.

3.3.3. Heat transfer rate through conduction in a tube

The heat transfer rate, through the tube, that is brought about by means of conduction in the radial direction is given by:

$$\dot{Q} = 2\pi L k \frac{\Delta T}{\ln(D_{i,o} / D_{i,i})} \tag{3.13}$$

where k is the conductivity of the tube and ΔT the temperature difference between the outer and inner wall.

Up to this point all the parameters, except the heat transfer coefficient, have been defined. The next section will encompass means to predict the value of the convection heat transfer coefficient, h_c. This coefficient is a function of Nu, which in turn is an empirical correlation.

3.4. Non-dimensional parameters

To calculate the convection heat transfer coefficient, it is firstly necessary to calculate three non-dimensional parameters, namely, Re, Pr and Nu.

3.4.1. The Reynolds number (*Re*)

Non-dimensional Re is a quantity that may be interpreted as the ratio of the inertial forces to the viscous forces in the velocity boundary layer (Rousseau, 2007). Re is defined by:

$$Re = \frac{\rho V L}{\mu} \tag{3.17}$$

Where μ is the viscosity of the fluid.

For the flow in a tube Re may be calculated by:

$$Re = \frac{\rho V D_H}{\mu} \tag{3.18}$$

3.4.2. The Prandtl number (*Pr*)

Non-dimensional Pr is a quantity that may be interpreted as the ratio of the ability to transport momentum *versus* the ability to transport energy through diffusion in both the velocity and thermal boundary layers (Rousseau, 2007). Pr is defined by:

$$Pr = \frac{c_p \mu}{k} \tag{3.19}$$

For laminar flow without secondary flow Nu is a constant and for turbulent flow Nu may be calculated by making use of a suitable empirical derived correlation. Such empirically derived correlations will be discussed in the following section.

3.4.3. The Nusselt number (*Nu*)

Non-dimensional *Nu* provides a measure of the convection heat transfer, and is defined by (Rousseau, 2007):

$$Nu = \frac{h_c L}{k} \tag{3.14}$$

For the flow in a tube, *Nu* is given by:

$$Nu = \frac{h_c D_H}{k} \tag{3.15}$$

where D_H is the hydraulic diameter, and is defined by:

$$D_H = \frac{4A_{ff}}{P_w} \tag{3.16}$$

where P_W is the wetted perimeter.

For laminar flow *Nu* is a constant and for turbulent flow *Nu* may be calculated by making use of a suitable empirical derived correlation. Such empirically derived correlations will be discussed in the following section.

3.5. Nusselt number correlations

In this study turbulent flow was assumed for both the water and R-744 fluid streams, therefore, empirical *Nu* correlations should be employed. For the water side the well known Dittus-Boelter correlation will be used to calculate *Nu* and eight different *Nu* correlations will be evaluated against each other for supercritical R-744 (Section 3.5.2 to 3.5.8).

3.5.1. Dittus-Boelter

Although the Dittus-Boelter correlation may be used to calculate *Nu* for a number of fluids, it is exceptionally suited to calculate *Nu* for turbulent water flow.

The Dittus-Boelter correlation (Nu_{DB}) is defined by (Dittus & Boelter, 1930):

$$Nu_{DB} = 0.023 Re_b^{0.8} Pr_b^n \tag{3.20}$$

$$\text{If } T_w > T_b, \text{ then } n = 0.4 \quad \text{and} \tag{3.21}$$

$$\text{if } T_w < T_b, \text{ then } n = 0.3$$

Re_b, Pr_b *and* T_b *are* calculated at the bulk of the fluid, whilst T_w represents the temperature at the wall of the fluid.

3.5.2. The Gnielinski and the modified Gnielinski correlations

The Gnielinski correlation (Nu_G) is defined by (Gnielinski, 1976):

$$Nu_G = \frac{f}{8}\left(Re_b - 1000\right)Pr_b\left[1.07 + 12.7\sqrt{\frac{f}{8}}\left(Pr_b^{2/3} - 1\right)\right]^{-1} \tag{3.22}$$

whilst the modified Gnielinski correlation (Nu_{GM}) is defined by (Gnielinski, 1976):

$$Nu_{G,M} = \frac{f}{8}\left(Re_b - 1000\right)Pr_b\left[1.07 + 12.7\sqrt{\frac{f}{8}}\left(Pr_b^{2/3} - 1\right)\right]^{-1}\left[1 + \left(\frac{D_H}{L}\right)^{2/3}\right] \tag{3.23}$$

where f represents either the Filonenko or Haaland friction factor correlation as defined in Section 3.7.[8]

3.5.3. The Krasnoshchekov Kuraeva Protopopov correlation

The Krasnoshchekov[9] correlation (Nu_{KKP}) is defined by (Krasnoshchekov *et al.*,. 1969):

$$Nu_{KKP} = Nu_{PK}\left(\frac{\rho_W}{\rho_b}\right)^n\left(\frac{\overline{c_p}}{c_{p,W}}\right)^m \tag{3.24}$$

where Nu_{PK} is the Petukhov-Kirillov correlation given by Eq (3.27), whilst ρ_W and ρ_b, respectively, are the density at the wall and bulk. The value of n is given in Table 3.1 at three different pressures (8, 10 and 12 MPa), whilst m is given by:

$$m = B\left(\frac{\overline{c}_p}{c_{p,W}}\right)^l \tag{3.25}$$

where $c_{p,w}$ is the specific heat capacity at constant pressure calculated at the wall conditions, l and B are given in Table 3.1 for three different pressures. The average specific heat, $\overline{c_p}$, is defined by (Krasnoshchekov *et al.*,. 1969):

[8] Unless stated otherwise, the Filonenko friction factor will be used in this study when using the Gnielinski and modified Gnielinski equations.

[9] Krasnoshchekov Kuraeva Protopopov correlation will be revered to as: Krasnoshchekov correlation.

$$\overline{c_p} = \frac{h_b - h_W}{T_b - T_W} \tag{3.26}$$

where h_b and h_w are the bulk and wall enthalpies respectively.

The Petukhov-Kirillov correlation, Nu_{PK}, used in Eq (3.24) is defined by (Petukhov & Kirillov, 1958):

$$Nu_{PK} = \frac{f}{8} Re_W Pr_W \left[1.07 + 12.7 \sqrt{\frac{f}{8}} \left(Pr_W^{2/3} - 1 \right) \right]^{-1} \tag{3.27}$$

where Re_W and Pr_W are Re and Pr at the wall conditions and f is the Filonenko friction factor correlation as defined in Section 3.7.1.

Table 3. 1. Pressure constants to be used for the calculation of Nu_{KKP} according to Eqs (3.24) and (3.25).

***p* [MPa]**	***n***	***B***	***l***
8.0	0.38	0.75	0.18
10.0	0.68	0.97	0.04
12.0	0.8	1.0	0.0

3.5.4. The Petrov-Popov correlation

The Petrov-Popov correlation (Nu_{PP}) is defined by (Petrov & Popov, 1985):

$$Nu_{PP} = Nu_{PK} \left(1 - 0.001 \frac{q}{G} \right) \left(\frac{\overline{c_p}}{c_{p,W}} \right)^n \tag{3.28}$$

where q and G, respectively, represent the heat flux and the mass flux, whilst n is defined by:

$$\begin{gathered} \text{If } n = 0.66 - 0.0004 \frac{q}{G}, \text{ then } \frac{\overline{c_p}}{c_{p,W}} \le 1 \\ \text{and} \\ \text{if } n = 0.90 - 0.0004 \frac{q}{G}, \text{ then } \frac{\overline{c_p}}{c_{p,W}} > 1 \end{gathered} \tag{3.29}$$

3.5.5. The Fang correlation

The Fang correlation (Nu_F) is defined by (Fang *et al.*, 2001):

$$Nu_F = \frac{f_W}{8}\left(\frac{(Re_W - 1000)Pr_W}{A + 12.7\sqrt{f_W/8}(Pr_W^{2/3} - 1)}\right)\left(\frac{1 - 0.001q_W}{G}\right)\frac{\bar{c}_p}{c_{p,W}} \tag{3.30}$$

where f_w and q_w, respectively, represents the friction factor correlation and heat flux at the wall, whilst f is either the Blasius or Filonenko friction factor correlation as defined in Section 3.7. A is defined by:

$$\begin{gathered}\text{If } A = 1 + 7\text{x}10^{-8}, \text{ then } Re_W < 10^6 \\ \text{and} \\ \text{if } A = 1.07, \text{ then } Re_W \geq 10^6\end{gathered} \tag{3.31}$$

3.5.6. The Yoon correlation

The Yoon correlation (Nu_Y) is defined by (Yoon *et al.*, 2003):

$$\begin{gathered}Nu_Y = 0.14Re_b^{0.69}Pr_b^{0.66} \\ \text{if } T_b/T_{pc} > 1\end{gathered} \tag{3.32}$$

$$\begin{gathered}Nu_Y = 0.14Re_b Pr_b^{-0.05}\left(\frac{\rho_{pc}}{\rho_b}\right)^{1.6} \\ \text{if } T_b/T_{pc} \leq 1\end{gathered} \tag{3.33}$$

where T_{pc} is the pseudocritical temperature and ρ_{pc} the density at the pseudocritical temperature.

3.5.7. The Son-Park correlation

The Son-Park correlation (Nu_{SP}) is defined by (Son & Park, 2006):

$$\begin{gathered}Nu_{SP} = Re_b^{0.55}Pr_b^{0.23}\left(\frac{c_{p,b}}{c_{p,W}}\right)^{0.15} \\ \text{if } T_b/T_{pc} > 1\end{gathered} \tag{3.34}$$

$$\begin{gathered}Nu_{SP} = Re_b^{0.35}Pr_b^{1.9}\left(\frac{\rho_b}{\rho_W}\right)^{-1.6}\left(\frac{c_{p,b}}{c_{p,W}}\right)^{-3.4} \\ \text{if } T_b/T_{pc} \leq 1\end{gathered} \tag{3.35}$$

3.5.8. The Huai correlation

The Huai correlation (Nu_H) is defined by (Huai *et al.*, 2005):

$$Nu_H = Re_W^{0.8} Pr_W^{0.3} \left(\frac{\rho_b}{\rho_W} \right)^{-1.47} \left(\frac{\bar{c}_p}{c_{p,W}} \right)^{0.083} \tag{3.36}$$

3.6. Pressure drop correlations

The pressure drop correlations are not only necessary for predicting pressure drops, but, as can be seen in Section 3.5, in some cases *Nu* is a function of the friction factor.

When predicting the pressure loss in a tube, with the assumption that there are no secondary losses, *i.e.* bends, T-pieces, etc., the pressure drop prediction (Δp_L) is given by:

$$\Delta p_L = f \frac{1}{2} \frac{\rho V^2 L}{D_H} \tag{3.37}$$

where f is the friction factor correlation.

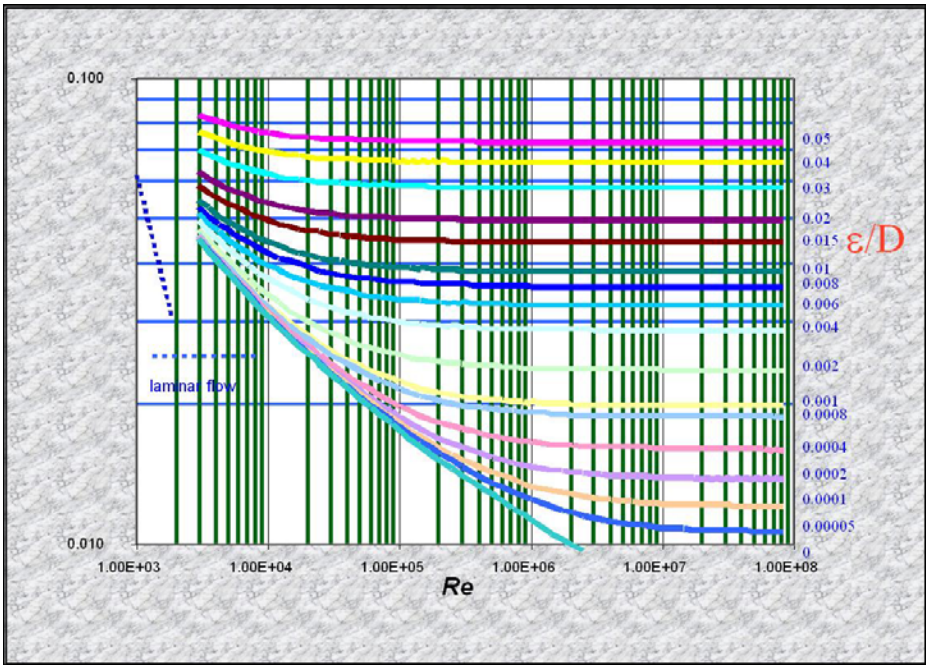

Figure 3.1. The Moody chart (taken from: Chen *et al.*, 2005).

For water flowing in a tube, the Darcy-Weisbach friction factor may be used. The Darcy-Weisbach friction factor may be obtained from the Moody chart (Figure 3.1), where ε is the relative tube roughness.

3.7. Friction factor correlations

Three friction factor correlations are given in this section, namely, the Filonenko, Haaland and Blasius correlations. It was, however, reported that the Blasius friction factor is the most accurate correlation that may be used to predict the pressure loss for cooling supercritical R-744 (Yoon *et al.*, 2003; Cheng *et al.*, 2008).

3.7.1. Filonenko friction factor correlation

The Filonenko friction factor correlation is given by (Filonenko, 1954):

$$f = (1.82 \log Re_b - 1.64)^{-2} \tag{3.38}$$

3.7.2. Haaland friction factor correlation

The Haaland friction factor correlation is given by (Haaland, 1983):

$$f = \left(-1.8 \log \left(\frac{6.9}{Re_b} + \left(\frac{\varepsilon}{3.7 D_H} \right)^{1.11} \right) \right)^{-2} \tag{3.39}$$

3.7.3. Blasius friction factor correlation

The Blasius friction factor correlation is given by (McAdams, 1954):

$$f = \frac{0.316}{Re_b^{1/4}} \tag{3.40}$$

3.8. Heat exchange for a tube-in-tube configuration

For the simulation of a tube-in-tube heat exchanger in this study (see Chapter 5), the heat transfer distribution pattern between the streams have to be defined. In this section the LMTD method will be defined.

The total rate of heat transfer to the fluid, $\dot{Q}$, is given by:

$$\dot{Q} = UA \cdot \Delta T_{lm} \tag{3.41}$$

where ΔT_{lm} represents a logarithmic temperature difference and UA is the overall heat transfer coefficient, whilst ΔT_{lm} is defined by:

$$\Delta T_{lm} = (\Delta T_1 - \Delta T_2) / \ln(\Delta T_1 / \Delta T_2)$$

$$\Delta T_{lm} = \frac{\Delta T_1 - \Delta T_2}{\ln(\Delta T_1 / \Delta T_2)} \tag{3.42}$$

For a counter flow heat exchange, the temperature differences, ΔT_1 and ΔT_2, are defined by:

$$\Delta T_1 = T_{p,i} - T_{s,e} \tag{3.43}$$

$$\Delta T_2 = T_{p,e} - T_{s,i} \tag{3.44}$$

where $T_{p,j}$, $T_{p,e}$, $T_{s,i}$ and $T_{s,e}$ represents the primary inlet and outlet, and the secondary inlet and outlet temperatures respectively.

The overall heat transfer coefficient, UA, is defined by:

$$\frac{1}{UA} = \frac{1}{(\eta_o h_c A)_p} + \frac{R''_{f',p}}{(\eta_o A)_p} + R_w + \frac{R''_{f',s}}{(\eta_o A)_s} + \frac{1}{(\eta_o h_c A)_s} \tag{3.45}$$

where η_0 is the overall surface efficiency, $R''_{f,p}$ and $R''_{f,s}$ are the surface foulness factors for the primary and secondary streams and R_W is the thermal wall resistance.

The surface efficiency, η_0, is defined by:

$$\eta_o = 1 - \frac{A_f}{A}(1 - \eta_f) \tag{3.46}$$

where A_f is the fin area, A the total area and η_f the fin efficiency.

The thermal wall resistance, R_W, for a tube is defined by:

$$R_W = \frac{\ln(D_{i,o} / D_{i,i})}{2\pi k L} \tag{3.47}$$

The simulation in this study (see Chapter 4) was performed on a smooth tube-in-tube heat exchanger, thus, the fin efficiency is unity, *i.e.* $\eta_f = 1$. If the fin efficiency is unity, then it follows from Eq (3.46) that the surface efficiency for this case will also be unity, thus $\eta_o = 1$.

All the relevant theory that is necessary to successfully simulate a tube-in-tube heat exchanger has been presented in this chapter. The next section will supply the statistical background, of some basic concepts, that will be used to interpret and process the computed and calculated results.

3.9. Statistical concepts[10]

Statistical concepts used in this study are:

- mean,
- standard deviation,
- linear regression and
- R^2-fitting.

The mean and standard deviation may probably be labelled the two most basic concepts of statistics.

The mean

The mean or average is the summation, $\bar{x}$, of numerical values, divided by the number of summation parameters and is defined by:

$$\bar{x} = \frac{1}{n}\sum_{i=1}^{n} x_i \tag{3.48}$$

where x_i may represent any numerical parameter.

Standard deviation

The standard deviation is defined by:

$$\sigma = \sqrt{\frac{1}{n}\sum_{i=1}^{n}(x_i - \bar{x})^2} \tag{3.49}$$

Linear regression

Linear regression is employed when it is suspected that the applicable data have an underlying linear relationship. Linear regression refers to an approach to identify a linear trend between data sets, *i.e.* to set up a linear model where a variable is manipulated in a linear fashion to predict another variable.

[10] The discussion in Section 3.9 is based on the notes of Rice (1995).

Linear regression is defined by:

$$y = \hat{\beta}x + \hat{\alpha} \tag{3.50}$$

where the gradient $\hat{\beta}$ and intercept $\hat{\alpha}$ are defined as follows:

$$\hat{\beta} = \frac{\sum_{i=1}^{n}(x_i - \bar{x})(y_i - \bar{y})}{\sum_{i=1}^{n}(x_i - \bar{x})^2} \tag{3.51}$$

and

$$\hat{\alpha} = \bar{y} - \hat{\beta}\bar{x} \tag{3.52}$$

R^2 method

The R^2 method is used to judge to what degree a linear regression line correlates with the particular data, and is defined by:

$$R^2 = 1 - \frac{\sum_{i=1}^{n}(y_i - y(x_i))^2}{\sum_{i=1}^{n}(y_i - \bar{y})^2} \tag{3.53}$$

where $y(x_i)$ is the expected outcome calculated by means of Eq (3.50).

3.10. Summary

The theoretical background that is necessary for the successful development and operation of the relevant simulation programs was given. This includes conservation laws, mass flow rate and the heat transfer rate through a tube-in-tube heat exchanger. The non-dimensional parameters *Nu*, *Re* and *Pr* were defined. A number of correlations were given that may be employed for the calculation of *Nu* for R-744, *Nu* for water (Dittus-Boelter) and friction factors. Finally, statistical concepts necessary for the analysis of the results were included.

CHAPTER

4

Simulation of a transcritical gas cooler

A theoretical simulation of R-744 is presented in the current chapter and supercritical R-744 will be scrutinised for water heating purposes. This chapter focuses on a theoretical simulation of Nu^s for turbulent supercritical R-744 in a gas cooler, based on different *Nu* correlations that were reported in the literature (see Section 3.5). These different *Nu* correlations will be compared with each other. As stated earlier, *Nu* is employed to determine the convection heat transfer coefficient, h_c, which is of utmost importance for executing accurate simulations.

4.1. Methodology

This section consists of theoretical simulations of a tube-in-tube heat exchanger, where the objective is to compute h_c by implementing different R-744 *Nu* correlations. The objective of each simulation is to deliver an outlet water temperature of 90 °C. Nekså and co-workers (1999) reported that an R-744 heat pump water heater may be constructed to deliver water with a temperature of up to 90 °C. White and co-workers (2002) constructed a prototype transcritical R-744 heat pump system, delivering water at 90 °C (Chapter 2). When a simulation is conducted for a practical setup, appropriate inputs are needed for prediction of the required outputs. For a heat exchanger simulation, the inlet conditions, *i.e.* temperature and pressure, of the fluids should be known before the outlet temperatures and pressures can be simulated. Since this chapter focuses only on a theoretical study, where no experimental data will be used, the outlet temperature, and not the inlet temperature, of the water will be chosen as a fixed boundary value. The decision to choose the outlet temperature as a fixed boundary value, does not by any means influence the simulation methodology of the simulation process.

Applicable thermodynamic boundary conditions are employed to uncover the appropriate thermodynamic properties[11] at the defined points. These properties are then used to compute, *via* simulation, the thermodynamic properties at the remaining points over the heat exchanger,

[11] Thermodynamic properties: conductivity (k), density (ρ), enthalpy (h), entropy (s), specific heat at constant pressure (c_p) and viscosity (μ).

i.e. at every discrete interval. During the process of simulation, the non-dimensional *Re*, *Pr* and *Nu*, need to be computed at every discrete point by applying knowledge of the underlying thermodynamic properties. The convection heat transfer coefficient, h_c, can only be computed after computation of *Nu* by means of a suitable empirical correlation.

For the water side of the heat exchanger, the well known Dittus-Boelter correlation may be employed to predict the Nu^s. An accurate *Nu* leads to an accurate h_c prediction, which in turn results in a true simulation of the temperature distribution. The various *Nu* correlations, mentioned in Section 3.5 were implemented for the R-744 side. Cheng and co-workers (2008) reported that a number of *Nu* correlations exist for the prediction of the h_c, but not enough data are available to verify which *Nu* correlation is the most suitable to employ.

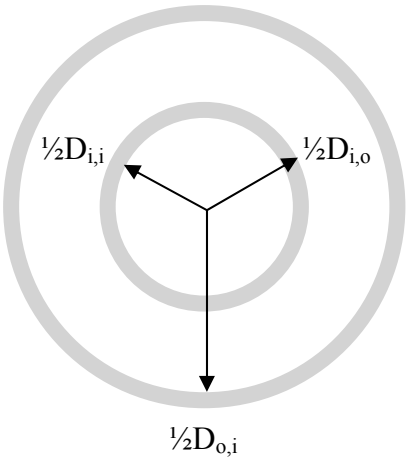

Figure 4.1. An annulus with $½D_{i,i}$ = inner radius of inner tube, $½D_{i,o}$ = outer radius of inner tube and $½D_{o,i}$ = inner radius of outer tube.

Figure 4.1 shows a tube-in-tube configuration, where R-744 flows in the inside tube and water in the outer annulus (Bruch *et al.*, 2009; Pitla *et al.*, 2002; Son & Park, 2006 and Yoon *et al.*, 2003). In the current study the following boundary conditions were specified for the simulation procedure of R-744 and water, for a tube-in-tube heat exchanger:

- The inlet pressures of the both fluids ($p_{R\text{-}744}$ = 12 MPa; p_{water} = 400 kPa).
- The inlet temperature of R-744 ($T_{R\text{-}744}$ = 120 °C).
- The outlet temperature of water (T_{water} = 90 °C).
- The mass flow rates of the fluids ($\dot{m}_{R-744}$.= 0.5 kg/s; $\dot{m}_{water}$ = 0.3 kg/s).

- Dimensions of the heat exchanger (length (25 m), inner diameters ($D_{i,i}$ = 0.04 m; $D_{o,i}$ = 0.05 m) and the inner tube thickness (½($D_{i,o} - D_{i,i}$) = 0.0015 m)).

The heat exchanger was divided into smaller, equal in length, increments and the thermodynamic properties of both fluids were computed for every discrete point, *i.e.* the inlet and outlet of the increments. The latter procedure was followed to improve the accuracy of the results. It should be noted, that the outlet conditions over an increment are the inlet conditions for the neighbouring increment. It were also assumed that:

- the flow was fully developed, and
- no heat loss occurred in the system at any point during the simulation process.

The thickness of the outer tube was not used as a parameter in this simulation, since it was assumed that the heat exchanger is perfectly insulated from the environment and that no heat loss will occur. Since all relevant dimensions were specified, the face flow areas could be calculated by employing Eqs (3.10) and (3.11).

It should be noted, however, that the effect of conduction through the inner tube was not taken into account. The conduction heat transfer coefficient, k, is a function of the temperature, but the effect of the temperature on k may be deemed negligible over the applicable range. This will result in a constant k and the effect will therefore be identical at every interval, irrespective of the *Nu* correlation used.

It follows from Eq (3.9) that the velocity of the fluid at a specific point can be computed if the mass flow rate, face flow area and density at that point are known. It is important to note, that at the chosen temperatures and pressures the fluids will at no stage be in a two phase state, therefore, the thermodynamic properties at a specific point may be determined if the relevant temperature and pressure are known.[12]

4.1.1. Computation of *Re*, *Pr*, *Nu* and h_c

With the density, velocity, hydraulic diameter (see Eq (3.16)) and viscosity known, *Re* was computed by using of Eq (3.17). *Pr* is a function of c_p, k and μ and was calculated by employing Eq (3.18). All *Nu* correlations (Section 3.5) are always a function of both *Re* and *Pr*. Therefore, it is imperative that the values of these two non-dimensional entities should be known, before the

[12] Fluid properties are calculated by means of built-in EES R-744 functions.

non-dimensional Nu[13] can be computed. Once Nu is known, h_c may be computed by making use of Eq (3.14).

For the incremental length of the tube, h_c of both streams may be computed if the Nu of these streams, *i.e.* the R-744 and water streams are known. These h_c^s are crucial parameters and are necessary for computing the temperature distribution throughout the heat exchanger for both streams (see Eqs (3.41) and (3.45)). The LMTD method, as described in Section 3.8, together with the energy conservation equation, Eq (3.8), may be employed to compute the incremental heat transfer rate between the fluids.

4.2. Computed results

The data shown in Figures 4.2 to 4.5 resulted from the theoretical simulations. The objective of this simulation study was to determine the R-744 Nu^s by employing the different Nu correlations. Note, that the Nu^s were computed for turbulent supercritical R-744 in cooling, while heating a turbulent water flow.

4.2.1. Nusselt number and convection heat transfer coefficient *versus* tube length

Figure 4.2 show the distribution of Nu^s over the length of the tube for R-744, as predicted by the different Nu correlations. In Figure 4.3 the heat transfer coefficient, h_c, is plotted against the length of the tube.

4.2.1.1. Nusselt number *versus* tube length

The different Nu^s, as predicted by the eight different Nu correlations employed in this study, are plotted against the length of the tube (Figure 4.2). As R-744 flows through the tube and cools, the correlations generally predict an initial increase in the values of Nu. The only exception is the Son-Park correlation that predicts an initial decline of Nu over almost two thirds of the tube length, where after Nu begin to rise. All the Nu^s, except Nu^s predicted by the Gnielinski correlation, eventually reach a maximum value over the length of the tube and then decline. The Gnielinski correlation increase over the entire length of the tube. If a longer tube should be employed, then one would expect that the Gnielinski correlation will also reach a maximum and then decline. Nu^s predicted by the Gnielinski and Modified Gnielinski correlations generally follow the same trend.

[13] For the calculation of Nu, the Filonenko friction factor correlation was chosen rather than the Blasius friction factor correlation, because the Filonenko correlation is more often employed for the calculation of R-744 Nu^s.

The Petrov-Popov and Fang correlations do not deviate much from each other up to about 22 m and are in close proximity up to about 7 m. From about 7 m, the Petrov-Popov correlation seems to rise steadily to about 20 m, where after it starts to decline. The Fang correlation tends to rise to a lesser extent than does the Petrov-Popov correlation. From about 17 m the Fang correlation rises more steeply to a maximum at about 23 m and then declines.

The Yoon, Huai and Krasnoshchekov correlations generally predict comparable patterns and overall the greatest Nu^s. Therefore, these correlations predict the most efficient heat transfer *via* convection. Krasnoshchekov predicts the most rapid increase of Nu^s over the pipe lenth. Up to a tube length of about 7 m, the Krasnoshchekov, Modified Gnielinski, Petrov-Popov, Fang and Modified Gnielinski correlations increase to more or less the same extend.

4.2.1.2. Convection heat transfer coefficient of R-744 *versus* tube length

The convection heat transfer coefficient, h_c, was computed by making use of Eq (3.14) and plotted against the tube length (Figure 4.3). Figures 4.2 and 4.3 follows an almost analogous distribution pattern, which is to be expected, since $h_c = f(Nu,k,L)$.

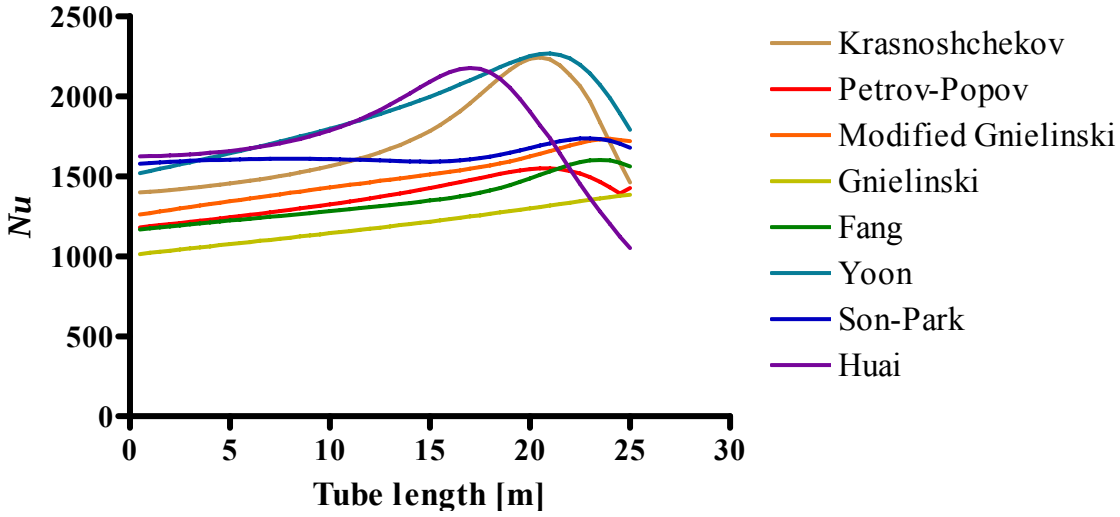

Figure 4.2. *Nu* plotted over the length of the heat exchanger for the different *Nu* correlations. Note the wide range of values predicted by the various correlations.

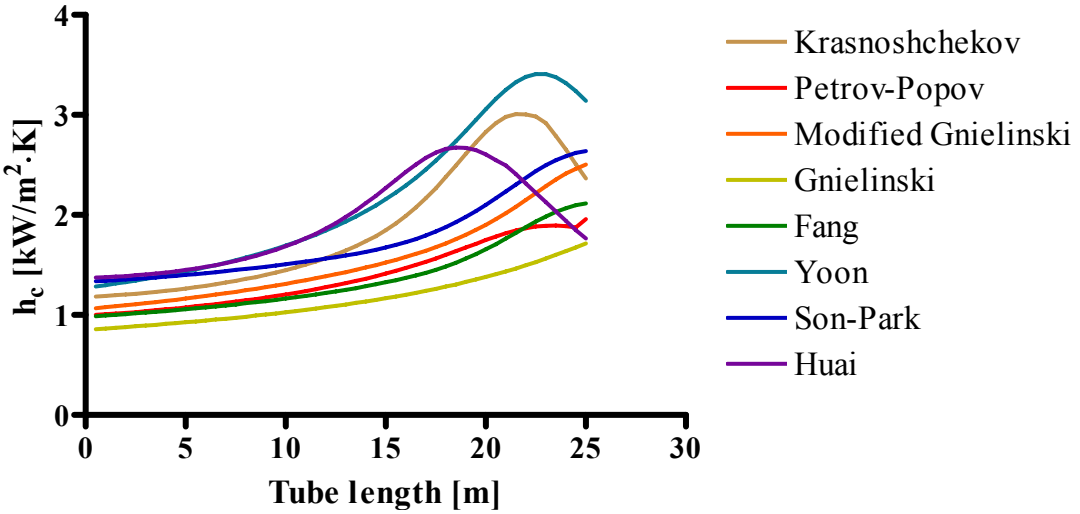

Figure 4.3. Heat transfer convection coefficient, h_c, of R-744 is plotted over the length of the heat exchanger for the different *Nu* correlations. Note the wide range of values predicted by the various correlations.

4.2.2. Temperature *versus* tube length

As mentioned previously, if *Nu* is known, then h_c may be computed. This was followed by the computation of the heat transfer rate for every incremental length. Ultimately, the temperature was computed at the inlet and outlet of every incremental length, *i.e.* the temperature distribution. This computation process is discrete and not continuous, thus, by increasing the increments over the tube length, the accuracy of the simulations results, and finally the distributions, should be improved.

The R-744 temperature distributions of the eight *Nu* correlations, employed in this study, are shown in Figure 4.4. It can be seen in Figure 4.4 that the temperature distributions differ substantially over the tube length. This is to be expected if one considers the distribution patterns of Nu^s and h_c^s, over the length of the heat exchanger, in Figures 4.2 and 4.3. The Gnielinski correlation is the most conservative in predicting *Nu*, resulting in an outlet temperature of 63.62 ºC for the supercritical R-744. On the other hand, the Yoon correlation is the most aggressive *Nu* predictor over the length of the heat exchanger and it predicted an outlet temperature of 46.23 ºC. Over the length of the heat exchanger this gives rise to a maximum temperature difference of 17.39 ºC between the various correlations.

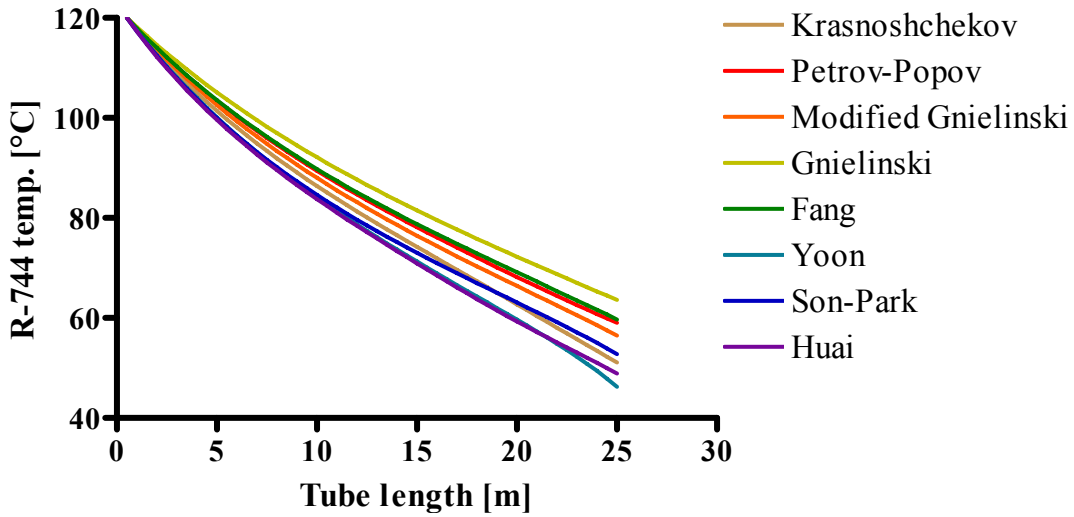

Figure 4.4. Temperature distribution for R-744 over the length of the heat exchanger for the different *Nu* correlations.

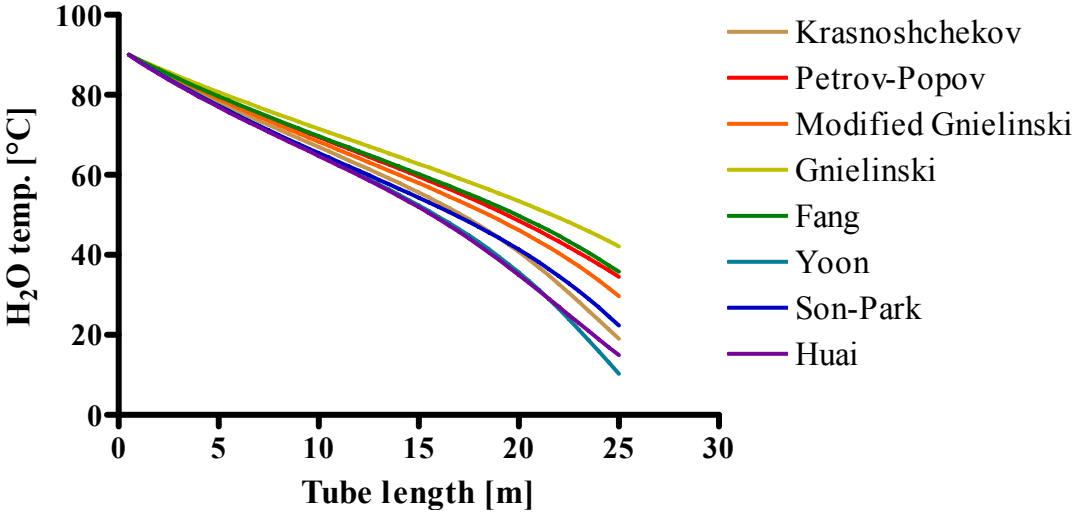

Figure 4.5. Graphs showing the influence on the temperature distribution of water over the length of the heat exchanger for the different R-744 *Nu* correlations. Due to a counter flow configuration, 0.0 m is the exit (specified to be 90 ºC) of the water stream.

Figure 4.5 shows the water temperature distribution throughout the heat exchanger. For the water stream, the well known Dittus-Boelter correlation was employed for the calculation of the relevant Nu^s. For the preset objective, *i.e.* heating water to 90 ºC over a fixed length of the tube, the Yoon correlation overall predicts the most efficient heat transfer rate of the cooling supercritical R-744 (Figure 4.4). According to the Yoon correlation, the water inlet temperature should be 7.55 ºC, which is the lowest inlet water temperature predicted by all the correlations used in this study. On the other hand, for the cooling of supercritical R-744 the Gnielinski

correlation is the most conservative of all these correlations (see Figure 4.2).[14] This correlation requires the highest inlet water temperature, namely 42.15 ºC, to eventually produce warm water at a temperature of 90 ºC at the outlet.

4.3. Conclusion

No explicit conclusions could be made regarding the accuracy of any of the correlations used in this study. However, the results in this chapter emphasise the importance of finding a more suitable *Nu* correlation for cooling supercritical R-744. Without an accurate *Nu* correlation, the simulation results will only remotely compare with reality.

4.4. Summary

A water-to-transcritical R-744 tube-in-tube heat exchanger was simulated by implementing various *Nu* correlations. These studies were theoretical in nature and only concentrated on the prediction of *Nu* by employing various *Nu* correlations, which ultimately gave rise to the prediction of a temperature distribution of R-744 flow in the inner tube. The theoretical data was not compared to experimentally acquired values, therefore, no conclusions could be made regarding the accuracy of the various *Nu* correlations concerning the cooling of supercritical R-744.

[14] The effect of the various *Nu* correlations on the heat transfer duty, may be seen in Figure A.5 in Appendix A

CHAPTER

5

Comparison of experimental and theoretical Nusselt numbers of R-744

In Chapter 4 a water-to-transcritical R-744 tube-in-tube heat exchanger was simulated by implementing various *Nu* correlations. These theoretical studies concentrated mainly on the prediction of *Nu* by employing various *Nu* correlations. In the current chapter theoretically calculated Nu^s will be compared to experimental Nusselt numbers ($Nu_{exp}{}^s$).[15] The various correlations will be compared to each other and evaluated. Eventually, a newly modified *Nu* correlation will be presented.

5.1. Experimental Nusselt numbers (Nu_{exp})

Yoon and co-workers (2003) published an innovative *Nu* correlation for supercritical R-744. The correlation is based on experimental data obtained on a test apparatus, which consisted of an 4.0 m long water-to-transcritical R-744 tube-in-tube heat exchanger, where supercritical R-744 was flowing in the inner tube, with an inner tube diameter of 7.73 mm. In the current study, the convection heat transfer coefficients, temperatures, pressures and tube diameter, reported by Yoon and co-workers (2003), were employed for the direct calculation of $Nu_{exp}{}^s$ (see Appendix B Table B.1 for calculation). These $Nu_{exp}{}^s$ are compared to theoretical Nu^s, calculated by means of the *Nu* correlations used in Chapter 4 (see Appendix B; Section B.2 for calculation). Note that the theoretical Nu^s were not computed according to various simulations of a water-to-transcritical R-744 tube-in-tube heat exchanger, as was the case in Chapter 4. The theoretical Nu^s in this chapter were calculated for every incremental length by using the known value for the inner tube diameter, R-744 mass flow, pressure and the relevant bulk and wall temperatures.

Figures 5.1 and 5.2, respectively, depict h_c and Nu_{exp} at different pressures, namely 7.5, 7.7, 8.0, 8.2, 8.5 and 8.8 MPa, over the length of the tube. In Figure 5.1 it can be seen that, at all the given pressures, h_c increases as the temperature decreases. In all instances h_c eventually reaches a maximal value, where after h_c decreases as the temperature increases. This is in accordance with

[15] All data given in this chapter is for cooling of supercritical R-744.

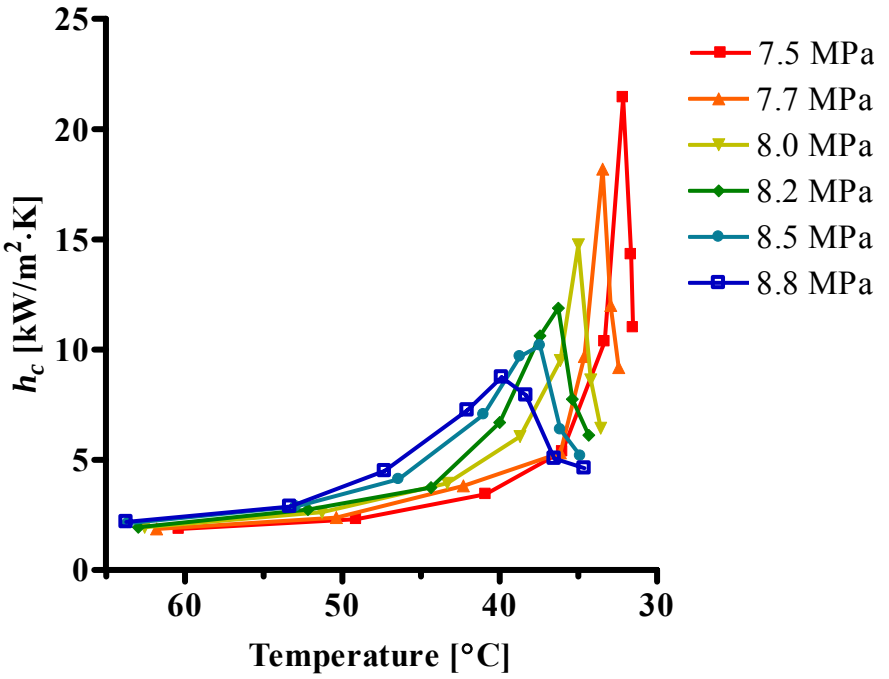

Figure 5.1. Heat transfer convection coefficient distribution at various pressures *versus* R-744 bulk temperature (Yoon *et al.*, 2003). Heat was transferred from supercritical R-744 to water in a water-to-transcritical R-744 tube-in-tube heat exchanger.

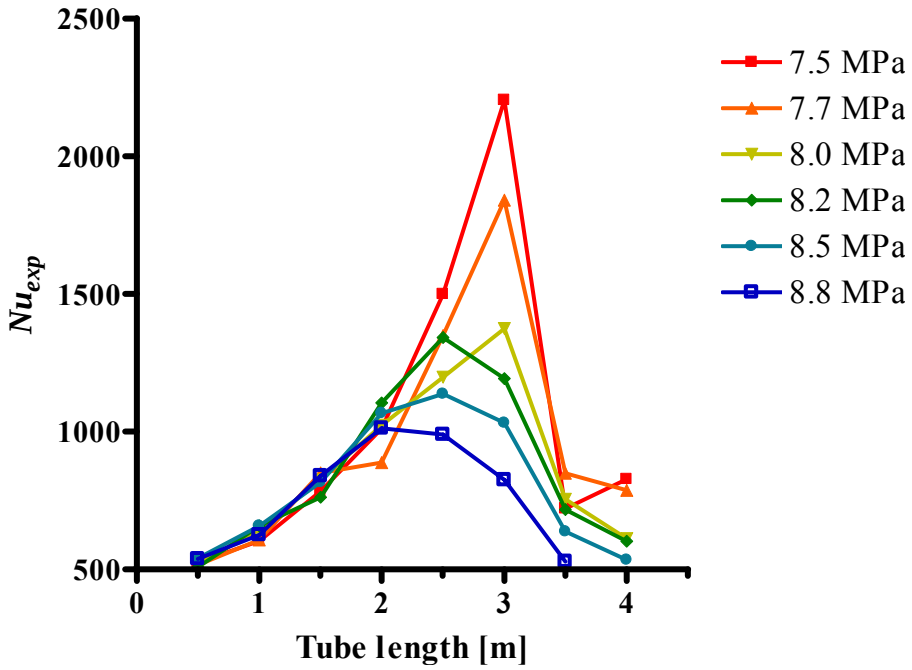

Figure 5.2. Experimental Nusselt numbers, Nu_{exp}, at various pressures *versus* the length of a tube-in-tube heat exchanger. Nu_{exp} was calculated by employing h_c data from Figure 5.1.

the finding of Bruch and co-workers (2006), namely, that the maximum heat transfer coefficient will be reached in a small interval around the pseudocritical temperature. At all the different pressures (Figure 5.1) the value of h_c, obtained after the maximal h_c, correlate to temperatures below the pseudocritical temperature for the pressure in question.

It follows indirectly from Figure 5.1, and directly from Figure 5.2, that the pressure affects the value of *Nu*. As the pressure increases, the maximal Nu_{exp}, obtained at each pressure, decreases. Note that the maximal Nu_{exp}^{s} at lower pressures were obtained at the greatest tube length, whilst the maximal Nu_{exp}^{s} at the highest pressures were obtained at shorter tube lengths. This is to be expected, since the temperature decreases over the tube length and passes through the pseudocritical temperature for every pressure set (7.5 to 8.8 MPa). A higher pressure results in a higher pseudocritical temperature. It follows that the maximal Nu_{exp}^{s} at lower pressures (7.5, 7.7 and 8.0 MPa) were obtained at a tube length of 3.0 m, whilst the maximal Nu_{exp}^{s} at medium pressures (8.2 and 8.5 MPa) were obtained at a tube length of 2.5 m. The maximal Nu_{exp}, obtained at the highest pressure (8.8 MPa), was observed at a tube length of 1.5 m.

5.2. Results and discussion

In Figures 5.3, 5.4 and 5.5 the results predicted by the various *Nu* correlations, as well as Nu_{exp}^{s}, were plotted against the length of the heat exchanger and for different pressures (7.5, 7.7, 8.0, 8.2, 8.5 and 8.8 MPa). Figure 5.3 depicts theoretical Nu^{s} obtained by means of the Gnielinski, Modified Gnielinski and Huai correlations, whilst Figure 5.4 depicts theoretical Nu^{s} obtained by means of the Krasnoshchekov, Petrov-Popov and Fang correlations. Figure 5.5 depicts theoretical Nu^{s} obtained by means of the Son-Park and Yoon correlations. The data in Figures 5.3, 5.4 and 5.5 were arbitrarily grouped together according to the general patterns observed for the various *Nu*–tube length curves.

It is important to note that Nu_{exp} increase progressively to a maximal value and then decline as the tube length increase. All the theoretical Nu^{s} in Figure 5.3 comply with this trend, whilst the predicted Nu^{s} are generally much smaller than the corresponding Nu_{exp}^{s}. The general curve patterns of the predicted *Nu*–tube length curves are almost identical, especially from a pressure of 8.0 MPa onwards.

In Figure 5.4 it can be seen that the various correlations in question also predict more or less identical *Nu*-tube length curves, however, these predicted curves generally differ rather substantially from the curves shown in Figure 5.3. At pressures of 7.5, 7.7 and 8.0 MPa, the

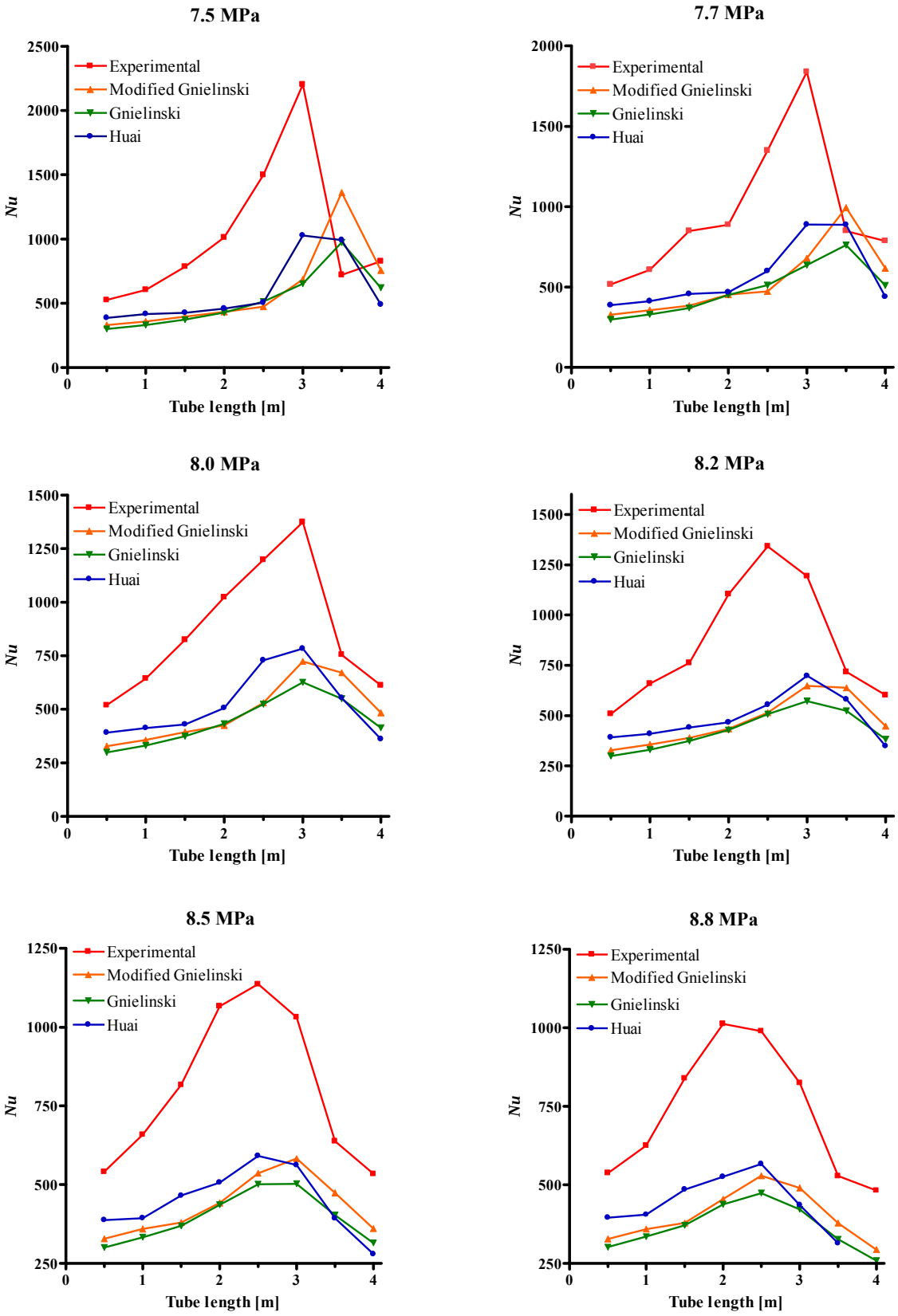

Figure 5.3. Experimentally obtained Nu^s compared to Nu^s calculated according to the Gnielinski, Modified Gnielinski and Huai correlations. *Nu*, at different pressures, plotted against the length of a tube-in-tube heat exchanger.

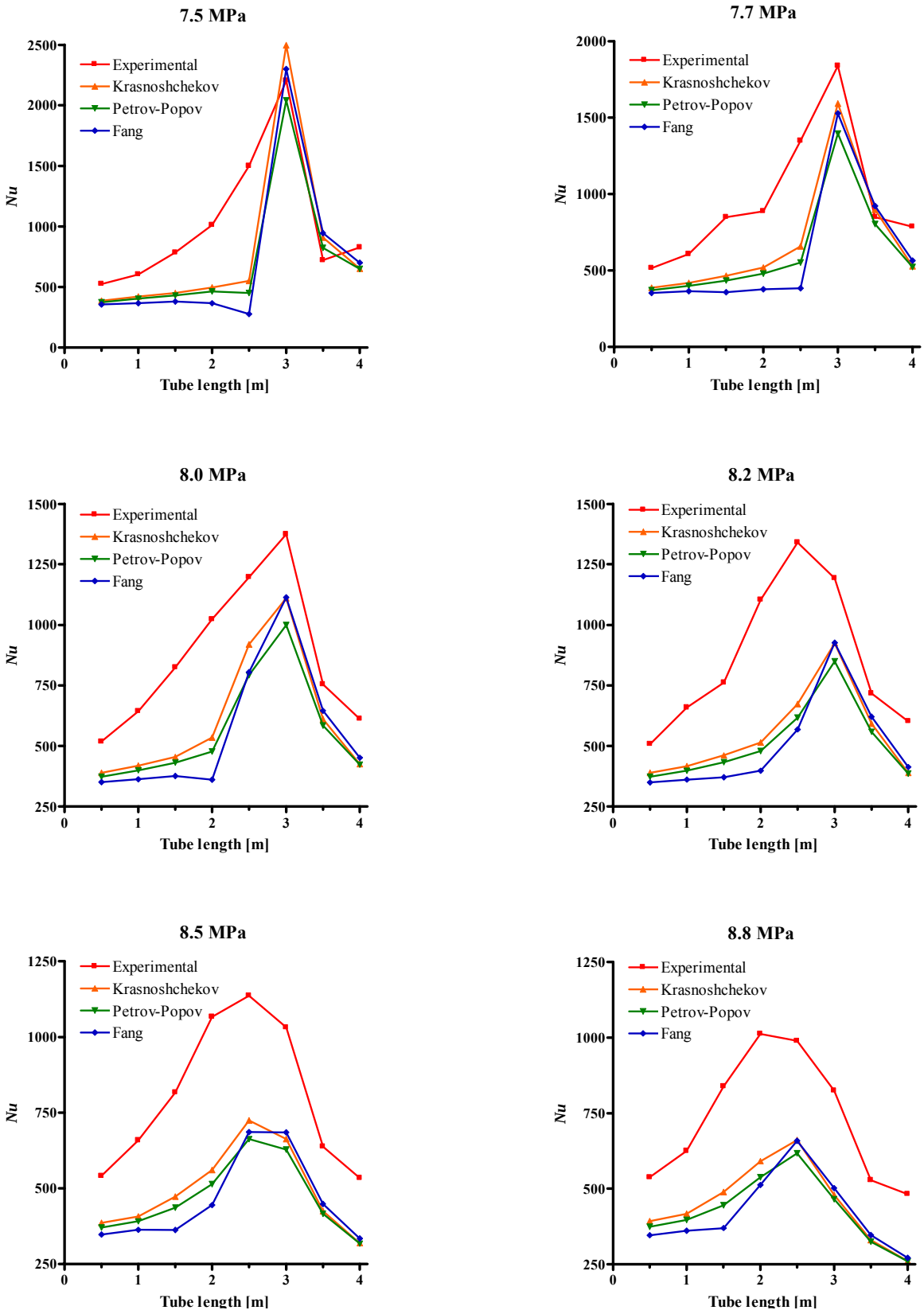

Figure 5.4. Experimentally obtained Nu^s compared to Nu^s calculated according to the Krasnoschchekov, Petrov-Popov and Fang correlations. *Nu*, at different pressures, plotted against the length of a tube-in-tube heat exchanger.

relevant correlations predict only a slight increase in *Nu* as the tube length increases. At a tube length of 2.5 m (7.5 and 7.7 MPa) and 2.0 m (8.0 MPa), the value of *Nu* increases abruptly to the maximal *Nu*. The correlations employed for data generation, at 7.5 to 8.0 MPa in Figure 5.4, predict maximal Nu^s that correlate very well with the corresponding $Nu_{exp}{}^s$. Note that all three of the correlations in Figure 5.4 use the wall conditions for determining *Nu* (see Section 3.5).

The *Nu*-tube length curves predicted by the Yoon- and Son-Park correlations are shown in Figure 5.5. The general pattern predicted by these two correlations does not fit in with that of the Gnielinski, Modified Gnielinski and Huai correlations (Figure 5.3) or the Krasnoshchekov, Petrov-Popov and Fang correlations (Figure 5.4). The Yoon correlation generally predicted some excessively high Nu^s as the pressure increases (Figure 5.4), but at tube lengths smaller than 3.0 m, the predicted Nu^s seemingly correlates rather well with the $Nu_{exp}{}^s$. At all pressures, except 8.2 MPa, the Son-Park correlation predicts an initial decline in Nu^s as the tube length increases.

5.2.1. Conclusion

All the *Nu* correlations included in this study generally tend to under predict *Nu* values, whereas the Yoon and Son-Park correlations constantly over predicted Nu^s at greater tube lengths, *i.e.* below the pseudocritical temperatures in question. The *Nu*-tube length graphs generally display a tendency that follows the trend of the experimental graphs, especially at more elevated pressures. Again, the Yoon and Son-Park correlations are the exceptions and deviate to some extend from the other correlations that were used.

5.3. Evaluation of the various *Nu* correlations

All the data (various correlations) was evaluated for possible use in developing a new *Nu* correlation for the cooling of turbulent supercritical R-744. This evaluation was performed by plotting Nu_{exp} against *Nu* predicted by all the correlations under investigation in this study.

If an ideal correlation scenario should be a reality, *i.e.* accurate Nu_{exp} and an ideal correlation, then a graph of the theoretical Nu^s against accurate Nu_{exp} should yield a linear relationship (the following holds for this linear relationship: $y = mx + c$ when $m = 1$ and $c = 0$). Figure 5.6 shows such linear graphs for the Gnielinski, Modified Gnielinski, Huai and Yoon correlations. In these graphs all data points for a temperature below the pseudocritical temperature, ($T < T_{pc}$), were removed.[16] It follows that the following Nu^s were excluded: Nu^s obtained for tube lengths greater than 3.0 m, and Nu^s obtained at 8.8 MPa for a tube length greater than 2.5 m. Not only

[16] Data points for $T < T_{pc}$ were removed due to the lack of sufficient quantity.

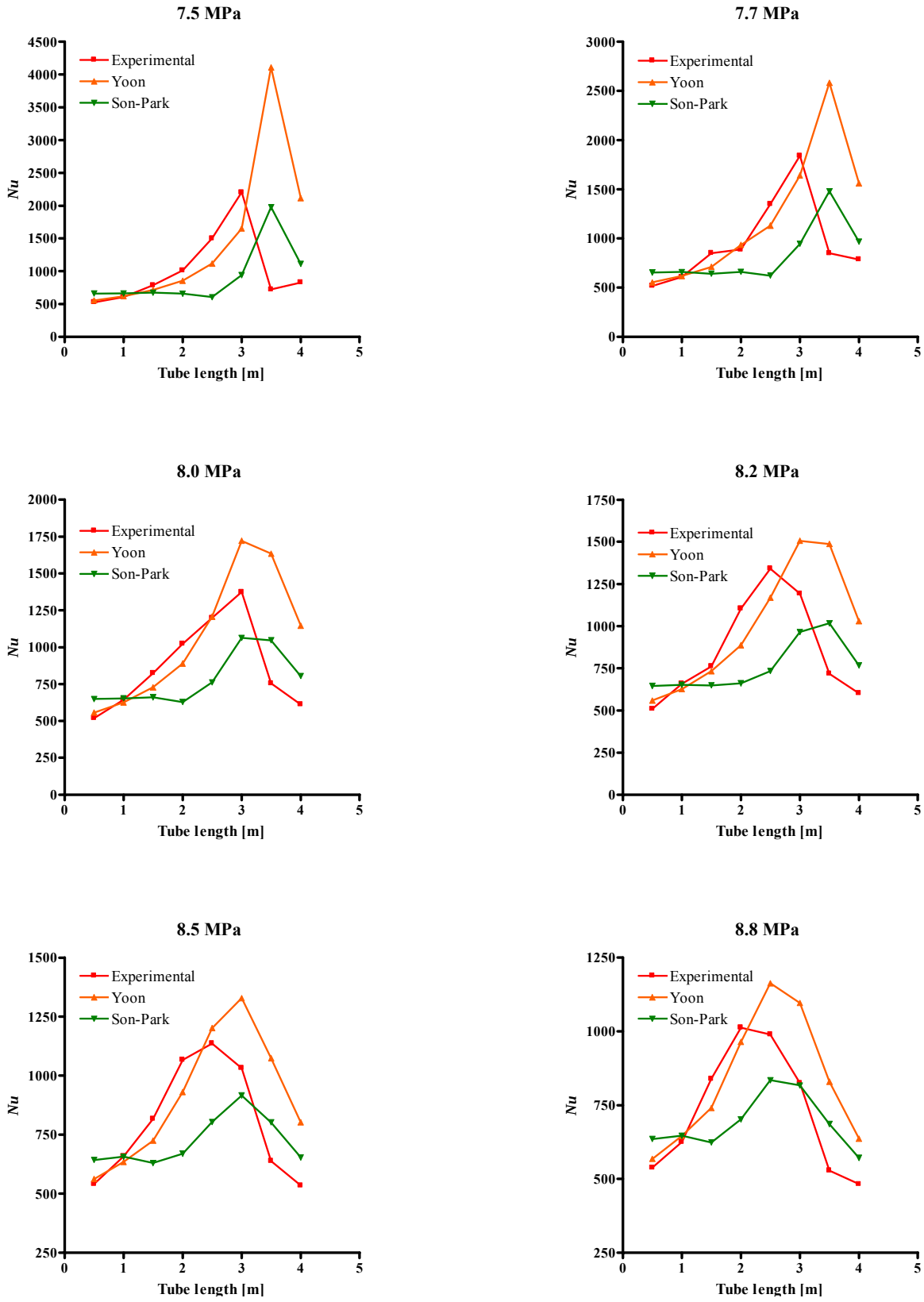

Figure 5.5. Experimentally obtained Nu^s compared to Nu^s calculated according to the Yoon and Son-Park correlations. *Nu*, at different pressures, plotted against the length of a tube-in-tube heat exchanger.

specific heat, but also all other fluid properties change rapidly around the pseudo-critical point (Tsuzuki *et al.*, 2009).

In Figure 5.6 the experimental graph was obtained by plotting Nu_{exp} against itself, which obviously yields a straight line originating at x = y = 0 and with a gradient of unity. The Nu^s, as predicted by the Gnielinski, Modified Gnielinski, Huai and Yoon correlations, were also plotted against Nu_{exp}.

The Gnielinski, Modified Gnielinski and Huai correlations under predict the Nu^s (as can also be seen in Figure 5.3), whilst the gradients of the linear regressions are generally much smaller than unity. The gradients of Gnielinski and Modified Gnielinski graphs are in close proximity at each given pressure, whilst the Modified Gnielinski correlation generally predicts Nu^s slightly larger (average: *9.7%*) than does the Gnielinski correlation (see Table B.3; Appendix B). A graph of *Nu,* predicted by the Yoon correlation, against the Nu_{exp} afforded linear regressions that seemingly compares well with the Nu_{exp} regression (Figure 5.6).

The R^2 values tabulated in Tables 5.1 give an overall idea of the validity of the linear regressions of the Gnielinski, Modified Gnielinski, Huai and Yoon Nu^s. It can be seen that the Nu^s, calculated according to the Gnielinski correlation, generally follow a linear regression with $R^2 > 0.9$ at all the given pressures, except at 8.2 MPa. It can be seen that the poorest linear fit for all three these correlations are found at a pressure of 8.2 MPa (see Table 5.1).

The R^2 values tabulated in Table 5.2 were obtained from linear regressions of the Nu^s depicted in Figure 5.4[17] and the Son-Park correlation depicted in Figure 5.5. All the R^2 values from the Krasnoshchekov, Petrov-Popov, Fang and Son-Park correlations are smaller than 0.9, which are indicative of rather poor linear fits.

Based on the R^2 values (Tables 5.1 and 5.2), the Gnielinski, Modified Gnielinski, Huai and Yoon correlations portray the best overall linear fit. Of these correlations, the Gnielinski correlation generally renders the best linear fit. It was, therefore, decided to proceed only with the Gnielinski correlation in an attempt to produce a newly modified and, hopefully, more accurate *Nu* correlation for cooling of supercritical R-744. Pettersen and co-workers (2000) also reported that the Gnielinski correlation showed an agreeable correspondence with their experimental results.

[17] Linear graphs not shown.

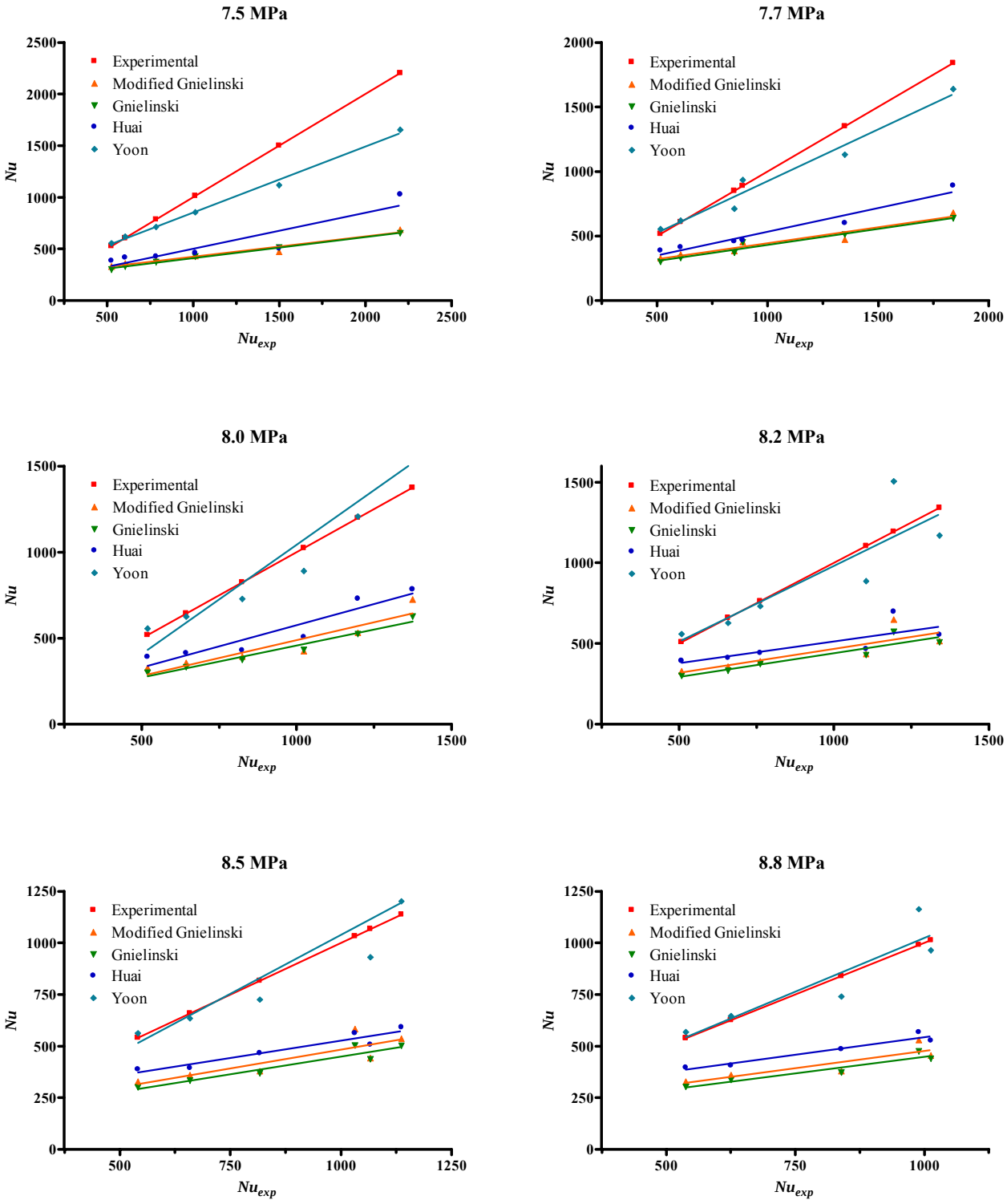

Figure 5.6. Linear regressions for the Gnielinski, Modified Gnielinski, Huai and Yoon correlations at the different pressures. The *Nu* and Nu_{exp} values were obtained from Figure 5.3.

Table 5.1. R^2 values of the linear regressions of Nu-Nu_{exp} graphs, at different pressures, for various correlations (data from Figure 5.6).
Note: in all cases the poorest linear fit was obtained at a pressure of 8.2 MPa.

P **[MPa]**	**Gnielinski**	**Modified Gnielinski**	**Huai**	**Yoon**
7.5	0.9950	0.9591	0.8396	0.9948
7.7	0.9612	0.9260	0.9512	0.9684
8.0	0.9634	0.8560	0.8870	0.8902
8.2	0.8418	0.6845	0.6064	0.7327
8.5	0.9057	0.7398	0.9079	0.7730
8.8	0.9140	0.7776	0.9367	0.8241

Table 5.2. R^2 values of the linear regressions of Nu-Nu_{exp} graphs, at different pressures, for various correlations (linear regressions not shown).
Note: in all cases the poorest linear fit was obtained at a pressure of 8.2 MPa.

p **[MPa]**	**K K P***	**Petrov-Popov**	**Fang**	**Son-Park**
7.5	0.7631	0.7366	0.6672	0.5294
7.7	0.8393	0.8037	0.6832	0.5665
8.0	0.8587	0.8390	0.7330	0.5847
8.2	0.6028	0.5862	0.4288	0.3417
8.5	0.8701	0.8367	0.6360	0.3983
8.8	0.8921	0.8363	0.6484	0.4412

* Krasnoshchekov Kuraeva Protopopov correlation

5.4. Correlations for cooling supercritical R-744

In this section three new successive correlations for cooling supercritical R-744 will be proposed. All three correlations will be based on the Gnielinski *Nu* correlation.

5.4.1. *Correlation I*: Formulation of an average equation based on the Gnielinski correlation

Linear regression equations, based on the Gnielinski correlation data presented in Figure 5.6, are tabulated in Table 5.3. It is important to note that the graphs in Figure 5.6 were plotted with Nu_{exp} as the independent variable, whilst Nu is the dependent variable. Note further, that for the linear regression data tabulated in Table 5.3 (calculated according to: Eq (3.48) and Eqs (3.50) to (3.52)), Nu is the independent variable, whilst, Nu_{exp} is the dependent variable.

From the data in Table 5.3 a new *Nu* correlation, based on the averages of the gradients and intersects, is proposed. The new *Nu* correlation, from here onwards referred to as *Correlation I*, is a linear manipulation of the existing Gnielinski correlation and is represented by:

$$Nu = 3.2897 Nu_G - 440.3 \tag{5.1}$$

where Nu_G is given by Eq (3.22). Eq (5.1) may be employed to calculate Nu^s for pressures ranging from 7.5 to 8.8 MPa when $T \geq T_{pc}$.

In Figure 5.7 the Nu^s, predicted by *Correlation I*, are plotted against the corresponding Nu_{exp}^s. Included in Figure 5.7 are three linear graphs, namely $y = x$, $y = 1.1x$ and $y = 0.9x$, *i.e.* the linear

Table 5.3. Gradients and intercepts of the linear regressions ($y = mx + c$) of Gnielinski data at different pressures.
Note: *Nu* is the independent variable, whilst Nu_{exp} is the dependent variable.
Average gradient = 3.2897 and average y-intercept = -440.3.

***p* [MPa]**	**Gradient (*m*)**	**y-Intercept (*c*)**
7.5	4.8780	-1004.5
7.7	3.8533	-660.03
8.0	2.5967	-188.92
8.2	2.8855	-280.44
8.5	2.6633	-208.73
8.8	2.8613	-299.16

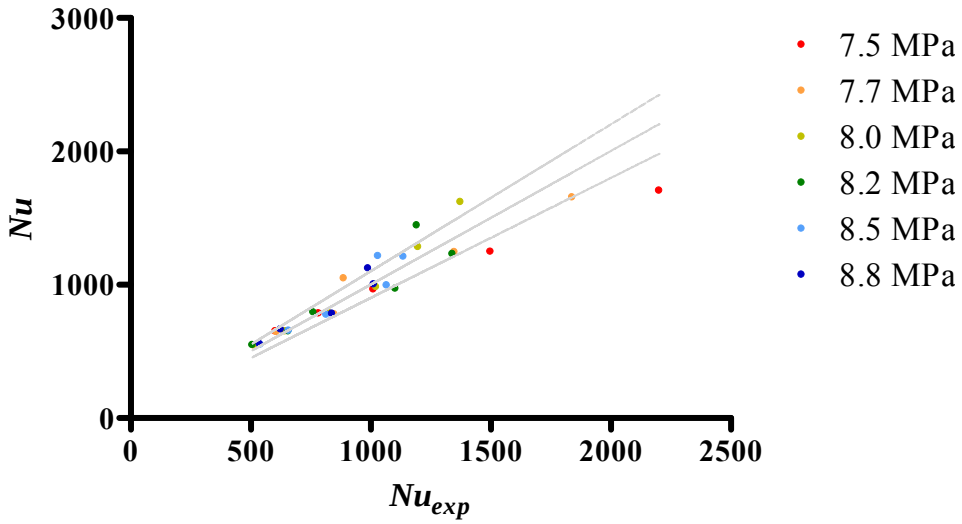

Figure 5.7. *Correlation I*: Linear graph *(x = 1)* of Nu_{exp} against *Nu*. *Nu* was calculated according to Eqs (5.1). The two outer linear graphs, *y = 1.1x* and *y = 0.9x,* indicate a 10% deviation interval.

direct proportional graph of unity with a 10% deviation interval. It can be seen in Figure 5.7 that the smaller values of *Nu* are within a 10% deviation interval. But, as *Nu* increase, the percentage deviation interval also increases.

In the following Section a second correlation, namely *Correlation II,* will be defined.

5.4.2. *Correlation II*: Formulation of an average equation based on the Gnielinski correlation using a modified Haaland friction factor correlation

It was mentioned in Section 3.5.2 that either the Filonenko or Haaland friction factor, as defined in Section 3.7, may be used with the Gnielinski correlation. Up to now (see Section 3.5.2), the Filonenko friction factor (independent of the tube roughness) was used in this study. In this section onwards, a modification on the Haaland friction factor, Eq (3.39), will be used with the Gnielinski correlation in an attempt to find a better *Nu* correlation.

5.4.2.1. Modification of the Haaland friction factor

Unlike the Filonenko friction factor, the Haaland friction factor depends on the tube roughness. However, the tube roughness was not reported in the study of Yoon and co-workers (2003), but, it was mentioned that R-744 was flowing through a copper tube (it will be assumed to be drawn tubing). For drawn tubing the tube roughness, namely ε, may be taken as 1.5 μm (see Table 5.4). By accepting a value of 1.5 μm for the tube roughness, the Haaland friction factor correlation was modified to yield a new friction factor correlation. This newly modified Haaland friction

Table 5.4. Average roughness of commercial pipes (Shames, 2003).

Material	ε [mm]
Glass	0.0003
Drawn tubing	0.0015
Steel, wrought iron	0.046
Asphalted cast iron	0.12
Galvanized iron	0.15
Cast iron	0.26
Wood stave	0.18 to 0.9
Concrete	0.3 to 3.0
Riveted steel	0.9 to 9.0

factor correlation is defined by:

$$f_{mH} = \left(-1.8 \log \left(\frac{6.9}{\mathrm{Re}_b} + \left(\frac{20\varepsilon}{3.7 D_H} \right)^{1.11} \right) \right)^{-2} \tag{5.2}$$

Eq (5.2) was obtained by multiplying the tube roughness factor, ε, in Eq (3.39) with a factor 20.[18]

5.4.2.2. Formulation of *Correlation II*

The modified Haaland friction factor, Eq (5.2), was combined with the Gnielinski correlation to yield a modified Gnielinski correlation, which will be referred to as Gnielinski MH. Nu_{GMH} calculated according to the Gnielinski MH correlation was calculated and plotted under exactly the same conditions that prevailed for the Gnielinski, Modified Gnielinski, Huai and Yoon correlations (Figure 5.6). These calculated $Nu_{GMH}{}^{s}$, and the Nu_{GMH}-tube length graphs are given in Appendix B (Section B.4). The linear regression equations and R^2 values obtained from the Gnielinski MH correlation are shown in Table 5.5, where Nu_{GMH} is the independent variable and Nu_{exp} the dependent variable. The 8.2 MPa linear regression has the poorest R^2 fitting, as compared to the R^2 fittings at 7.5, 7.7, 8.0, 8.5 and 8.8 MPa (also see Tables 5.1 and 5.2).

Table 5.5. Gradients and intercepts of the linear regressions (y = *m*x + *c*) of Gnielinski MH data at different pressures. Note: Nu_{GMH} is the independent variable, whilst Nu_{exp} is the dependent variable.
Average gradient = 3.1852 and average y-intercept = -1060.91.

***p* [MPa]**	**R^2**	**Gradient (*m*)**	**y-Intercept (*c*)**
7.5	0.9916	4.2933	-1720.2
7.7	0.9579	3.4593	-1253.2
8.0	0.9754	2.4755	-661.65
8.2	0.8675	2.8457	-851.22
8.5	0.9599	2.9025	-872.58
8.8	0.9518	3.1840	-1006.6

The average gradient and intersect values of the linear regressions of the Gnielinski MH correlation, obtained from the values tabulated in Table 5.5, were now employed to create the second new *Nu* correlation. This new correlation, from here onwards referred to as *Correlation II*, incorporates Nu_{GMH} and is defined by:

[18] The factor 20 was arbitrarily chosen. It was not in the scope of this study to find the optimal multiplication factor for ε.

$$Nu = 3.1852 Nu_{GMH} - 1060.91 \tag{5.3}$$

where Nu_{GMH} represents the Gnielinski MH *Nu*. correlation.

Eq (5.3) may be employed to calculate *Nu* for pressures ranging from 7.5 to 8.8 MPa when $T \geq T_{pc}$. In Figure 5.8 the Nu^s, predicted by *Correlation II*, are plotted against the corresponding $Nu_{exp}{}^s$. Included in Figure 5.8 are three linear graphs, namely $y = x$, $y = 1.1x$ and $y = 0.9x$, *i.e.* the linear direct proportional graph of unity with a 10% deviation interval. It can be seen in Figure 5.8, as for *Correlation I* in Figure 5.7, that the smaller of *Nu* are within a 10% deviation interval. As *Nu* increase, the percentage deviation interval also increases, but to a lesser degree than was observed for *Correlation I* (Figure 5.7). It follows from Figure 5.8 that *Correlation II* predicts more accurate Nu^s than does *Correlation I*.

In the following Section, a third correlation, namely *Correlation III* will be defined.

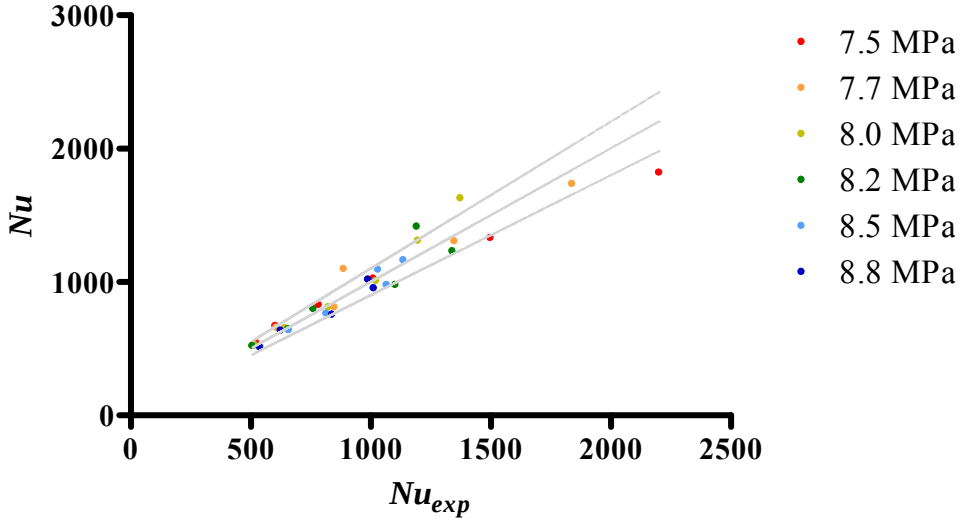

Figure 5.8. *Correlation II*: Linear graph *(x = 1)* of Nu_{exp} against *Nu*. *Nu* was calculated according to Eqs (5.3). The two outer linear graphs, $y = 1.1x$ and $y = 0.9x$, indicate a 10% deviation interval.

5.4.3. *Formulation* of a linear equation based on the Gnielinski Modified Haaland correlation

Although *Correlation II*, represented by Eq (5.3), was formulated from data tabulated in Table 5.5, this tabulated data may also be used to formulate a third and more advanced correlation. This was accomplished by plotting the data in Table 5.5, *i.e.* the gradients and y-intercepts against pressure, to yield the graphs shown in Figures 5.9a and 5.9b. These graphs display a

noteworthy trend for both the gradient and intersect. In Figure 5.9a the gradient seems to decrease linearly from a pressure of 7.5 to 8.0 MPa. From a pressure of 8.0 to 8.8 MPa, the gradient rise in a seemingly linear fashion. However, for the y-intercept (Figure 5.9b), the trend is exactly the opposite. For pressures 7.5 to 8.0 MPa, there is a linear rise in the intercept values, whereas a seemingly linear decline is found for the intercept values at pressures 8.0 to 8.8 MPa.

In both Figures 5.9a and 5.9b linear regressions may be performed in two sections. In Figures 5.9a and 5.9b, linear regressions were firstly carried out for pressures of 7.5 to 8.0 MPa and, secondly for pressures of 8.0 to 8.8 MPa.

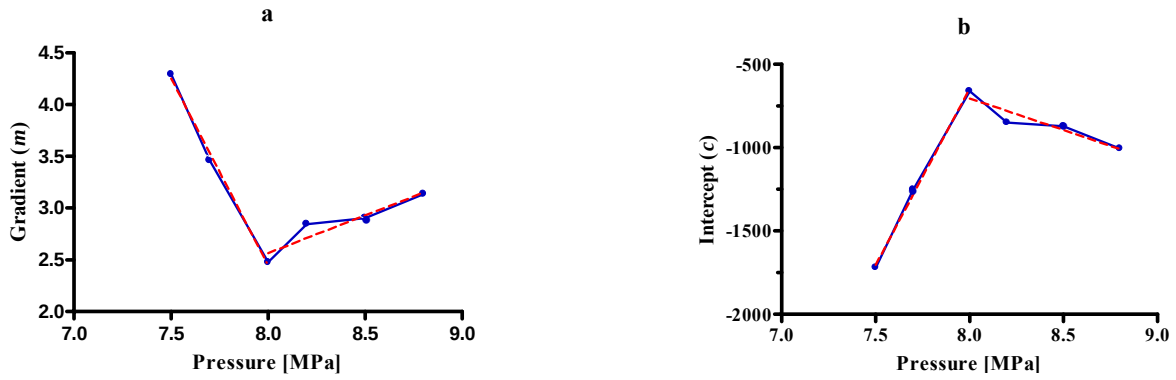

Figure 5.9. Graphs of the linear regression data given in Table 5.5. Note the so called *'turning point pressure'* at 8.0 MPa.
a. Solid line: Gradient (*m*)-pressure (*p*) graph. Broken lines: Linear regressions (data shown in Table 5.6).
b. Solid line: Intercept (*c*)-pressure (*p*) graph. Broken lines: Linear regressions (data shown in Table 5.7).

Tables 5.6 and 5.7 display equations for the gradient and intercept regressions at pressures ranging from 7.5 to 8.8 MPa, respectively. For pressures ranging from 7.5 to 8.0 MPa, both the gradient and intercept linear regressions demonstrate R^2 values of almost unity. For the pressure

Table 5. 6. Linear regressed equations obtained from the Gnielinski MH gradient-pressure graphs (see Figure 5.9a and Table 5.5). The equations were obtained for the given pressure range.

Pressure range [MPa]*	Gradient equations	R^2
7.5 to 8.0	$m(p) = -3.6075p + 31.307$	0.9955
8.0 to 8.8	$m(p) = 0.7314p - 3.2859$	0.8788

Table 5.7. Linear regressed equations obtained from the Gnielinski MH intercept-pressure graphs (see Figure 5.9b and Table 5.5). The equations were obtained for the given pressure range.

Pressure range [MPa]	Intercept equations	R^2
7.5 to 8.0	$c(p) = 2105.6p - 17495$	0.9978
8.0 to 8.8	$c(p) = -380.4p + 2337.8$	0.8790

range of 8.0 to 8.8 MPa, the R^2 values of the linear regressions for both the gradients and intercepts are smaller than 0.9. This deviation from linearity may be attributed to the influence of Nu^s obtained at a pressure of 8.2 MPa. In Figures 5.7a and 5.7b it can be seen that the values obtained at 8.2 MPa deviate much more from the linear trend than the rest of the values. This observation correlates with previous observations (see Sections 5.3 and 5.4.2.2).[19]

It follows from Figures 5.7a and 5.7b that 8.0 MPa is a turning point for both the gradients and intercepts. This pressure will be referred to as the *'turning point pressure'* for cooling supercritical R-744, and will be denoted by p_{TP}. A non-dimensional pressure ratio, namely the *turning point pressure ratio*, may now be defined as:

$$\chi_p = \frac{p}{p_{TP}} \tag{5.4}$$

5.4.3.1. Correlation III

From the data in Tables 5.6 and 5.7 a new correlation, namely *Correlation III*, for turbulent cooling supercritical R-744, based on the linear regressions from Gnielinski MH can be defined as:

$$Nu = m(p)Nu_{GMH} + c(p) \tag{5.5}$$

Eq (5.5) is a basic equation that may converted to a practically useful equation by substituting $m(p)$ and $c(p)$ with relevant equations.

A practically useful Nu correlation for R-744, that is valid for pressures from 7.5 to 8.0 MPa, was obtained by substituting $m(p)$ and $c(p)$, in Eq (5.5), with the relevant data from Tables 5.6 and 5.7. Substitution of p in the obtained equation with Eq (5.4), gives:

$$Nu = \left(-28.86\chi_p + 31.307\right)Nu_{GMH} + 16844.8\chi_p - 17495 \tag{5.6}$$

[19] It is a possibility that the values obtained at a pressure of 8.2 MPa may be somewhat suspect. It should be noted that the experimental data employed in this chapter was obtained from the literature, thus no conclusion can be made regarding the correctness of the particular value or values.

Eq (5.6) is valid if 7.5 MPa $\leq p <$ 8.0 MPa and $T \geq T_{pc}$.

The following equation, which is valid when 8.0 MPa $\leq p \leq$ 8.8 MPa and $T \geq T_{pc}$, is obtained analogous to Eq (5.6):

$$Nu = \left(5.8512\chi_p - 3.2859\right)Nu_{GMH} - 3043.2\chi_p + 2337.8 \tag{5.7}$$

In Eqs (5.6) and (5.7) Nu_{GMH} is the Gnielinski correlation given by Eq (3.22), when a modified Haaland friction factor, Eq (5.2), is used. This modified Eq (3.22) is represented by:

$$Nu_{GMH} = \frac{f_{MH}}{8}\left(\mathrm{Re}_b - 1000\right)\mathrm{Pr}_b\left[1.07 + 12.7\sqrt{\frac{f_{MH}}{8}}\left(\mathrm{Pr}_b^{2/3} - 1\right)\right]^{-1} \tag{5.8}$$

Eqs (5.6), (5.7) and (5.8) may be employed to calculate Nu at defined pressures, when $T \geq T_{pc}$.

No relevant data for the calculation of Nu^s could be obtained for pressures not included in this study, *i.e.* pressures outside the range 7.5 to 8.8 MPa. It follows that the new proposed correlation, represented by Eqs (5.6), (5.7) and (5.8), may possibly only be valid within this given pressure range. It is important to note that this correlation is only applicable for turbulent R-744 subjected to supercritical cooling and, when $T \geq T_{pc}$.

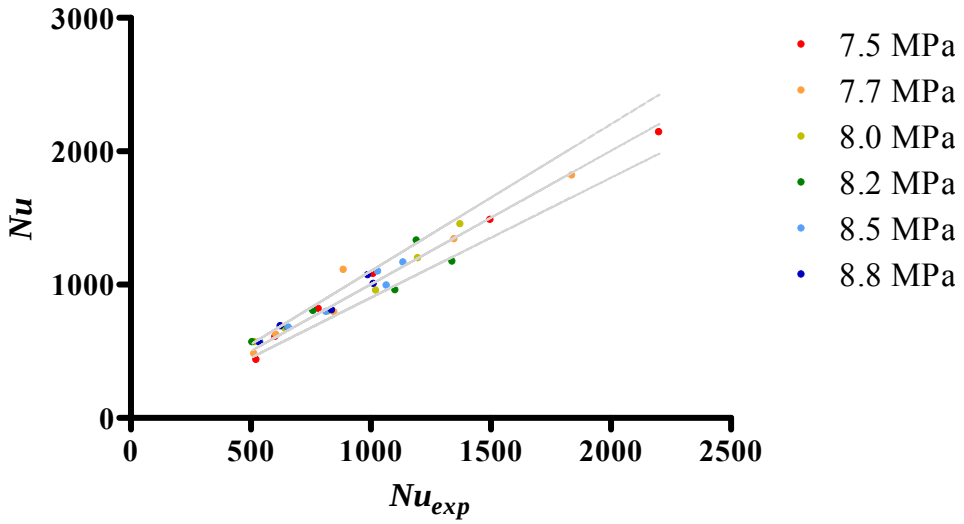

Figure 5.10. *Correlation III:* Linear graph *(x = 1)* of Nu_{exp} against Nu. Nu was calculated according to Eqs (5.6), (5.7) and (5.8). The two outer linear graphs, $y = 1.1x$ and $y = 0.9x$, indicate a 10% deviation interval.

Figure 5.10 shows the predicted *Correlation III* Nu^s plotted against the $Nu_{exp}{}^s$. Included in Figure 5.10 are three linear graphs ($y = x$, $y = 1.1x$ and $y = 0.9x$), *i.e.* the linear direct proportional graph of unity and two graphs representing a 10% deviation interval. It can be seen

in Figure 5.10 that *Nu* and the corresponding Nu_{exp} are within a 10% deviation interval, except for six data points (see Table 5.9). These six data points will be discussed in Section 5.6. When comparing Figures 5.7, 5.8 and 5.10, it seems that *Correlation III* is the more accurate correlation for the prediction of *Nu*.

5.5. Comparing the results predicted by the three new *Nu* correlations

The accuracy of the three new *Nu* correlations, defined in Sections 5.4.1, 5.4.2.2 and 5.4.3, will be scrutinised in this section. The correlation that predicts the most accurate Nu^s, will be the correlation employed in this study for the calculation of Nu^s for cooling supercritical R-744.

Table 5.8 shows the average deviation at every pressure set, namely $\overline{dev}_p$, and the average deviation, $\overline{dev}$, for all the data, as predicted by the three *Nu* correlations (see Appendix B; Section B.5 for *Correlations I* and *II dev's* and Table 5.9 for *Correlation III dev's*). The deviation, as a percentage, for every data point can be calculated according to the following equation:

$$dev = 100\frac{\left|Nu_{\exp} - Nu\right|}{Nu_{\exp}} \tag{5.6}$$

where *dev* is the percentage deviation at a particular point and $\overline{dev}$ is the average deviation for all the data points, according to Eq (3.48).

Table 5.8. The $\overline{dev}_p$ for the correlations, at each of the given pressures, is the average deviation of *Nu* over the entire length of the heat exchanger.
$\overline{dev}$ for *Correlation I* = 7.77; $\overline{dev}$ for *Correlation II* = 6.69; $\overline{dev}$ for *Correlation III* = 6.11

p **[MPa]**	$\overline{dev}_p$ **for *Correlation I*** **Eq (5.1)**	$\overline{dev}_p$ **for *Correlation II*** **Eq (5.3)**	$\overline{dev}_p$ **for *Correlation III*** **Eqs (5.4) and (5.6) to (5.8)**
7.5	9.29	8.20	5.42
7.7	9.20	7.97	7.29
8.0	6.41	5.49	4.81
8.2	9.05	7.94	9.30
8.5	6.33	5.22	4.26
8.8	6.03	5.05	5.52

It can be seen in Table 5.8 that all three correlations, namely Eq (5.1), Eq (5.3) and Eqs (5.6), (5.7) and (5.8), predict the *Nu* on average (per pressure) within a 10% deviation interval. *Correlation II*, Eq (5.3), has more acceptable average deviations than C*orrelation I*, Eq (5.1), at

every one of the following pressures: 7.5, 7.7, 8.0, 8.2, 8.5 and 8.8 MPa. Therefore, *Correlation II* is deemed to be the more accurate of these two correlations. However, *Correlation III*, Eqs (5.6), (5.7) and (5.8), has lower average deviations than C*orrelation II*, at every pressure except 8.2 MPa and is, therefore, deemed to be the more accurate of the latter two correlations. *Correlation III* is thus the most accurate correlation of the three proposed correlations, which may be employed to predict Nu^s for cooling supercritical R-744. The respective $\overline{dev}^s$ for *Correlations I, II* and *III*, are $\overline{dev}$ = 7.77%, $\overline{dev}$ = 6.69% and $\overline{dev}$ = 6.11% (Table 5.8).

5.5.1. Conclusion

Correlation III proved to be more accurate than *Correlations I* and *II*. For the applicable experimental data, it also seems to be more accurate than the existing correlations found in the literature that was employed in this study. Due to the lack of experimental data, no conclusion could be made regarding the validity of the correlation(s) outside the specified pressure range. Although the correlation(s) may possibly be employed outside the specified pressure range, it should certainly not be employed for temperatures below the pseudocritical temperature.

5.6. Summary

In this chapter Nu_{exp}, obtained from the literature, were compared with various *Nu* correlations found in the literature. The *Nu* correlations included in this study generally tend to under predict *Nu* values. It was possible to group correlations according to the general patterns of their *Nu*-tube length graphs.

Graphs of Nu_{exp} against Nu^s, calculated according to the Gnielinski correlation, generally follow a linear regression with $R^2 > 0.9$ when $T \geq T_{pc}$. From this data a new correlation, *Correlation I*, based on average gradients and intersects, was proposed. A modified Haaland friction factor was used with the Gnielinski correlation to yield a second correlation, namely *Correlation II*. By mathematically manipulating Nu^s predicted by the Gnielinski correlation, a third and more advanced correlation, *Correlation III*, was formulated. For the formulation of *Correlation III* a new parameter, namely the *turning point pressure ratio of cooling supercritical R-744*, was defined.

Correlations I, II and *III* for cooling supercritical R-744 may only be valid for a diameter in the order of the experimental diameter of 7.73 mm, temperatures that are equal or above the pseudocritical temperatures and at pressures ranging from 7.5 to 8.8 MPa.

CHAPTER

Summary and Conclusions 6

This study consisted of three independent investigations given in Chapters 4 and 5. The main aim for this study was to implement and compare various Nusselt number correlations for the cooling of v R-744.

Chapter 4

In Chapter 4 the various *Nu* correlations found in the literature were compared *via* theoretical simulations of an R-744-to-water heat exchanger. The heat exchanger was of a tube-in-tube configuration. No experimental data was displayed in this chapter, so that theoretical Nu^s were compared only to theoretical Nu^s. It was concluded that, even though there was no experimental data to compare the theoretical data with, an accurate *Nu* correlation for supercritical R-744 in cooling needs to be found. This conclusion was made due to the fact that the various *Nu* correlations varied considerably, in the prediction of the *Nu* numbers, over the length of the heat exchanger.

Chapter 5

This chapter formed the crux of this study. In Chapter 5 the various *Nu* correlations employed in Chapter 4 were compared to experimental Nu^s, reported in the literature. Chapter 5 did not consist of simulations, but the theoretical Nu^s for the various correlations were calculated by applying knowledge of the applicable pressure, mass flow rate, bulk temperature and wall temperatures. A new *Nu* correlation was also presented in this chapter. The validity of the proposed correlation could, however, only be guaranteed for a diameter in the order of the experimental diameter and the given range of pressures used to obtain the experimental data. It was emphasised that the new correlation should not be employed for a temperature less than the applicable pseudocritical temperature.

Future studies

There exist great opportunities for employing R-744 for heating and cooling purposes. However, heating and cooling systems may only be simulated with accuracy if accurate *Nu* correlations are available for all operational diameters, pressures and temperatures.

It is thus proposed that an experimental test unit should be constructed. From this test unit it should be possible to attain data for higher temperatures and pressures, preferably up to 120 ºC and 12 MPa, than the experimental test unit of Yoon and co-workers (2003). The experimental test section must also be able to generate adequate data for temperatures lower than the pseudocritical temperature at every pressure and for a variety of tube diameters. Once accurate *Nu* correlations for R-744 are obtained, accurate simulations may be performed for the simulation and eventual construction of R-744 systems for heating and cooling purposes.

References

AICHER, T. & MARTIN, H. 1997. New correlation for mixed turbulent natural and forced convection heat transfer in vertical tubes. *International Journal of Heat and Mass Transfer,* 40(15):3617-3626.

ALDANA, J.P., GEORGIADIS, J.G. & JACOBI, A.M. 2002. Critical Heat Flux of CO2 in a Microchannel at Elevated Subcritical Pressures. *Air-conditioning and Refrigeration Center,* CRC TR-195, March. The University of Illinois, Urbana-Champaign. 90 p.

ANDRESEN, U.C. 2007. Supercritical gas cooling and near-critical-pressure condensation of refrigerant blends in microchannels. Georgia Institute of Technology, Atlanta. (Thesis – Ph.D.). 17 – 23 p.

BASKOV, V.L., KURAEVA, I.V. & PROTOPOPOV, V.S. 1977. Heat transfer with the turbulent flow of a liquid at supercritical pressure in tubes under cooling conditions. *High Temperature,* 15(1):81–86. *(English translation of Teplofizika Vysokikh Temperatur, 15(1):96–102).*

BREDESEN, A.M., AFLEKT, K., PETTERSEN, J., HAFNER, A., NEKSÅ, P. & SKAUGEN, G. 1997a. Studies on CO_2 heat exchange and heat transfer. (*In* CO_2 technology in refrigeration, heat pumps and air conditioning systems. IEA Heat pump centre, Trondheim, Norway).

BREDESEN, A.M., HAFNER, A., PETTERSEN, J. & NEKSÅ, K. 1997b. Heat transfer and pressure drop for in-tube evaporation of CO_2. (*In* Heat transfer in natural refrigerants. College Park, Maryland). 1-15 p.

R.P. BRINGER, R.P. & SMITH, J.M. 1957. Heat Transfer in the Critical Region. *American Institute of Chemical Engineers,* 3(1):49–55.

BRUCH, A., BONTEMPS, A. & COLASSON, S. 2009. Experimental investigation of heat transfer of supercritical carbon dioxide flowing in a cooled vertical tube. *International Journal of Heat and Mass Transfer,* 52:2589-2598.

CHEN, N., KWON, H., RAY, A. & WONG, R. 2005. Flow in the Pipes: Correlation between Fanning Friction Factor and Reynolds Number. Transport Process Laboratory, Carnegie Mellon University, Pittsburgh, Pennsylvania.

CHENG, L., RIBATSKI, G. & THOME, J.R. 2008. Analysis of supercritical CO_2 cooling in macro- and micro-channels. *International Journal of Refrigeration*, 31:1301-1316.

DANG, C. & HIHARA, E. 2004. In-tube cooling heat transfer of supercritical carbon dioxide. Part 1. Experimental measurement. *International Journal of Refrigeration,* 27:736-747.

DITTUS, F.W. & BOELTER, L.M.K. 1930. Heat transfer in automobile radiators of the tubular type. *University of California, Berkeley, Publications in Engineering,* 2:443-461.

DORIN, F. 1999. Semi-hermetic CO_2 compressors for commercial applications. (*In* CO_2 technology in refrigeration, heat pump and air conditioning system. Mainz, Germany).

FANG, X., BULLARD, C.W. & HRNJAK, P.S. 2001. Modelling and analysis of gas coolers. *Ashrae Transactions,* 107(1):4-13.

FILONENKO, G.K. 1954. Hydraulic Resistance in Pipes. *Teploenergetika,* 1:10-44.

GHAJAR, A.J. & ASADI, A. 1986. Improved Forced Convective Heat Transfer Correlations for Liquids in the near-Critical Region. *American Institute of Aeronautics and Astronautics Journal*, 24(12):2030-2037.

GNIELINSKI, V. 1976. New equations for heat and mass transfer in turbulent pipe and channel flow. *International Chemical Engineering,* 16(2):359-368.

HAALAND, S.E. 1983. Simple and explicit formulas for the friction-factor in turbulent pipe flow. *Transactions of the ASME (Journal of Fluids Engineering),* 105:89-90.

HUAI, X.L., KOYAMA, S. & ZHAO, T.S. 2005. An experimental study of flow and heat transfer of supercritical carbon dioxide in multiport mini channels under cooling conditions. *Chemical Engineering Science*, 60:3337-3345.

INCROPERA, F.P., DEWITT, D.P. BERGMAN, T.L. & LAVINE, A.S. 2006. Fundamentals of Heat and Mass Transfer. 6th Edition. New York: John Wiley and Sons.

JACKSON, J. D. & FEWSTER, J. 1975. AERE-R8158. Harwell.

JACKSON, J.D. & HALL, W.B. 1979. Forced convection heat transfer to fluids at supercritical pressures. (*In* Kakac, S. & Spalding, D.B., eds. Turbulent forced convection in channels and bundles 2. Washington: Hemisphere). 563-611 p.

KRASNOSHCHEKOV, E.A. & PROTOPOPOV, V.S. 1966. Experimental study of heat exchange in carbon dioxide in the supercritical range at high temperature drops. *High Temperature,* 4(3):375–382. *(English translation of Teplofizika Vysokikh Temperatur, 4:(3):389–398)*.

KRASNOSHCHEKOV, E.A., KURAEVA, I.V. & PROTOPOPOV, V.S. 1969. Local heat transfer of carbon dioxide at supercritical pressure under cooling conditions. *High Temperature,* 7(5):856–861. *(English translation of Teplofizika Vysokikh Temperatur, 7(5):922-930)*.

KURGANOV, V.A. 1998a. Heat Transfer and Pressure Drop in Tubes under Supercritical Pressure of the Coolant. Part 1: Specifics of the Thermophysical Properties, 258 Hydrodynamics, and Heat Transfer of the Liquid. Regimes of Normal Heat Transfer. *Thermal Engineering,* 45(3):177-185. *(English translation of Teploenergetika)*.

KURGANOV, V.A. 1998b. Heat Transfer and Pressure Drop in Tubes under Supercritical Pressure. Part 2. Heat Transfer and Friction at High Heat Fluxes. The Influence of Additional Factors. Enhancement of Deteriorated Heat Transfer. *Thermal Engineering,* 45(4):301-310. *(English translation of Teploenergetika).*

LIAO, S.M. & ZHAO, T.S. 2002. Measurements of Heat Transfer Coefficients From Supercritical Carbon Dioxide Flowing in Horizontal Mini/Macro Channels. *Journal of Heat Transfer,* 124:413-420.

McADAMS, W.H. 1954. Heat transmission. New York: McGraw-Hill.

MITRA, B. 2005. Supercritical Gas Cooling and Condensation of Refrigerant R410a at near-Critical Pressures. Georgia Institute of Technology, Atlanta. (Thesis - Ph.D.). 34 – 35; 43 – 45 p.

NEKSÅ, P., DORIN, F., REKSTAD, H., BREDESEN, A.M. & SERBISSE, A. 1999. Development of semi-hermetic CO_2-compressors. (*In* 20th *International Congress of Refrigeration IIR/IIF*. Sydney. Australia).

NEKSÅ, P., REKSTAD, H., ZAKERI, G.R. & SCHIEFLOE, P.A. 1998. CO_2-heat pump water heater: characteristics, system design and experimental results. *International Journal of Refrigeration,* 21:172-179.

OLSEN, D.A., ALLEN, D. 1998. Heat Transfer in Turbulent Supercritical Carbon Dioxide Flowing in a Heated Horizontal Tube. *NISTIR 6234, U.S. Department of Commerce Report, National Institute of Standards and Technology (NIST)*. Gaithersburg, Maryland.

PEARSON, A. 2005. Carbon dioxide – new uses for an old refrigerant. *International Journal of Refrigeration,* 28:1140-1148.

PETROV, N.E. & POPOV, V.N. 1985. Heat transfer and resistance of carbon dioxide being cooled in the supercritical region. *Thermal Engineering,* 32(3):131-134.

PETTERSEN, J., RIEBERER, R. & LEISTER, A. 2000. Heat transfer and pressure drop characteristics of supercritical carbon dioxide in microchannel tubes under cooling. *(In Proc. of the 4th IIR-Gustav Lorentzen Natural Working Fluids Conference. Purdue).* 99–106 p.

PETUKHOV, B.S. 1970. Heat transfer and friction in turbulent pipe flow with variable physical properties. *Advances in Heat Transfer*, 6:511-564.

PETUKHOV, B.S. & KIRILLOV, V.V. 1958. On heat exchange at turbulent flow of liquid in pipes. *Teploenergetika,* 4:63-68.

PETUKHOV, B.S., KRASNOSHCHEKOV, E.A. & PROTOPOPOV, V.S. 1961. An investigation of heat transfer to fluids flowing in pipes under supercritical conditions. *(In the 1961 ASME International Heat Transfer Conference, Part 3. University of Colorado, Boulder, Colorado, USA).* 569–578 p.

PITLA, S.S., GROLL, E.A. & RAMADHYANI, S. 2002. New correlation to predict the heat transfer coefficient during in-tube cooling of turbulent supercritical CO_2. *International Journal of Refrigeration,* 25:887-895.

PITLA, S.S., ROBINSON, M.D., GROLL, E.A. & RAMADHYANI, S. 1998. Heat Transfer from Supercritical Carbon Dioxide in Tube Flow: A Critical Review. *International Journal of HVAC&R Research,* 4(3):281-301.

RICE, J.A. 1995. Mathematical Statistics and Data Analysis. 2nd Edition. Belmont, California: Duxbury Press.

ROUSSEAU, P.G. 2007. Thermal-fluid Systems Modelling. Potchefstroom: Platinum Press.

SHAMES, I.H. 2003. Mechanics of fluid. 4th Edition. New York: McGraw-Hill. 412 p.

SHITSMAN, M. E. 1963. Impairment of the Heat Transmission at Supercritical Pressures. *High Temperature,* 1(2):237–244. *(English translation of Teplofizika Vysokikh Temperatur, 1(2):267-275)*.

SON, C.H. & PARK, S.J. 2006. An experimental study on heat transfer and pressure drop characteristics of carbon dioxide during gas cooling process in a horizontal tube. *International Journal of Refrigeration,* 29:539-546.

SONNTAG, R.E., BORGNAKKE, C. & VAN WYLEN, G.J. 2003. Fundamentals of Thermodynamics. 6th Edition. New York: John Wiley and Sons.

TANAKA, H., NISHIWAKI, N., HIRATE, M. & TSAGE, A. 1971. Forced Convection Heat Transfer to a Fluid near Critical Point Flowing in Circular Tube. *International Journal of Heat and Mass Transfer,* 14:739-750.

TSUZUKI, N., UTAMURA, M. & NGO, T.L. 2009. Nusselt number correlations for a microchannel heat exchanger hot water supplier with S-shaped fins. *Applied Thermal Engineering,* 29(16):3299-3308.

WHITE, S.D., YARRAL, M.G., CLELAND, D.J. & HEDLEY, R.A. 2002. Modelling the performance of a transcritical CO_2 heat pump for high temperature heating. *International Journal of Refrigeration,* 25:479-486.

YOON, S.H., KIM, J.H., HWANG, Y.W., KIM, M.S., MIN, K. & KIM, Y. 2003. Heat transfer and pressure drop characteristics during the in-tube cooling process of carbon dioxide in the supercritical region. *International Journal of Refrigeration,* 26:857-864.

Appendix A: *Thermodynamic graphs of supercritical R-744*

A.1. Thermodynamic graphs of a turbulent supercritical R-744 gas cooler simulation

Figures A.1 to A.4 show the thermodynamic graphs of specific heat over constant pressure, c_p, conductivity, k, density, ρ and viscosity, μ, for the theoretical simulation of the supercritical R-744 gas cooler (Chapter 4).

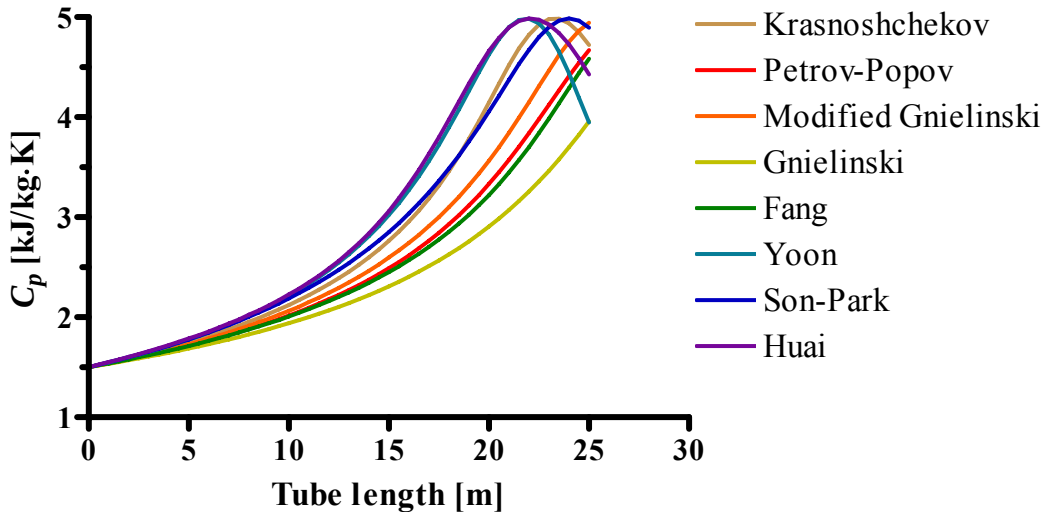

Figure A.1. Specific heat over constant pressure, c_p, is plotted over the length of the heat exchanger for different *Nu* correlations.

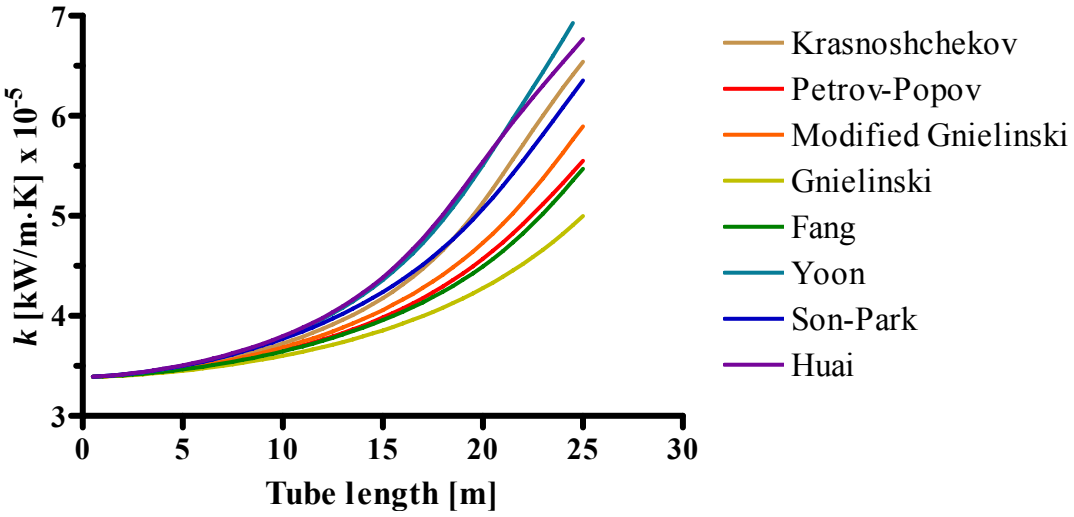

Figure A.2. Conductivity, k is plotted over the length of the heat exchanger for different *Nu* correlations.

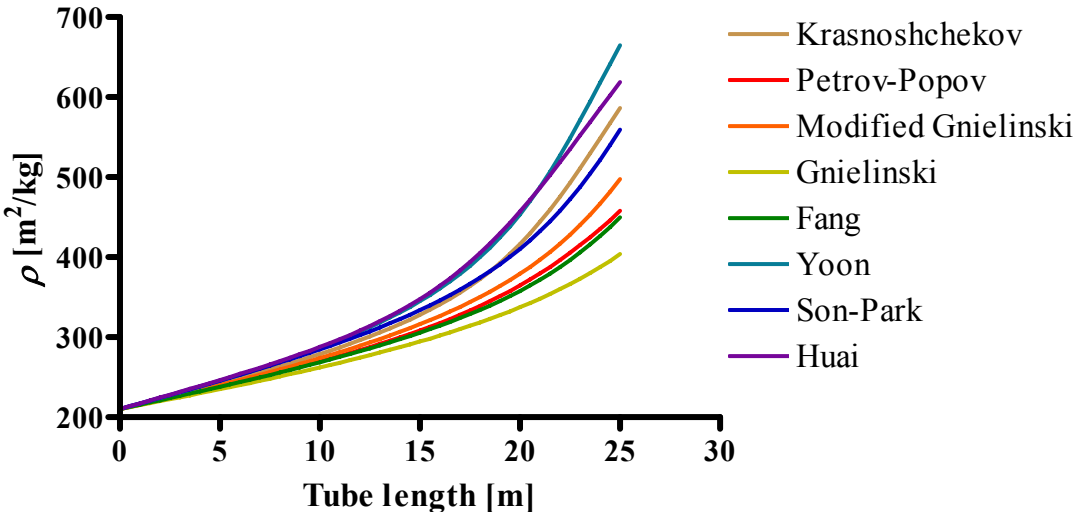

Figure A.3. Density, ρ, is plotted over the length of the heat exchanger for different *Nu* correlations.

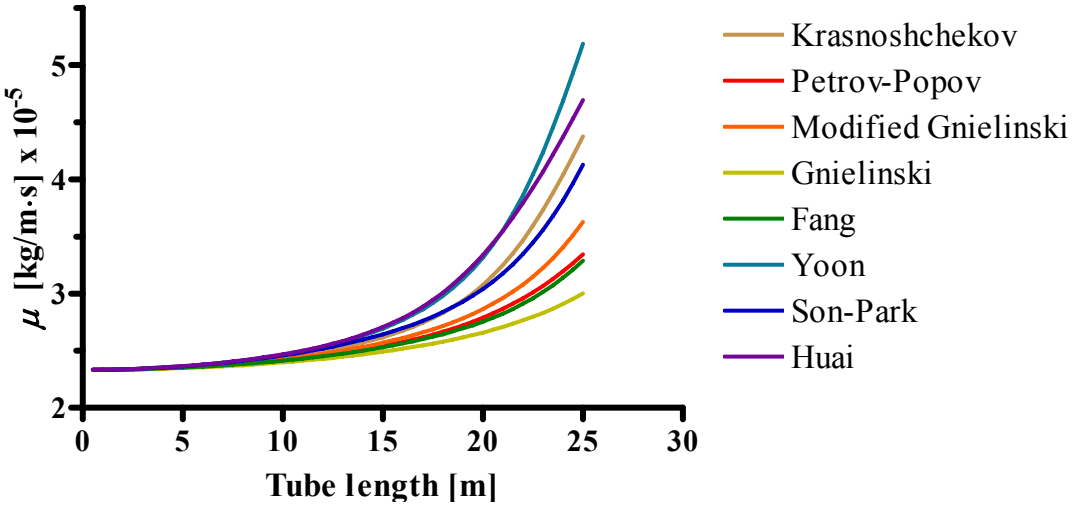

Figure A.4. Viscosity, μ, is plotted over the length of the heat exchanger for different *Nu* correlations.

A.2. Predicted heat transfer duty graphs of a turbulent supercritical R-744 gas cooler simulation

Figure A.5 shows the predicted heat transfer duty graphs for the various *Nu* correlations, used in the theoretical simulation of the supercritical R-744 gas cooler (Chapter 4).

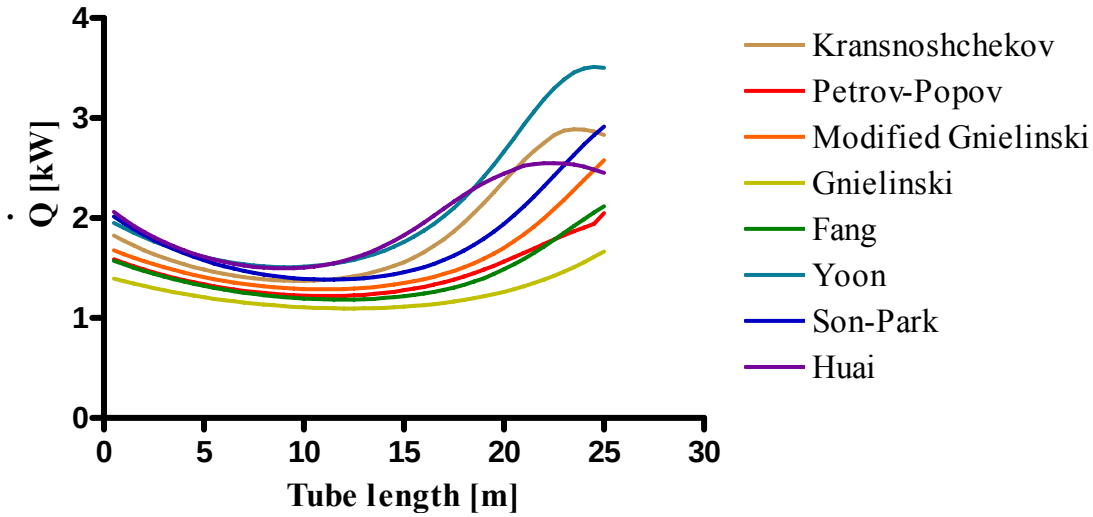

Figure A.5. The predicted heat transfer duty, $\dot{Q}$, is plotted over the length of the heat exchanger for different *Nu* correlations.

Appendix B: *Calculation of Nu and Nu_{exp}*

B.1. Nu_{exp} obtained from Yoon and co-workers (2003)

Experimentally obtained data (convection heat transfer coefficients with bulk temperatures) from Yoon and co-workers (2003) and Nu_{exp} are shown in Table B.1. Nu_{exp} was calculated according to Eq 3.14 by employing the hydraulic diameter (D_H = 7.73 mm) reported by Yoon and co-workers (2003).

Table B.1. Experimental h_c and T_b data,were taken from Yoon and co-workers (2003) to calculate Nu_{exp}, according to Eq (3.14).

p [MPa]	h_c	T_b	Nu_{exp}	p [MPa]	h_c	T_b	Nu_{exp}
7.5	1.875	60.38	524.5657	**8.2**	1.9375	62.95	508.2075
	2.3125	49.10	603.7023		2.75	52.18	658.3308
	3.4375	40.90	784.0624		3.75	44.36	761.6264
	5.375	36.03	1011.657		6.6875	40.00	1104.109
	10.375	33.33	1498.762		10.625	37.44	1340.918
	21.4375	32.18	2202.737		11.875	36.28	1192.746
	14.3125	31.67	721.2231		7.75	35.38	717.1116
	11	31.54	827.1401		6.125	34.36	602.1398
7.7	1.875	61.79	516.3431	**8.5**	2.125	63.59	540.6929
	2.375	50.38	607.3023		2.875	52.95	658.4815
	3.8125	42.31	849.7873		4.125	46.41	816.5493
	5.3125	36.15	887.7135		7.0625	41.03	1066.689
	9.6875	34.62	1349.025		9.6875	38.72	1136.678
	18.1875	33.46	1839.453		10.1875	37.44	1031.696
	12	32.82	849.4505		6.375	36.15	637.9126
	9.1875	32.44	787.5291		5.1875	34.87	533.9464
8.0	1.9375	62.56	518.5899	**8.8**	2.1875	63.72	537.659
	2.625	51.28	643.7579		2.875	53.33	625.3165
	3.9375	43.33	824.4007		4.5	47.31	839.0014
	6.0625	38.72	1022.989		7.25	42.05	1012.511
	9.5	36.15	1197.57		8.75	39.87	989.431
	14.75	35.00	1374.036		7.9375	38.21	824.8
	8.625	34.23	754.7119		5.0625	36.54	528.1123
	6.4375	33.59	612.2278		4.625	34.62	482.1477

B.2. Calculation of theoretical *Nu*

The theoretical Nu^s tabulated in Tables B.2.a to B.2.f have been calculated for every coordinate on the graphs shown in Figure 5.1. These Nu^s were calculated by means of:

- Gnielinski correlation *via* Eq 3.22.
- Modified Gnielinski correlation *via* Eq 3.23.
- Krasnoshchekov correlation *via* Eqs (3.24) to (3.26) and Table 3.1.
- Petrov-Popov correlation *via* Eqs (3.27) to (3.29).
- Fang correlation *via* Eqs (3.30) and (3.31).
- Yoon correlation *via* Eq (3.32).
- Son-Park correlation *via* Eq (3.34).
- Huai correlation *via* Eq (3.36).

The Nu^s calculated according to these correlations, at various pressures, are tabulated in Tables B.2a to B.2f.

For the successful calculation of the theoretical Nu^s, the following parameters need to be known (note: every correlation does not require all of the parameters):

- T_b and T_W. T_b is given by Yoon and co-workers (2003) and T_W was calculated by using data from Yoon.
- p is given by Yoon and co-workers (2003).
- D_H is given by Yoon and co-workers (2003) as 7.73 mm.
- L is given by Yoon and co-workers (2003). Note that Yoon and co-workers reported that the length of every sub section is 500 mm, but the annulus is only 470 mm in length per sub section.
- Re_b and Re_W calculated according to Eq (3.18).
- Pr_b and Pr_W calculated according to Eq (3.19).
- f calculated according to Eq (3.38).
- Enthalpies h_b and h_W.
- Densities ρ_b and ρ_W.

- Specific heat capacities at constant pressure c_p and $c_{p,W}$.
- $\overline{c_p}$ calculated according to Eq (3.26).
- G/q. G was given as 337 kg/m^{2}s by Yoon and co-workers (2003) and q was calculated calculated according to Eqs (3.8). Note that:

$$q = \frac{\dot{Q}}{\pi DL}$$

The Krasnoshchekov, Petrov-Popov, Fang, Son-Park and Huai correlations can only be calculated if the wall temperatures are known. To calculate the wall temperature, Eq (3.12) can be used. From Eq (3.12) it follows that the heat transfer rate, $\dot{Q}$, should be known. $\dot{Q}$ can be calculated with Eq (3.8) if the inlet and outlet temperature are known. Yoon and co-workers (2003) defined the bulk temperature as follows:

$$T_b = \frac{T_{b,in} + T_{b,out}}{2}$$

where $T_{b,in}$ and $T_{b,out}$ are, respectively, the bulk temperatures at the inlet and outlet. To calculate the inlet and outlet bulk temperature of every section (eight sections per pressure set), appropriate assumptions need to be made. In Table B.1 it can be seen that as the bulk temperature decreases, the difference between the bulk temperatures decreases as well, resulting in the formation of unequal intervals. For the calculation of T_W two possible routes may be followed:

1. As mentioned, Yoon and co-workers (2003) reported that each section was 500 mm in length, but the annulus heat exchanger at each section was only 470 mm (see Figure B.1). It may be assumed that the exit bulk temperature at a section is halfway between the applicable bulk temperature and the inlet bulk temperature of the same section (note that the R-744 stream is cooling down, therefore, the midpoint between the smaller intervals were chosen). The inlet bulk temperature will thus be an equal distance to the warmer side. This assumption gives rise to a situation where there is a temperature loss between the outlet of the previous section and the inlet at the current section. This assumption will be valid if it is further assumed that there is a heat loss between the sections (*i.e.* in the excess 30 mm).
2. If the assumption is made that there is no heat loss between the outlet of the previous section and the inlet of the current section, then the inlet bulk temperature at the first

section, or the outlet bulk temperature at the last section, should be known. If the temperature difference between the inlet bulk temperature and the bulk temperature, at the first section is assumed to be equal to half the difference between the first and second bulk temperature, then no legitimate results can be generated for any of the six pressure sets. However, if the difference in the exit bulk temperature at the last (8^{th}) section and the bulk temperature at the last section is assumed to be equal to half the difference between the bulk temperatures of second last and last (7^{th} and 8^{th}) sections, then plausible results may be generated for all eight of the pressure sets.

For this study, the first option was chosen. It should be noted that the Gnielinski correlation, which is the foundation of the newly formulated *Nu* correlation, requires only bulk temperatures and pressures. Note, *Correlations I*, *II* and *III* are independent of T_W, and thus of the method used to calculate T_W.

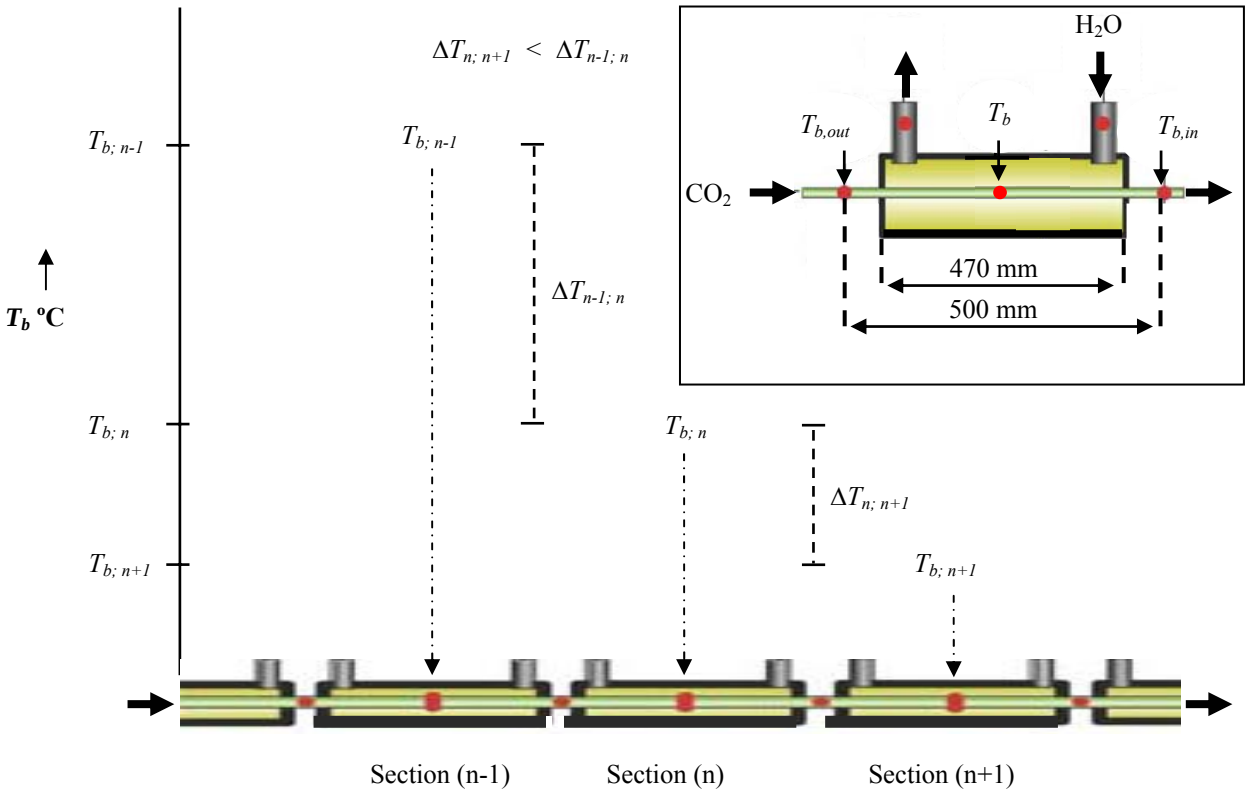

Figure B.1. Schematic illustration for determination of the inner wall temperature (T_W). T_b is the average temperature at bulk of section, $T_b = ½(T_{b,in} + T_{b,out})$.
Inset: Schematic illustration of a single annulus section.

Table B.2.a. Values calculated according to abovementioned Equations at a pressure of 7.5 MPa.

T_b ºC	Nu_G	$Nu_{G,M}$	Nu_{KKP}	Nu_{PP}	Nu_F	Nu_Y	Nu_{SP}	Nu_H
60.38	299.8	330.3	386.1	372	354.8	555	658.8	385.3
49.10	330.8	357.4	422.1	402.7	366.3	619.3	660.8	416.5
40.90	372	394.8	449.5	429.7	379.4	713.1	671.9	425.6
36.03	426.7	432.2	497.6	462.4	365.6	854.4	655.9	459.1
33.33	512.8	472.9	551.6	448.9	275.7	1117	603.3	505.4
32.18	651.7	685.1	2497	2040	2300	1653	939.4	1028
31.67	973.5	1361	907.3	823.1	944.6	4107	1976	991.5
31.54	620	755.9	651.8	649.1	700.7	2115	1112	490.9

Table B.2.b. Values calculated according to abovementioned Equations at a pressure of 7.7 MPa.

T_b ºC	Nu_G	$Nu_{G,M}$	Nu_{KKP}	Nu_{PP}	Nu_F	Nu_Y	Nu_{SP}	Nu_H
61.79	298.4	328.2	386.7	371.7	352.9	553.2	654.1	387
50.38	329.5	356.1	418.6	399.6	364.5	618.4	658.6	412.7
42.31	369.8	383.5	466.1	433.9	357.8	711.4	640.8	457
36.15	451.6	452.1	519.7	480	376	934.5	660.5	467
34.62	511.6	473.1	659.2	553.5	384.7	1130	621.8	599.9
33.46	636.8	680.5	1593	1396	1528	1639	945.5	888.9
32.82	762.3	994.2	898.4	803.8	923	2583	1479	887.4
32.44	511.3	616.4	528	522.9	565	1561	966.1	440.2

Table B.2.c. Values calculated according to abovementioned Equations at a pressure of 8.0 MPa.

T_b ºC	Nu_G	$Nu_{G,M}$	Nu_{KKP}	Nu_{PP}	Nu_F	Nu_Y	Nu_{SP}	Nu_H
62.56	299	327.7	389.3	373.1	351.1	556.1	648.3	390.7
51.28	331.1	356.5	419.1	399.6	362.8	624.9	653.8	412.7
43.33	374.2	393.6	454.5	431.6	376.4	728.2	660.3	429.3
38.72	432.4	424.6	535.5	477.4	360.9	890.4	628.1	506.5
36.15	523.4	531.1	920.1	792.9	804.6	1207	762.2	728.5
35.00	625.8	724	1110	1000	1114	1721	1063	783.2
34.23	549.2	670.7	611.2	584.6	645.5	1634	1047	553.4
33.59	413	483.7	426	423.2	451.4	1146	803.9	360.9

Table B.2.d. Values calculated according to abovementioned Equations at a pressure of 8.2 MPa.

T_b ºC	Nu_G	$Nu_{G,M}$	Nu_{KKP}	Nu_{PP}	Nu_F	Nu_Y	Nu_{SP}	Nu_H
62.95	299.6	327.7	390	373	349.6	558.6	645.1	391.7
52.18	330.9	356.1	416.9	397.8	361.8	626.5	651.8	409.7
44.36	374	390	461.4	433.4	370.8	732	649.2	440.5
40.00	428.1	434.5	514.3	479.5	397.6	886.8	661	465.9
37.44	507	514.9	672.9	617.3	568.6	1169	733.3	554.1
36.28	572.5	648.1	924.8	850	926.9	1506	964.9	697.1
35.38	523.8	637.8	592.7	558.7	620.9	1487	1017	580.8
34.36	382.8	447.8	390.2	386.3	412.8	1029	766.5	348.3

Table B.2.e. Values calculated according to abovementioned Equations at a pressure of 8.5 MPa.

T_b ºC	Nu_G	$Nu_{G,M}$	Nu_{KKP}	Nu_{PP}	Nu_F	Nu_Y	Nu_{SP}	Nu_H
63.59	300.3	328.2	386.5	370.4	347.6	561.9	642.9	387.5
52.95	332.6	359.4	407.2	391.2	362.8	633.9	656.4	393.7
46.41	368.8	379.2	473.3	436	362.3	725	629.4	465.2
41.03	436.2	441.7	560.3	514.6	444.8	930.8	669.3	506.7
38.72	501.1	536.1	724.5	662.6	685.8	1201	803.5	591.1
37.44	502.8	582.6	663	628.2	684.7	1328	916	561.9
36.15	403.4	473.6	424.8	415.8	448.2	1074	802	393
34.87	314.8	360.4	318.9	317.5	334.2	802.1	653.6	279.4

Table B.2.f. Values calculated according to abovementioned Equations at a pressure of 8.8 MPa.

T_b ºC	Nu_G	$Nu_{G,M}$	Nu_{KKP}	Nu_{PP}	Nu_F	Nu_Y	Nu_{SP}	Nu_H
63.72	302.1	328.1	392.9	374.2	346.1	567.8	635.3	395.9
53.33	335.7	359.3	417	396.8	360.9	645.5	646.1	405.3
47.31	371.6	379	489.1	445.3	370.1	740.4	623.7	485.3
42.05	438.4	454.4	591.4	538.1	512.4	964.3	701.9	526.1
39.87	474.3	529.4	660.9	616.9	658.5	1163	834.7	566.7
38.21	422.1	490.4	479.3	465	501.8	1096	816.9	435.9
36.54	327	378.6	329.7	325	346.6	829.5	685.7	314.4
34.62	259.4	294.1	260.2	259.4	271.1	636.3	571.1	232.3

B.3. Average deviation between the Gnielinski and modified Gnielinski correlations

Table B.3 shows the average deviation, $\Delta\%$, at every point between the Gnielinski and modified Gnielinski correlations. $\Delta\%$ is defined by:

$$\Delta\% = 100\left(\frac{Nu_{G,M} - Nu_G}{Nu_G}\right) \tag{B.1}$$

Table B.3. The average deviation at every point between the Gnielinski and modified Gnielinski correlations. The average for all the points is *9.7%*.

p [MPa]	Nu_G	$Nu_{G,M}$	$\Delta\%$	p [MPa]	Nu_G	$Nu_{G,M}$	$\Delta\%$	p [MPa]	Nu_G	$Nu_{G,M}$	$\Delta\%$
7.5	299.8	330.3	10.2	**8.0**	299	327.7	9.6	**8.5**	300.3	328.2	9.3
	330.8	357.4	8.0		331.1	356.5	7.7		332.6	359.4	8.1
	372	394.8	6.1		374.2	393.6	5.2		368.8	379.2	2.8
	426.7	432.2	1.3		432.4	424.6	-1.8		436.2	441.7	1.3
	512.8	472.9	-7.8		523.4	531.1	1.5		501.1	536.1	7.0
	651.7	685.1	5.1		625.8	724	15.7		502.8	582.6	15.9
	973.5	1361	39.8		549.2	670.7	22.1		403.4	473.6	17.4
	620	755.9	21.9		413	483.7	17.1		314.8	360.4	14.5
7.7	298.4	328.2	10.0	**8.2**	299.6	327.7	9.4	**8.8**	302.1	328.1	8.6
	329.5	356.1	8.1		330.9	356.1	7.6		335.7	359.3	7.0
	369.8	383.5	3.7		374	390	4.3		371.6	379	2.0
	451.6	452.1	0.1		428.1	434.5	1.5		438.4	454.4	3.6
	511.6	473.1	-7.5		507	514.9	1.6		474.3	529.4	11.6
	636.8	680.5	6.9		572.5	648.1	13.2		422.1	490.4	16.2
	762.3	994.2	30.4		523.8	637.8	21.8		327	378.6	15.8
	511.3	616.4	20.6		382.8	447.8	17.0		259.4	294.1	13.4

B.4. Gnielinski MH correlation graphs

Figure B.2 show the prediction of *Nu* by the Gnielinski MH correlation over the entire tube length of the heat exchanger. Figure B.3 show Nu_{exp} against. *Nu* (predicted by the Gnielinski MH correlation) for temperatures equal and greater than that of the pseudocritical temperature.

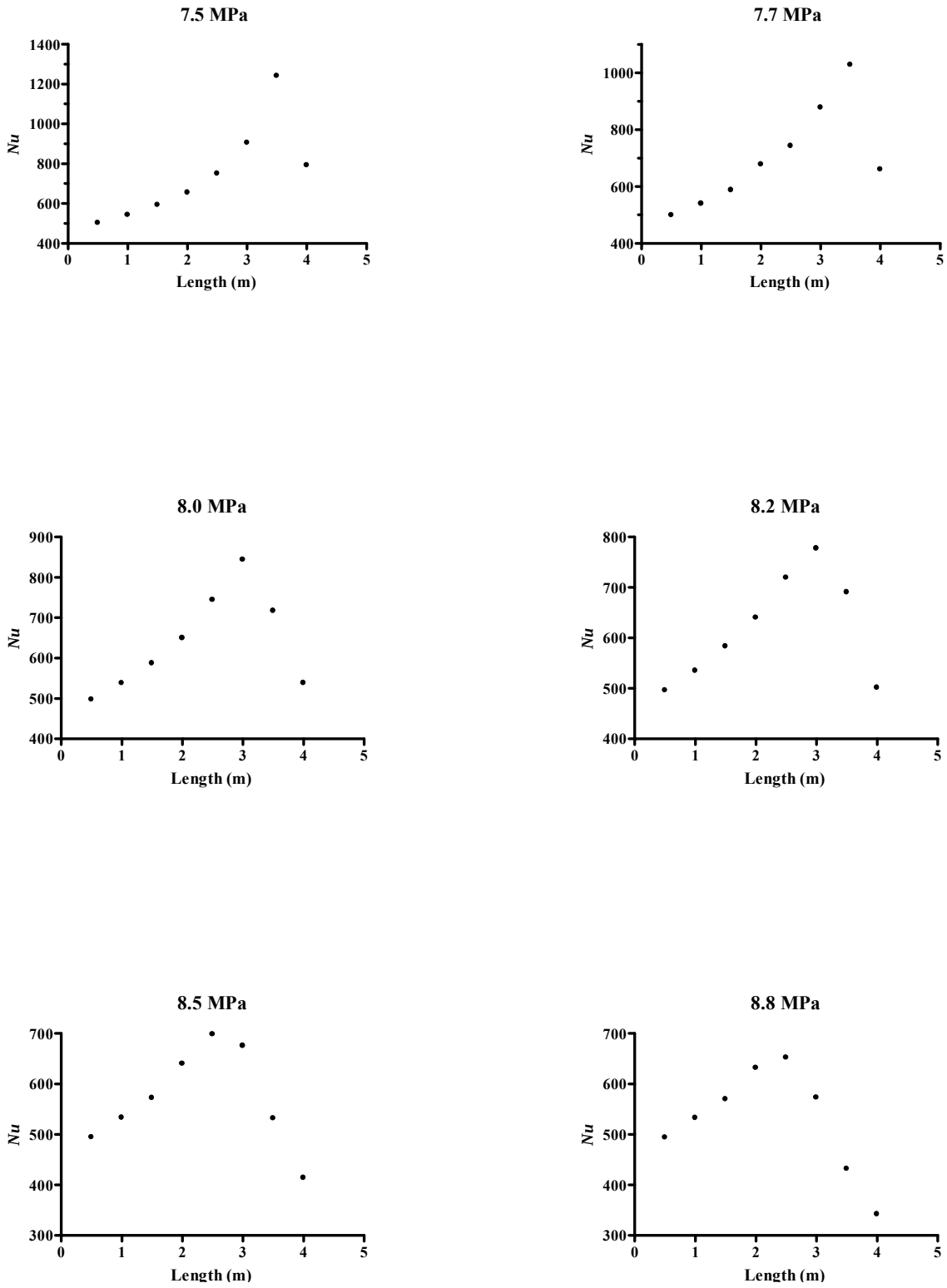

Figure B.2. *Nu* was calculated according to the Gnielinski MH correlation at different pressures, over the tube length of a tube-in-tube heat exchanger.

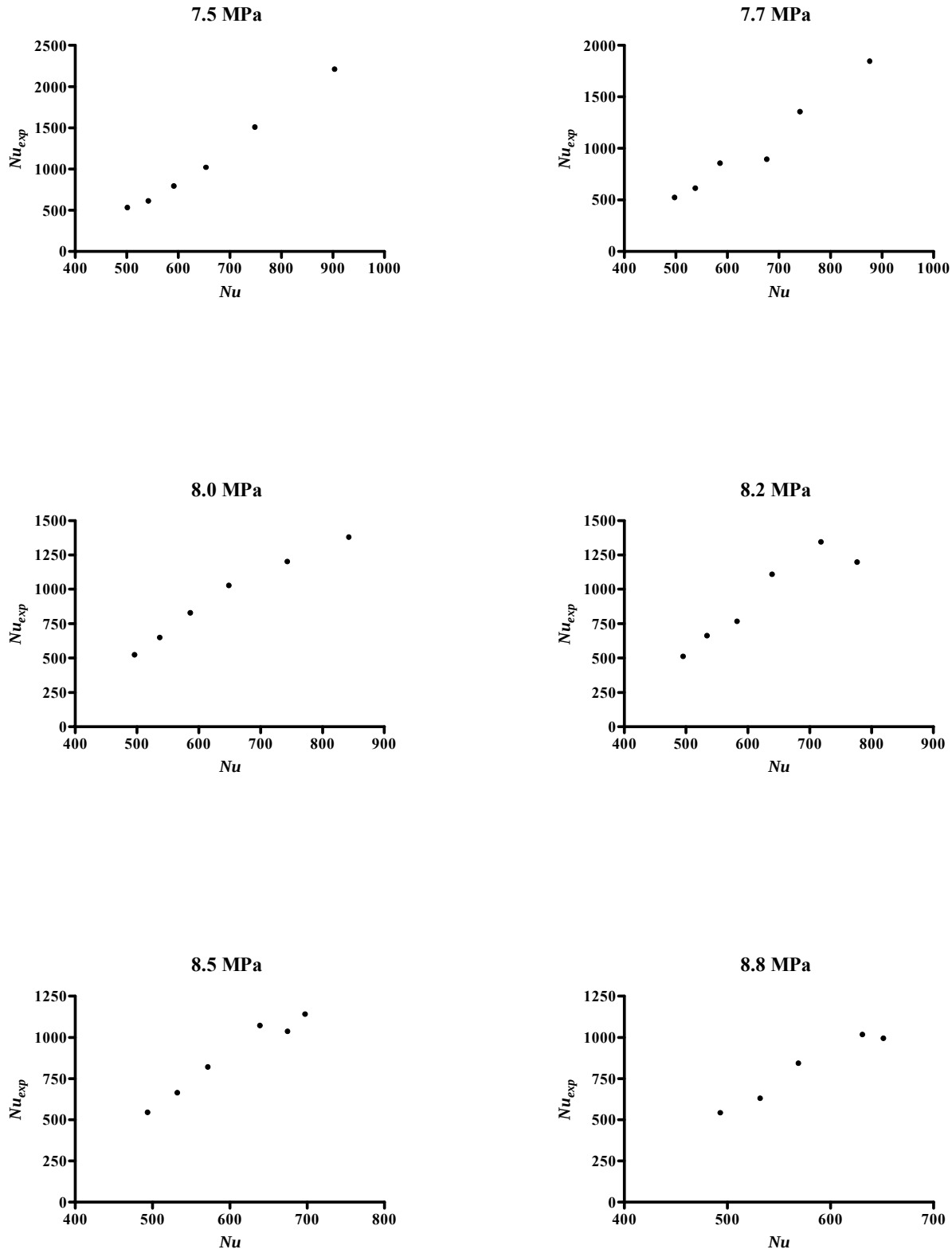

Figure B.3. *Nu* was calculated according to the Gnielinski MH correlation at different pressures and for temperatures equal or greater than the pseudocritical temperature.

B.5. Correlations I, II an III dev's

Tables B.4 and B.5, respectively, give *dev* at every point for *Correlations I* (Eq (5.1)) and *II* (Eq (5.3)).

Table B.4. The *dev* at every point between Nu_{exp} and *Correlation I Nu*. Only Nu_{exp} (and thus *Nu*) obtained when $T \geq T_{pc}$ are included. The average of all the *dev* values ($\overline{dev}$) is equal to 7.77%.

***p* [MPa]**	**Nu_{exp}**	***Nu***	***dev***	***p* [MPa]**	**Nu_{exp}**	***Nu***	***dev***
57.	524.5657	545.9521	4.08	**8.2**	508.2075	545.2941	7.30
	603.7023	647.9328	7.33		658.3308	648.2617	1.53
	784.0624	783.4684	0.08		761.6264	790.0478	3.73
	1011.657	963.415	4.77		1104.109	968.0206	12.33
	1498.762	1246.658	16.82		1340.918	1227.578	8.45
	2202.737	1703.597	22.66		1192.746	1443.053	20.99
7.7	516.3431	541.3465	4.84	**8.5**	540.6929	547.5969	1.28
	607.3023	643.6562	5.99		658.4815	653.8542	0.70
	849.7873	776.2311	8.66		816.5493	772.9414	5.34
	887.7135	1045.329	17.76		1066.689	994.6671	6.75
	1349.025	1242.711	7.88		1136.678	1208.169	6.29
	1839.453	1654.581	10.05		1031.696	1213.761	17.65
8.0	518.5899	543.3203	4.77	**8.8**	537.659	553.5184	2.95
	643.7579	648.9197	0.80		625.3165	664.0523	6.19
	824.4007	790.7057	4.09		839.0014	782.1525	6.78
	1022.989	982.1663	3.99		1012.511	1001.904	1.05
	1197.57	1281.529	7.01		989.431	1120.005	13.20
	1374.036	1618.394	17.78				

Table B.5. The *dev* at every point between Nu_{exp} and *Correlation II Nu.* Only Nu_{exp} (and thus *Nu*) obtained when $T \geq T_{pc}$ are included. The average of all the *dev* values ($\overline{dev}$) is equal to 6.69%.

***p* [MPa]**	Nu_{exp}	***Nu***	***dev***
7.5	524.5657	539.3278	2.81
	603.7023	669.2833	10.86
	784.0624	826.9498	5.47
	1011.657	1024.431	1.26
	1498.762	1327.661	11.42
	2202.737	1819.771	17.39
7.7	516.3431	527.8611	2.23
	607.3023	656.861	8.16
	849.7873	809.1128	4.79
	887.7135	1096.735	23.55
	1349.025	1303.453	3.38
	1839.453	1734.09	5.73
8.0	518.5899	522.4463	0.74
	643.7579	651.4462	1.19
	824.4007	808.7943	1.89
	1022.989	1007.231	1.54
	1197.57	1308.55	9.27
	1374.036	1625.475	18.30

***p* [MPa]**	Nu_{exp}	***Nu***	***dev***
8.2	508.2075	519.5796	2.24
	658.3308	642.8462	2.35
	761.6264	796.6906	4.60
	1104.109	977.2905	11.49
	1340.918	1229.557	8.30
	1192.746	1414.935	18.63
8.5	540.6929	513.8463	4.97
	658.4815	636.7944	3.29
	816.5493	761.9721	6.68
	1066.689	976.972	8.41
	1136.678	1162.35	2.26
	1031.696	1090.364	5.69
8.8	537.659	511.9352	4.78
	625.3165	634.8833	1.53
	839.0014	753.3721	10.21
	1012.511	951.172	6.06
	989.431	1015.831	2.67

Table B.6. The *dev* at every point between Nu_{exp} and *Nu* (calculated by means of C*orrelation III)*. The average of all the *dev* values; $\overline{dev}$ = 6.11%. Only Nu_{exp} (and thus *Nu*) obtained for $T \geq T_{pc}$ are included.

p **[MPa]**	Nu_{exp}	***Nu***	***dev***
7.5*	524.5657	432.577	17.54
	603.7023	606.007	0.38
	784.0624	816.42	4.13
	1011.657	1079.97	6.75
	1498.762	1484.64	0.94
	2202.737	2141.38	2.79
7.7*	516.3431	478.51	7.33
	607.3023	621.445	2.33
	849.7873	790.143	7.02
	887.7135	1108.83	24.91
	1349.025	1337.88	0.83
	1839.453	1815.04	1.33
8.0**	518.5899	565.337	9.01
	643.7579	668.867	3.90
	824.4007	795.148	3.55
	1022.989	954.406	6.70
	1197.57	1196.23	0.11
	1374.036	1450.58	5.57

p **[MPa]**	Nu_{exp}	***Nu***	***dev***
8.2**	508.2075	565.187	11.21
	658.3308	670.217	1.81
	761.6264	801.301	5.21
	1104.109	955.183	13.49
	1340.918	1170.13	12.74
	1192.746	1328.08	11.35
8.5**	540.6929	563.102	4.14
	658.4815	676.99	2.81
	816.5493	792.943	2.89
	1066.689	992.098	6.99
	1136.678	1163.81	2.39
	1031.696	1097.13	6.34
8.8**	537.659	563.991	4.90
	625.3165	687.007	9.87
	839.0014	805.561	3.99
	1012.511	1003.47	0.89
	989.431	1068.16	7.96

* Calculated according to Eq (5.6). ** Calculated according to Eq (5.7).

Appendix C: *EES program for simulation of supercritical R-744*

```
"Simple LMTD method for CO2 heating water, crossflow"


Function n(c_p_CO2,c_p_wl_CO2,k_k,rho_CO2,u_pp,q_w_pp)

if ((c_p_CO2/c_p_wl_CO2) <=1) then
   n = 0.66 - k_k*q_w_pp/(rho_CO2*u_pp)
else
   n = 0.9 - k_k*q_w_pp/(rho_CO2*u_pp)
endif

end


        "Dimensions of tube in tube water in annulus"
d_i_CO2 = 0.04
d_o_CO2 = d_i_CO2+0.0015
d_i_water = 0.05
d_h_CO2 = d_i_CO2
d_h_water = d_i_water - d_o_CO2
A_CO2 = pi/4*d_i_CO2^2
A_water = pi/4*(d_i_water^2 - d_o_CO2^2)
epsilon = 0.0015e-3



        "Conditions"
m_dot_CO2 = 0.5
m_dot_water = 0.3

T_CO2_in = 393.15
T_water_out = 363.15

L = 25

P_CO2_in = 12000
P_water_in = 400

k_pp = 4e-4
n=50


T_water_in = T_water[0]          "n"
T_water_out = T_water[n]         "0"
T_CO2_in = T_CO2[n]              "0"
T_CO2_out = T_CO2[0]             "n"


P_CO2_in = P_CO2[0]
P_water_in = P_water[0]

c_p_CO2[0] = CP(CarbonDioxide,T=T_CO2[0],P=P_CO2[0])
c_p_water[0] = CP(Water,T=T_water[0],P=P_water[0])

rho_CO2[0] = Density(CarbonDioxide,T=T_CO2[0],P=P_CO2[0])
rho_water[0] = Density(Water,T=T_water[0],P=P_water[0])
```

```
mu_CO2[0] = VISCOSITY(CarbonDioxide,T=T_CO2[0],P=P_CO2[0])
mu_water[0] = VISCOSITY(Water,T=T_water[0],P=P_water[0])

k_CO2[0] = CONDUCTIVITY(CarbonDioxide,T=T_CO2[0],P=P_CO2[0])/1000
k_water[0] = CONDUCTIVITY(Water,T=T_water[0],P=P_water[0])/1000

Pr_CO2[0] = PRANDTL(CarbonDioxide,T=T_CO2[0],P=P_CO2[0])
Pr_water[0] = PRANDTL(Water,T=T_water[0],P=P_water[0])

m_dot_CO2 = rho_CO2_m[0]*V_CO2[0]*A_CO2
m_dot_water = rho_water_m[0]*V_water[0]*A_water

rho_CO2_m[0] = rho_CO2[0]
rho_water_m[0] = rho_water[0]

A_CO2_heat = A_CO2_heat[n]
A_water_heat = A_water_heat[n]

factor = 0

Duplicate i = 1,n

A_CO2_heat[i] = pi*d_i_CO2*(L/n)
A_water_heat[i] = pi*d_i_water*(L/n)

P_CO2[i]=  P_CO2[i-1] - DELTAP_oL_CO2[i]
P_water[i]=P_water[i-1] - DELTAP_oL_water[i]

DELTAT_1[i] = T_CO2[i] - T_water[i]
DELTAT_2[i] = T_CO2[i-1] - T_water[i-1]
DELTAT_lm[i]=(DELTAT_1[i]-DELTAT_2[i])/ln(DELTAT_1[i]/DELTAT_2[i])

-Q_[i] = m_dot_CO2*1/2*(c_p_CO2[i]+c_p_CO2[i-1])*(T_CO2[i-1] - T_CO2[i])
-Q_[i] = m_dot_water*1/2*(c_p_water[i]+c_p_water[i-1])*(T_water[i-1] - T_water[i])
-Q_[i] = UA_CO2_[i]*(T_wl_CO2[i]-0.5*(T_CO2[i-1] + T_CO2[i]))
UA_CO2_[i]=(h_CO2[i]*A_CO2_heat[i])

c_p_wl_average_CO2[i]=(h_enthalpy_CO2[i]-h_enthalpy_wl_CO2[i])/(T_CO2[i]-T_wl_CO2[i])
c_p_wl_CO2[i]=CP(CarbonDioxide,T=T_wl_CO2[i],P=P_CO2[i])
c_p_CO2[i] = CP(CarbonDioxide,T=T_CO2[i],P=P_CO2[i])
c_p_water[i] = CP(Water,T=T_water[i],P=P_water[i])

rho_wl_CO2[i] = Density(CarbonDioxide,T=T_wl_CO2[i],P=P_CO2[i])
rho_CO2[i] = Density(CarbonDioxide,T=T_CO2[i],P=P_CO2[i])
rho_water[i] = Density(Water,T=T_water[i],P=P_water[i])

mu_wl_CO2[i] = VISCOSITY(CarbonDioxide,T=T_wl_CO2[i],P=P_CO2[i])
mu_CO2[i] = VISCOSITY(CarbonDioxide,T=T_CO2[i],P=P_CO2[i])
mu_water[i] = VISCOSITY(Water,T=T_water[i],P=P_water[i])

k_CO2[i] = CONDUCTIVITY(CarbonDioxide,T=T_CO2[i],P=P_CO2[i])/1000
k_water[i] = CONDUCTIVITY(Water,T=T_water[i],P=P_water[i])/1000

m_dot_CO2 = 1/2*(rho_CO2[i]+rho_CO2[i-1])*V_CO2[i]*A_CO2
m_dot_water = 1/2*(rho_water[i]+rho_water[i-1])*V_water[i]*A_water

Q_[i] = UA_[i]*DELTAT_lm[i]

Re_wl_CO2[i]=rho_wl_CO2[i]*V_CO2[i]*D_h_CO2/mu_wl_CO2[i]
Re_CO2_m[i] = 1/2*(rho_CO2[i]+rho_CO2[i-1])*V_CO2[i]*D_h_CO2/(1/2*(mu_CO2[i]+mu_CO2[i-1]))
```

```
Re_water_m[i] = 1/2*(rho_water[i]+rho_water[i-1])*V_water[i]*D_h_water/(1/2*(mu_water[i]+mu_water[i-1]))

Pr_wl_CO2[i] = PRANDTL(CarbonDioxide,T=T_wl_CO2[i],P=P_CO2[i])
Pr_CO2[i] = PRANDTL(CarbonDioxide,T=T_CO2[i],P=P_CO2[i])
Pr_water[i] = PRANDTL(Water,T=T_water[i],P=P_water[i])

N_U_water[i] = 0.023*abs(Re_water_m[i])^0.8*abs(1/2*(Pr_water[i]+Pr_water[i-1]))^0.4


        "Gnielinski correlation using the Haaland friction factor"
N_U_G_CO2[i] = N_U_G_m[i]*(1/2*(Pr_CO2[i]+Pr_CO2[i-1])/Pr_wl_CO2[i])^0.11
N_U_G_m[i] = (f_fil[i]/8*(Re_CO2_m[i] - 1000)*(1/2*(Pr_CO2[i]+Pr_CO2[i-1])))/(1 + 12.7*sqrt(abs(f_fil[i])/8)*(abs(1/2*(Pr_CO2[i]+Pr_CO2[i-1]))^(2/3)-1))*(1 + abs((d_i_CO2/(L/n)))^(2/3))
f_CO2[i] = (-1.8*log10(6.9/Re_CO2_m[i] + (epsilon/d_i_CO2/3.7)^1.11))^(-2)

        "Pitla91; Popov"
N_U_CO2[i]=N_U_Hu_CO2[i]*(1-factor)+N_U_sp_CO2[i]*factor

        "Pitla '99"
N_U_mean_CO2[i] = (N_U_wall_CO2[i] + N_U_balk_CO2[i])/2
        "Gnielinski"
N_U_wall_CO2[i] = f_fil[i]/8*(Re_CO2_m[i] - 1000)*1/2*(Pr_CO2[i]+Pr_CO2[i-1])/(1.07 + 12.7*sqrt(f_fil[i]/8)*((1/2*(Pr_CO2[i]+Pr_CO2[i-1]))^(2/3)-1))
N_U_balk_CO2[i] = (f_fil[i]/8*(Re_CO2_m[i] - 1000)*1/2*(Pr_CO2[i]+Pr_CO2[i-1]))/(1.07 + 12.7*sqrt(f_fil[i]/8)*((1/2*(Pr_CO2[i]+Pr_CO2[i-1]))^(2/3)-1))

        "Kransnoshcheko-Kuraeva-Protopopov for cooling of supercritical CO2 turbulent flow conditions in horizontal tubes"
        "Pitla '91"
N_U_w_CO2[i] = N_U_o_w_CO2[i]*(rho_wl_CO2[i]/rho_CO2[i])^n_kkp[i]*(c_p_wl_average_CO2[i]/c_p_wl_CO2[i])^m_kkp[i]
        "Petukhov-Kirillov"
N_U_o_w_CO2[i] = (f_fil[i]/8*Re_wl_CO2[i]*Pr_wl_CO2[i])/(1.07 + 12.7*sqrt(f_fil[i]/8)*(Pr_wl_CO2[i]^(2/3) - 1))

n_kkp[i]=0.8
m_kkp[i]=1
m_pp[i]=0.001
q_w_pp[i]= (Q_[i]*1000)/A_CO2_heat[i]

        "Petrov and Popov '85"
N_U_w_Pp_CO2[i] = N_U_o_w_CO2[i]*(1 - m_pp[i]*q_w_pp[i]/(rho_CO2[i]*V_CO2[i]))*(c_p_wl_average_CO2[i]/c_p_wl_CO2[i])^n_pp[i]

n_pp[i] =  n(c_p_CO2[i],c_p_wl_average_CO2[i],k_pp,rho_CO2[i],V_CO2[i],q_w_pp[i])

        "Fang"
N_U_fang_CO2[i]=f_fil_wl[i]/8*(Re_wl_CO2[i]-1000)*Pr_wl_CO2[i]/(1.00000007+12.7*sqrt(f_fil_wl[i]/8)*(Pr_wl_CO2[i]^(2/3)-1))*(1-m_pp[i]*q_w_pp[i]/(rho_CO2[i]*V_CO2[i]))*(c_p_wl_average_CO2[i]/c_p_wl_CO2[i])
f_fil[i]=(1.82*log10(Re_CO2_m[i])-1.64)^(-2)
f_fil_wl[i]=(1.82*log10(Re_wl_CO2[i])-1.64)^(-2)

        "Yoon"
N_U_yoon_CO2[i]=0.14*Re_CO2_m[i]^0.69*Pr_CO2[i]^0.66

        "Son-Park"
N_U_sp_CO2[i]=Re_CO2_m[i]^0.55*Pr_CO2[i]^0.23*(c_p_CO2[i]/c_p_wl_CO2[i])^0.15
```

```
        "Huai"
N_U_Hu_CO2[i]=0.0222*Re_wl_CO2[i]^0.8*Pr_wl_CO2[i]^0.3*(rho_CO2[i]/rho_wl_CO2[i])^(-
1.47)*(c_p_wl_average_CO2[i]/c_p_wl_CO2[i])^0.083

f_water[i]= MoodyChart(Re_water_m[i],epsilon/d_h_water)

f_CO2_Blasius[i] = 0.316/Re_CO2_m[i]^0.25
DELTAP_oL_CO2[i] = f_CO2_Blasius[i]*((L/n)/d_h_CO2)/2*(1/2*(rho_CO2[i]+rho_CO2[i-
1]))*V_CO2[i]^2/1000
DELTAP_oL_water[i] = f_water[i]*((L/n)/d_h_water)/2*(1/2*(rho_water[i]+rho_water[i-
1]))*V_water[i]^2/1000

N_U_CO2[i] = h_CO2[i]*d_h_CO2/(1/2*(k_CO2[i]+k_CO2[i-1]))
N_U_water[i] = h_water[i]*d_h_water/(1/2*(k_water[i]+k_water[i-1]))

1/UA_[i] = 1/(h_CO2[i]*A_CO2_heat[i]) + 1/(h_water[i]*A_water_heat[i]) + qas*R_wall_cond

L_[i] = L*(i/n)

h_enthalpy_wl_CO2[i] = ENTHALPY(CarbonDioxide,T=T_wl_CO2[i],P=P_CO2[i])
h_enthalpy_CO2[i] = ENTHALPY(CarbonDioxide,T=T_CO2[i],P=P_CO2[i])
h_enthalpy_water[i] = ENTHALPY(Water,T=T_water[i],P=P_water[i])

s_CO2[i] = ENTROPY(CarbonDioxide,T=T_CO2[i],P=P_CO2[i])
s_water[i] = ENTROPY(Water,T=T_water[i],P=P_water[i])

T_C_water[i]= T_water[i] - 273.15
T_C_CO2[i] = T_CO2[i] - 273.15
T_C_wl_CO2[i]=T_wl_CO2[i] - 273.15

End

qas=0
R_wall_cond=ln(d_o_CO2/d_i_CO2)/(2*pi*cond*L/n)
```

Appendix D: *EES program for calculating Nu*

```
"Determination of Experimental and Theoretical Nu numbers"

function factor(cp_av,cp)
if cp_av/cp >1 then
  factor=0.9-4e-4
else
  factor=0.66-4e-4
endif
end


K=273.15

T_7.5[1]=60.38+K      ; T_7.5[2]=49.1+K      ;T_7.5[3]=40.9+K      ;T_7.5[4]=36.03+K
T_7.5[5]=33.33+K      ;T_7.5[6]=32.18+K      ;T_7.5[7]=31.67+K      ;T_7.5[8]=31.54+K

T_7.7[1]=61.79+K      ; T_7.7[2]=50.38+K     ;T_7.7[3]=42.31+K      ;T_7.7[4]=36.15+K
T_7.7[5]=34.62+K      ;T_7.7[6]=33.46+K      ;T_7.7[7]=32.85+K      ;T_7.7[8]=32.44+K

T_8[1]=62.56+K        ; T_8[2]=51.28+K       ;T_8[3]=43.33+K              ;T_8[4]=38.72+K
T_8[5]=36.15+K       ;T_8[6]=35+K           ;T_8[7]=34.23+K              ;T_8[8]=33.59+K

T_8.2[1]=62.95+K      ; T_8.2[2]=52.18+K     ;T_8.2[3]=44.36+K      ;T_8.2[4]=40+K
T_8.2[5]=37.44+K      ;T_8.2[6]=36.28+K      ;T_8.2[7]=35.38+K      ;T_8.2[8]=34.36+K

T_8.5[1]=63.59+K      ; T_8.5[2]=52.95+K     ;T_8.5[3]=46.41+K      ;T_8.5[4]=41.03+K
T_8.5[5]=38.72+K      ;T_8.5[6]=37.44+K      ;T_8.5[7]=36.15+K      ;T_8.5[8]=34.87+K

T_8.8[1]=63.72+K      ; T_8.8[2]=53.33+K     ;T_8.8[3]=47.31+K      ;T_8.8[4]=42.05+K
T_8.8[5]=39.87+K      ;T_8.8[6]=38.21+K      ;T_8.8[7]=36.54+K      ;T_8.8[8]=34.62+K

h_7.5[1]=1.875       ;h_7.5[2]=2.3125             ;h_7.5[3]=3.4375             ;h_7.5[4]=5.375
h_7.5[5]=10.375             ;h_7.5[6]=21.4375      ;h_7.5[7]=14.3125      ;h_7.5[8]=11

h_7.7[1]=1.875       ;h_7.7[2]=2.375        ;h_7.7[3]=3.8125             ;h_7.7[4]=5.3125
h_7.7[5]=9.6875             ;h_7.7[6]=18.1875      ;h_7.7[7]=12           ;h_7.7[8]=9.1875

h_8[1]=1.9375         ;h_8[2]=2.625          ;h_8[3]=      3.9375         ;h_8[4]=6.0625
h_8[5]=9.5           ;h_8[6]=      14.75          ;h_8[7]=8.625          ;h_8[8]=6.4375

h_8.2[1]=1.9375             ;h_8.2[2]=2.75         ;h_8.2[3]=3.75         ;h_8.2[4]=6.6875
h_8.2[5]=10.625             ;h_8.2[6]=11.875             ;h_8.2[7]=7.75         ;h_8.2[8]=6.125

h_8.5[1]=2.125       ;h_8.5[2]=2.875        ;h_8.5[3]=4.125        ;h_8.5[4]=7.0625
h_8.5[5]=9.6875             ;h_8.5[6]=10.1875      ;h_8.5[7]=6.375        ;h_8.5[8]=5.1875

h_8.8[1]=2.1875             ;h_8.8[2]=2.875        ;h_8.8[3]=4.5          ;h_8.8[4]=7.25
h_8.8[5]=8.75         ;h_8.8[6]=7.9375       ;h_8.8[7]=5.0625             ;h_8.8[8]=4.625


P_7.5=7500
P_7.7=7700
P_8=8000
P_8.2=8200
P_8.5=8500
P_8.8=8800
```

```
epsilon=1.5e-6
m_dot_CO2=337*A_f_CO2
A_f_CO2=1/4*pi*D_i_CO2^2
D_i_CO2=0.00773
D_t=0.0009
D_o_CO2=D_i_CO2+2*D_t
D_i_water=0.016
D_h_water=D_i_water-D_o_CO2
L= 0.47
A_CO2=pi*D_i_CO2*L

T_max=80+K
T_min=50+K

T_7.5_in[8]=T_7.5_out[7]

x_[1]=1
Duplicate j =1,7
  T_7.5_in[j]=T_7.5[j]+0.5*(T_7.5[j]-T_7.5[j+1])
  x_[j+1]=x_[j]+1
end

Duplicate j =1,8

T_b_7.5[j]=T_7.5[j]-K
c_p_7.5_CO2[j]=CP(CarbonDioxide,T=T_7.5[j],P=P_7.5)

c_p_7.5_CO2_in[j]=CP(CarbonDioxide,T=T_7.5_in_x[j],P=P_7.5)
c_p_7.5_CO2_out[j]=CP(CarbonDioxide,T=T_7.5_out_x[j],P=P_7.5)

rho_7.5_CO2[j]=DENSITY(CarbonDioxide,T=T_7.5[j],P=P_7.5)
rho_wl_CO2[j]=DENSITY(CarbonDioxide,T=T_wl_7.5[j],P=P_7.5)
m_dot_CO2=rho_7.5_CO2[j]*V_7.5_CO2[j]*A_f_CO2
Pr_7.5_CO2[j]=PRANDTL(CarbonDioxide,T=T_7.5[j],P=P_7.5)
Pr_wl_CO2[j]=PRANDTL(CarbonDioxide,T=T_wl_7.5[j],P=P_7.5)
mu_7.5_CO2[j] = viscosity(CarbonDioxide,T=T_7.5[j],P=P_7.5)
mu_wl_CO2[j] = viscosity(CarbonDioxide,T=T_wl_7.5[j],P=P_7.5)
Re_7.5_CO2[j]=rho_7.5_CO2[j]*V_7.5_CO2[j]*D_i_CO2/mu_7.5_CO2[j]
Re_wl_CO2[j]=rho_wl_CO2[j]*V_7.5_CO2[j]*D_i_CO2/mu_wl_CO2[j]
k_7.5_CO2[j]=CONDUCTIVITY(CarbonDioxide,T=T_7.5[j],P=P_7.5)/1000
f_wl_CO2[j]=(1.82*log10(Re_wl_CO2[j])-1.64)^(-2)
f_7.5_CO2[j]=(-1.8*log10(6.9/Re_7.5_CO2[j]+(epsilon/D_i_CO2/3.7)^1.11))^(-2)

T_7.5[j]=0.5*(T_7.5_in[j]+T_7.5_out[j])
T_7.5_in_x[j]=T_7.5_in[j]
T_7.5_out_x[j]=T_7.5_out[j]

Q_7.5[j]=h_7.5[j]*A_CO2*(T_wl_7.5[j]-0.5*(T_7.5_in[j]+T_7.5_out[j]))
Q_7.5[j]=m_dot_CO2*c_p_7.5_CO2[j]*(T_7.5_out[j]-T_7.5_in[j])
N_u_7.5[j]=h_7.5[j]*D_i_CO2/k_7.5_CO2[j]
rho_w[j]=DENSITY(CarbonDioxide,T=T_wl_7.5[j],P=P_7.5)
h_b_7.5[j]=ENTHALPY(CarbonDioxide,T=T_7.5[j],P=P_7.5)
h_w_7.5[j]=ENTHALPY(CarbonDioxide,T=T_wl_7.5[j],P=P_7.5)
c_p_wl_7.5[j]=(h_b_7.5[j]-h_w_7.5[j])/(T_7.5[j]-T_wl_7.5[j])
c_p_W_7.5[j]=CP(CarbonDioxide,T=T_wl_7.5[j],P=P_7.5)



"Giniel Halaad"
```

N_u_GH_7.5[j]=N_u_m_7.5[j]*(Pr_7.5_CO2[j]/Pr_wl_CO2[j])^0.11
N_u_m_7.5[j]=(f_7.5_CO2[j]/8*(Re_7.5_CO2[j]-
1000)*Pr_7.5_CO2[j])/(1+12.7*(f_7.5_CO2[j]/8)^0.5*(Pr_7.5_CO2[j]^(2/3)-1))*(1+(D_i_CO2/L)^(2/3))

"Giniel"
N_u_wall_G_7.5[j]=f_7.5_CO2[j]/8*(Re_7.5_CO2[j]-
1000)*Pr_7.5_CO2[j]/(1.07+12.7*(f_7.5_CO2[j]/8)^0.5*(Pr_7.5_CO2[j]^(2/3)-1))

"Krasnoshchekov Kuraeva Protopopov"
N_u_KKP_7.5[j] = N_u_ow_7.5[j]*(rho_w[j]/rho_7.5_CO2[j])^n[j]*(c_p_wl_7.5[j]/c_p_W_7.5[j])^m[j]
n[j]=0.38
m[j]=B[j]*(c_p_wl_7.5[j]/c_p_W_7.5[j])^l_l[j]"0.2"
B[j]=0.75
l_l[j]=0.18

N_u_ow_7.5[j]=f_7.5_CO2[j]/8*Re_wl_CO2[j]*Pr_wl_CO2[j]/(1.07+12.7*(f_7.5_CO2[j]/8)^0.5*(Pr_wl_CO2
[j]^(2/3)-1))

"Petrov Popov"
N_u_PP_7.5[j]=N_u_ow_7.5[j]*(1-0.001*Q_7.5[j]/m_dot_CO2)*(c_p_wl_7.5[j]/c_p_W_7.5[j])^n_pp_7.5[j]
n_pp_7.5[j]=factor(c_p_wl_7.5[j],c_p_W_7.5[j])

"Fang"
N_u_F_7.5[j]=f_wl_CO2[j]/8*(Re_wl_CO2[j]-1000)*Pr_wl_CO2[j]/(1+7e-
8+12.7*(f_wl_CO2[j]/8)^0.5*(Pr_wl_CO2[j]^(2/3)-1))*(1-
0.001*Q_7.5[j]/m_dot_CO2)*(c_p_wl_7.5[j]/c_p_W_7.5[j])

"Yoon"
N_u_Yoon_7.5[j]=0.14*Re_7.5_CO2[j]^0.69*Pr_7.5_CO2[j]^0.66

"Son-Park"
N_u_SP_7.5[j]=Re_7.5_CO2[j]^0.55*Pr_7.5_CO2[j]^0.23*(c_p_7.5_CO2[j]/c_p_W_7.5[j])^0.15

"Huai"
N_u_Hu_7.5[j]=0.0222*Re_7.5_CO2[j]^0.8*Pr_7.5_CO2[j]^0.3*(rho_7.5_CO2[j]/rho_w[j])^(-
1.47)*(c_p_wl_7.5[j]/c_p_W_7.5[j])^0.083

end